MULTIFUNCTIONAL POLYMER COATINGS VIA CHEMICAL VAPOR DEPOSITION COPOLYMERIZATION

by

Yaseen Mohamed Elkasabi

A dissertation submitted in partial fulfillment
of the requirements for the degree of
Doctor of Philosophy
(Chemical Engineering)
in The University of Michigan
2009

Doctoral Committee:

       Associate Professor Joerg Lahann, Chair
       Professor Erdogan Gulari
       Professor Nicholas Kotov
       Assistant Professor Matthew R. Chapman

Then tell Me about the seed that you sow in the ground.
Is it you that make it grow, or are We the grower?
Were it Our will, We could crumble it to dry pieces, and you would lament:
"We are indeed ruined!"
"Nay, but we are deprived!"

Then tell Me about the water that you drink.
Is it you who send it down from the rain clouds, or are We the sender?
If We willed, We verily could make it salty: why then do you not give thanks?

Then tell Me about the fire which you kindle.
Is it you that produce the trees for it, or are We the producer?
We have made it a reminder, and an article of use for the travelers
Then glorify with praises the name of your Lord, the Most Great.

– The Noble Quran, 56:63-74

ACKNOWLEDGEMENTS

TABLE OF CONTENTS

LIST OF SCHEMES

LIST OF TABLES

LIST OF APPENDICES

ABSTRACT

The dissertation investigates how reactive polymer coatings can facilitate controlled immobilization of multiple biomolecules and can control multiple surface properties independently for biomedical applications. Chemical vapor deposition (CVD) copolymerization technology was chosen for the surface modification of substrates and biological devices, due to its high degree of conformal deposition. This feature was evidenced by the conformal deposition of reactive coatings within pre-assembled microfluidic channels, with aspect ratios as high as 37.

A superhydrophobic reactive CVD-coated surface was designed. The coating can immobilize proteins, despite its extremely high contact angle ($> 155^{\circ}$). Also, multipotent copolymer coatings presenting two different biological ligands in controllable ratios were prepared via CVD copolymerization of two functionalized PCPs. These polymer coatings are designed so that different reactive groups can be orthogonally introduced, making them attractive for a wide range of biomedical devices.

Preliminary biocompatibility of these coatings was assessed in short-term experiments (24-48 hr), using human umbilical vein endothelial cells and 3T3 murine fibroblasts. Both cell types adhered and spread on PPX polymers, with limited growth occurring on fluorinated PPX coatings. G6PD assays indicated significantly low cytotoxicity of CVD surfaces, when cultured with fibroblasts. We also demonstrate the immobilization of two different antithrombotic biomolecules onto a CVD-based

copolymer via orthogonal immobilization strategies. The antithrombotic biomolecules retained their bioactivity after immobilization. Furthermore, a modified CVD process was used to produce coatings which possess reactive surface composition gradients. The as-deposited gradient compositions range from 85% to 20%. Also, the CVD system can deposit various gradient slopes, such that the same composition range is deposited over distances of 1'', 3'', or 6''. These surface gradients can immobilize two biomolecules as gradients, allowing for further adaptation to specific biological environments.

Applications from this dissertation include the development of novel analytical biodevices, tissue engineering protocols, and combinatorial screening platforms. For instance, growth and differentiation of neurons occur along a chemical gradient. CVD copolymer gradients could mimic biological environments to guide their growth. Also, gradient deposition allows for the mass production of many copolymer compositions in one deposition. These samples could then be simultaneously screened for their interactions with cells.

CHAPTER 1

INTRODUCTION

The materials in this chapter have been adapted with minor modifications from the following book chapter: Y. Elkasabi, J. Lahann, "Recent Progress in Microstructured Surfaces Based on Chemical Vapor Deposition Methods", Biological Microarrays: Methods in Molecular Biology Series, Humana Press (in press).

1.1 Surface Modification Techniques

Controlled surface engineering has been a long-standing challenge in the development of bioarrays, artificial implants, and biomedical devices. Moreover, miniaturized diagnostic systems, such as micro-total analysis systems (μTAS),[1] cell-based assays,[2] microseparators for proteins,[3,4] DNA,[5] and polysaccharides,[6] often require universally applicable surface engineering protocols. Some general surface modification techniques have proven to be versatile in alleviating adverse biological effects. One technique that is widely used to tailor the interfacial properties of metals, metal oxides and semiconductor surfaces is the use of self-assembled monolayers (SAMs).[7] Based on the terminal functional groups exposed on the surface of a SAM, the surface reactivity can be varied. SAMs have been used for the direct immobilization of DNA, polypeptides and proteins.[8] However the use of SAMs is limited due to the relative chemical instability of the monolayer and the specificity of the substrates. In contrast, the above-mentioned applications require robust surface chemistry.

Extensive efforts have been made to create topological surface modifications using printing methods, such as dip/pen lithography,[9] patterning via scanning probes,[10] imprinting lithographies,[11,12] or soft lithography.[13,14] Included within soft lithography are: micromoulding in capillaries,[15] microcontact printing,[16] replica moulding,[17] microtransfer moulding,[18] solvent-assisted micromoulding,[19] and capillary force lithography.[20] Soft lithographical methods rely on the use of elastomeric stamps or replica structures to transfer material from a solution onto a surface. Patterned substrates created using shadow masks included a range of different materials, such as semiconductors,[21-23] organic metals,[24] polymers,[25] biomaterials[26] or cells.[27-29] Surface patterns have also been fabricated using lithographical techniques, on the basis of light,[30] X-rays,[31] electron[32] and ion beams,[33] or atoms[34].

Furthermore, patterned substrates can be incorporated into microfluidic systems subsequently used for high-throughput proteomics applications, pharmaceutical screening of cellular assays, or cell-based biosensors. Methods for creating patterns in microfluidic channels previously depended on patterning of a flat substrate, which is then sealed to the microchannel. Some specific processes utilize microfluidic patterning,[35] laminar flow patterning,[36-38] robotic spotting,[39-41] and jet printing,[42,43] and selective plasma etching.[44] These patterning methods have been used to pattern hydrogels[45-47], cells,[48,49] and proteins[36] within microfluidic systems. However, they often have several shortcomings. For example, patterns generated by laminar flow patterning and microfluidic patterning are limited to a relatively narrow range of continuous patterns, which are mainly determined by the flow geometry.

1.2 Chemical Vapor Deposition Polymerization

In addition to solvent-based methods that are being utilized for biomedical surface modification, solventless surface modification methods, such as chemical vapor deposition (CVD) polymerization, are currently being explored for biomedical devices.
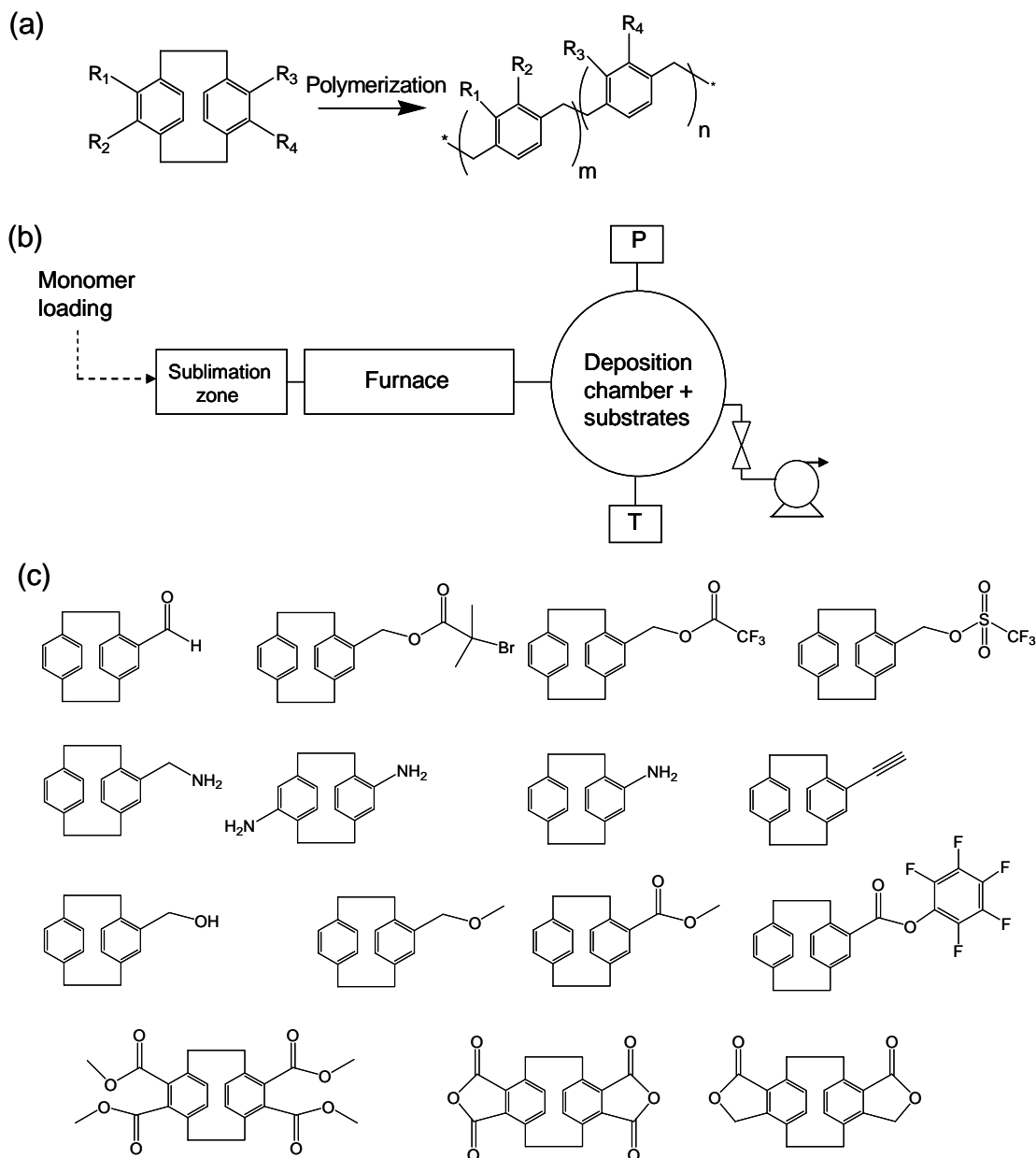
Figure 1.1. Functionalized [2.2]paracyclophanes (PCPs) can be polymerized into functionalized poly(*p*-xylylenes) (PPXs) with tailored reactivity. Taken from [64]

Many of the advantages to CVD polymerization are unique when compared to solvent-based coating processes. First, impurities associated with the use of solvents, initiators, or plasticizers are non-existent. Second, CVD coatings are conformal, allowing for simple and uniform modification of three-dimensional substrate geometries.[50] Third, although the initiation step requires high temperatures, initiation takes place away from the substrate, and the substrates can be controlled and maintained at room temperature. The control over substrate temperature allows for the deposition of polymers onto delicate substrates, as well as onto mechanically strong materials made of inorganic substances. Several examples of CVD-based polymer coatings have been reported: Frank and coworkers[51,52] have grafted polypeptide chains onto a surface using CVD. Gleason and coworkers[53,54] have shown that polymerization initiators can be introduced together with the monomer through basic process modification, thus facilitating the polymerization of monomers which do not contain an initiator. Hot filaments within the deposition chamber can be used for initiation of radical polymerizations, which often yields conformal coatings.

A major focus of CVD polymerization has been the polymerization of substituted [2.2]paracyclophanes (PCP) to yield functionalized poly(p-xylylenes) (PPX). This CVD polymerization is adapted from a process first developed by Gorham for parylene coatings.[55] In this procedure (Figure 1.1), a cyclic dimer is sublimated under vacuum (0.2-0.3 Torr), and transported by a carrier gas through an external heat source (T = 600 – 800 $^{\circ}$C). If the temperature is sufficiently high, a homolytic cleavage occurs across both bridge bonds, resulting in two quinodimethane diradicals, serving as an initiation step. The radicals then deposit and polymerize onto a sample that is fixed at a particular

temperature. For deposition of PPX polymers, the substrate temperature is critical for obtaining high-quality coatings. Generally, as substrate temperature decreases, the thickness of the PPX coating increases accordingly.[56] However, under normal CVD conditions for other materials, the substrate temperature and resulting film thickness are directly proportional to each other.[57] Much work has been done to model the mechanisms behind this trend.[56,58]

For a given substrate temperature, the pyrolyzed quinodimethane monomer will adsorb onto the substrate at a given surface density. Adsorption is then followed by spontaneous propagation reaction, resulting in growth of the polymer chain. At the same time, monomers and/or oligomers can desorb back into the CVD atmosphere. Thus, the rate of propagation is limited by the desorption rate. The fraction of adsorbed monomers that undergo polymerization is referred to as the sticking coefficient.[59] As the substrate temperature increases, the rate of monomer desorption increases, resulting in a lower sticking coefficient. Propagation rates remain constant, so long as the CVD process conditions remain at steady-state. This is because the rate of radical generation (pyrolysis) equals the rate at which radicals are buried in the growing film.[56] The termination of radical polymerization is dominated by coupling with ambient O_2. Hence, a contaminated CVD system can result in unstable, low molecular weight polymer films.

Typically, CVD polymers are deposited using substrate temperatures between -40 and 60 $^{\circ}$C, where 60 $^{\circ}$C represents the maximum temperature of significant PPX deposition.[56] Temperatures below -40 are not practical for real applications, and such a low temperature can damage delicate substrates. Room-temperature substrates facilitate the deposition of robust PPX coatings at controlled thicknesses and deposition rates, and

they can accommodate any type of substrate. We have successfully modified PCPs with a wide variety of functional groups,[60-64] which can then serve as reactive sites for immobilization of biomolecules. Vapor-based polymerization of PCPs produces a conformal PPX coating with mechanical integrity and low dielectric constants. Such properties are useful attributes for various applications including MEMS devices.[65-68] Recently-developed methods of fabricating micropatterns onto substrates via CVD of reactive poly(*p*-xylylenes) are discussed in this chapter. For this purpose, the CVD technology can be utilized in one of two general ways (Figure 1.2): (1) Deposition of a homogenous polymer coating that is reactive, then chemically pattern the coating after CVD treatment, and (2) Fabrication of polymer patterns during the CVD process *in situ*.
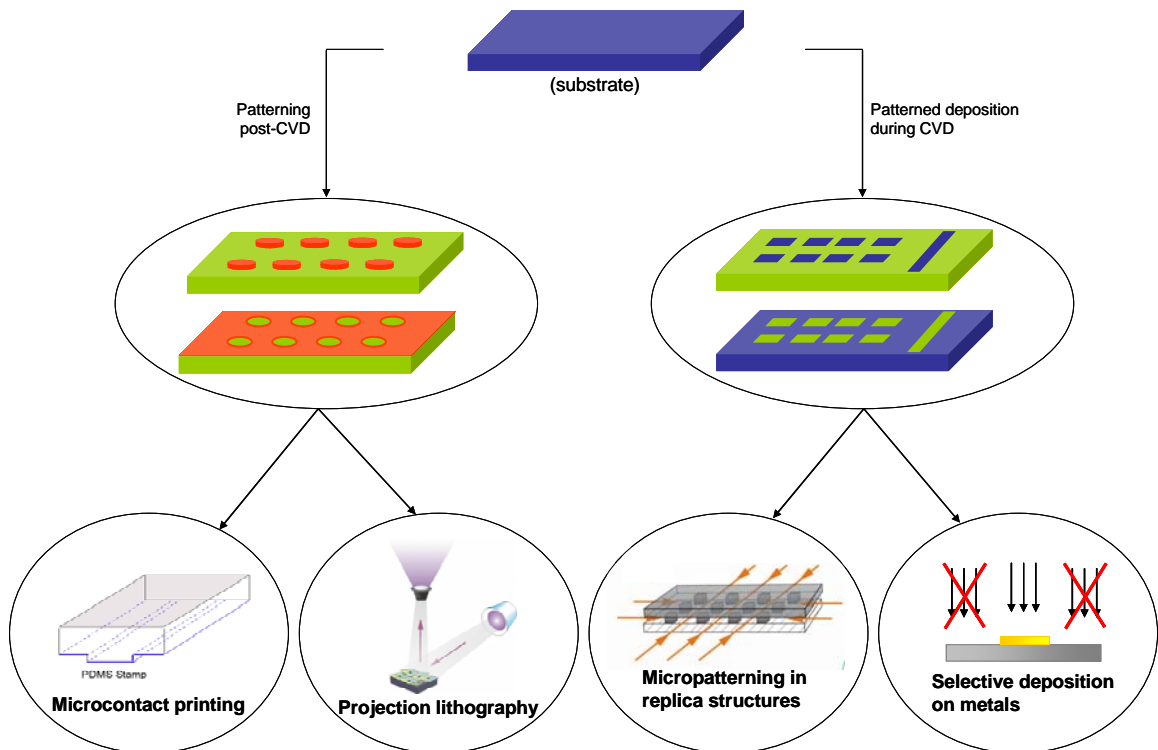
Figure 1.2. Two general protocols for fabrication of micropatterned surfaces are described. 1) CVD process, followed by subsequent patterning of the reactive coating. 2) Patterned deposition of the CVD polymer.

1.3 Modification of CVD Polymer Coatings

1.3.1 Microcontact Printing

Microcontact printing technology can be used to fabricate micropatterns of immobilized biomolecules onto reactive CVD coatings post-deposition. In this method, a PDMS stamp is cast from a photolithographically produced master made of silicon. Once the PDMS is cured, the biomolecule of interest is dissolved in a buffer, and the resulting solution is inked onto the PDMS pattern. The patterned PDMS substrate is then laid onto the surface, and the biomolecules are allowed to react (Figure 1.3a). The PDMS stamp can be removed and reused multiple times.

One recent example[69] exploits the specificity of hydrazides toward aldehydes and ketones.[70] Carbonyl-containing surfaces can be modified using dihydrazide homobifunctional linkers to form hydrazone bonds on one side, yielding alkyl hydrazide spacers on the other side, which can react further with formyl-containing groups in saccharides.[70] Adipic acid dihydrazide was chosen as the linker due to its intermediate-length spacer arm, which leads to accessible reactive sites for further reaction. A substrate coated with poly(4-formyl-*p*-xylylene-co-*p*-xylylene) (formyl-PPX) was patterned with adipic acid dihydrazide, hence creating hydrazide-activated surfaces suitable for targeting saccharides. The hydrazide-modified polymer surface was then reacted with 2—mannobiose, a disaccharide. One mannose group reacted with the hydrazide while leaving the other saccharide group free. Rhodamine-labeled concanavalin A, a mannose-specific lectin that recognizes the free mannose unit,[71] was used to investigate saccharide binding. Patterned substrates were visualized using fluorescence microscopy (Figure 1.3a, inset). The rhodamine-labeled lectin bound
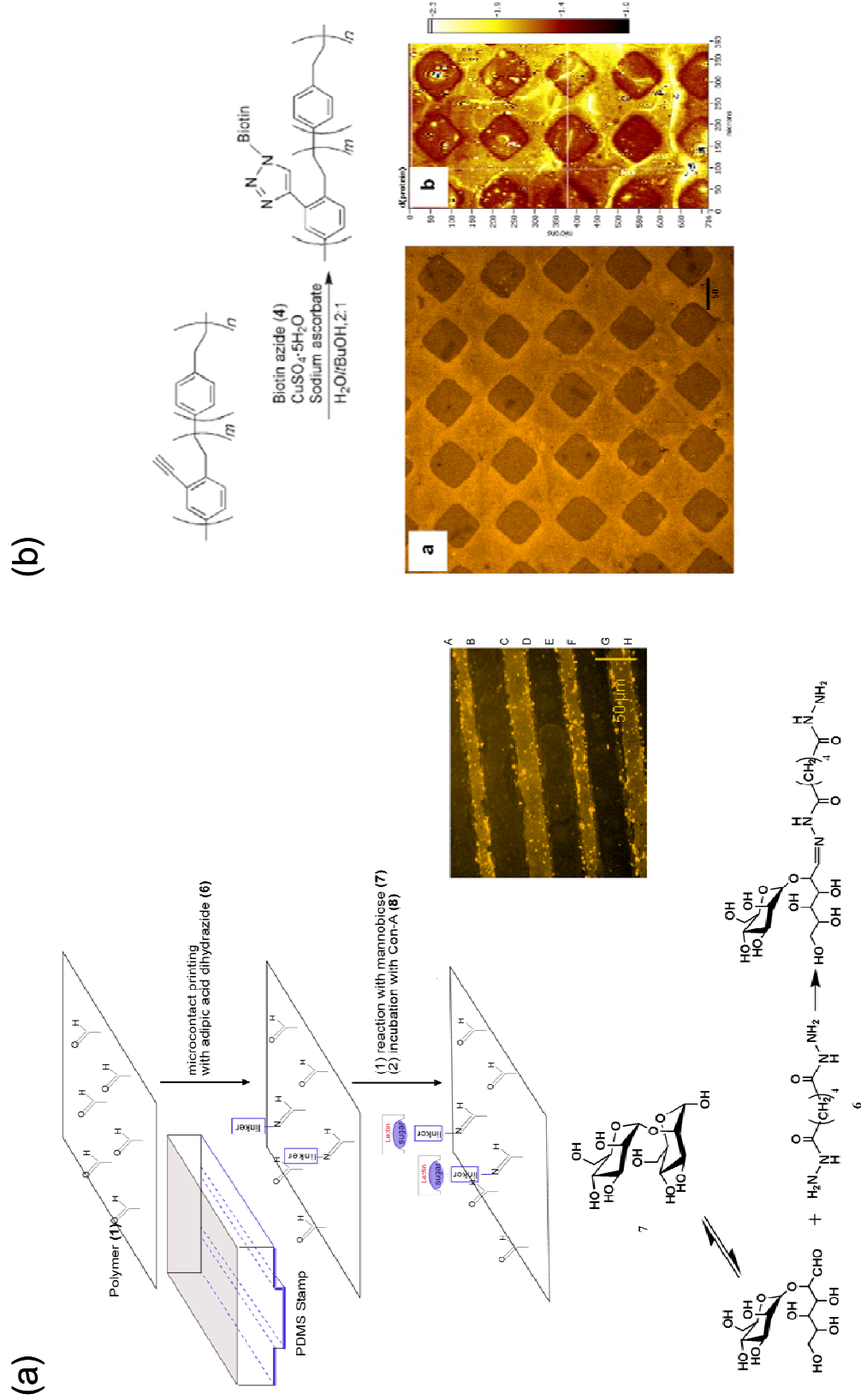
Figure 1.3. Microcontact printing process for (a) the immobilization of sugars onto aldehyde-functionalized PPX and (b) click chemistry. Taken from [69] and [73].

specifically to the disaccharide-presenting surface, which was then immobilized onto a substrate coated with formyl-PPX and patterned with lines of adipic acid dihydrazide. Immobilization of microscale patterns on formyl-PPX can also be extended towards DNA immobilization.[72] Supermolecular nanostamping (SuNS) was used to fabricate DNA nanopatterns immobilized onto formyl-PPX. The patterns can be lines or spots, an important feature for the operation of DNA microarrays.

Another example[73] involved the use of poly(4-ethynyl-*p*-xylylene-co-*p*-xylylene) (ethynyl-PPX), a polymer specifically tailored for use in click chemistry. Its reactivity against azides was studied, in order to assess whether the coating can be used for heterogeneous click reactions. Huisgen 1,3-dipolar cycloaddition between ethynyl-PPX and an azide-containing biotin-based ligand in the presence of copper(II) sulfate and sodium ascorbate was examined (Figure 1.3b). This coupling reaction yields triazoles, as described for solvent-based systems.[74] Sodium ascorbate acts as a reductant, generating CuI ions in situ, which then function as the catalyst.[74] Biotin azide (Photoprobe biotin, Vector Labs) was chosen as the representative ligand in this study, because biotin forms a strong noncovalent interaction with streptavidin (which has been widely used for binding biotinylated biomolecules).[60]

A thin layer of biotin azide and sodium ascorbate was spread onto a film of ethynyl-PPX and dried using N_2. In comparison to the concurrent microcontact printing of catalyst and azide, a two-step approach was found to be superior. A patterned PDMS stamp was then inked with a $CuSO_4$ solution and kept in contact with the substrate for 12-18 h. The patterned substrate was rinsed and incubated with an aqueous solution of rhodamine-labeled streptavidin. The immobilization of biotin azide onto ethynyl-PPX

was assed using fluorescence microscopy. The fluorescence micrograph and ellipsometric thickness map shown in Figure 1.3b confirm selective protein coupling in the regions where the $CuSO_4$ solution was microcontact printed, thus demonstrating the spatially directed binding of biotin azide to ethynyl-PPX. Thus, the alkyne groups on the polymer surface are reactive and can be effectively used as anchoring sites for various biomolecules.

1.3.2 CVD within Confined Microgeometries

Even though miniaturized bioanalytical devices contain dimensions of high aspect ratios, the homogeneous modification of their surfaces can be challenging. In an attempt to expand CVD polymerization to the coating of complex microgeometries with high aspect ratios, a recent study[75] examined the deposition behavior of functionalized poly(*p*-xylylenes) within preassembled microfluidic devices. It was demonstrated that CVD polymerization can be used to deposit a range of functionalized poly(*p*-xylylenes) within confined microgeometries.

Seven different poly(*p*-xylylenes) were deposited via CVD polymerization within both removable and sealed PDMS microchannels.[76] A subgroup of five poly(*p*-xylylenes) had reactive side groups (so-called reactive coatings), while two commercially available poly(*p*-xylylenes) were included as nonfunctionalized references (Parylene[TM] N and C). The PDMS microchannels used in this study were open at both ends and were 75 μm high and 100 μm wide. Both straight (1600 m long) and meandering channel (2800 m long) layouts with high aspect ratios were studied (Figure 1.4). For both straight and
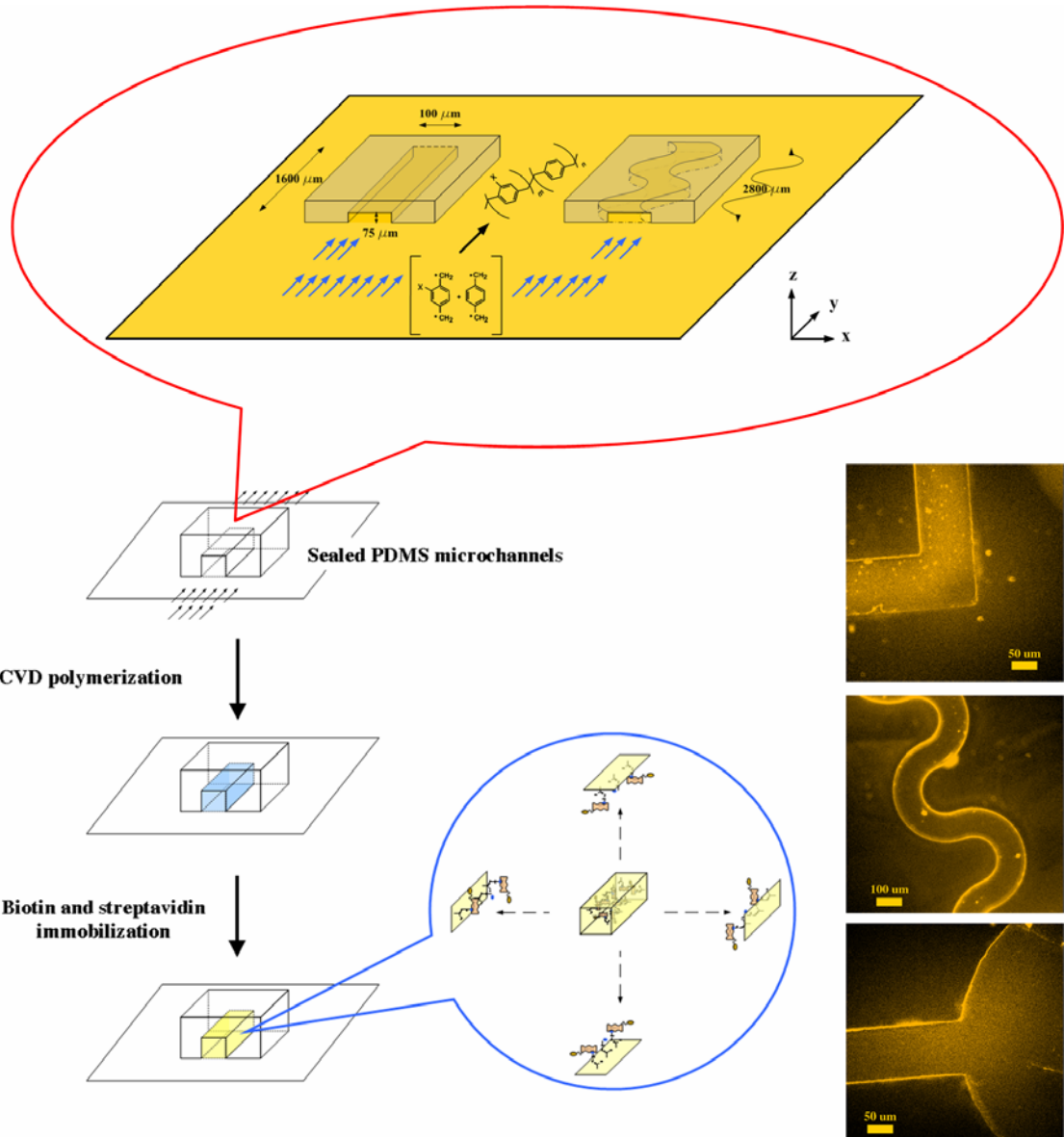
Figure 1.4. Conformal deposition of CVD polymers occurs even within microscale geometries. Facile modification and biofunctionalization of microfluidic channels can be attained. Adapted from [75].

meandering microchannels the degree of deposition was constant and did not change with increasing film thickness. Homogenous surface coverage of different microgeometries has been demonstrated for all reactive coatings. Deposition within aspect ratios of up to 37 was accomplished, based on optical microscopy and imaging XPS results.

In addition to the deposition studies, immobilization studies were conducted using permanently sealed PDMS devices[76] after CVD polymerization. The microchannels

11

were coated with either poly(4-amino-*p*-xylylene-co-*p*-xylylene) (amino-PPX) or poly(4-trifluoroacetyl-*p*-xylylene-co-*p*-xylylene) (PPX-COCF$_3$) prior to immobilization. While amino-PPX provides primary amino groups for coupling with activated carboxyl groups (amide formation), PPX-COCF$_3$ has keto groups that can react with hydrazines or hydrazides. To assess the chemical activity of both reactive coatings, a PFP-derived biotin ligand and a biotin hydrazide ligand were used to evaluate chemical reactivity of amino-PPX and PPX-COCF$_3$, respectively. These ligands undergo nearly quantitative conversion with amines or ketones; also, the interactions between biotin and streptavidin result in tight confinement of streptavidin on the biotin-modified surface. For all ligand immobilization reactions, aqueous solutions of the corresponding biotin derivative were filled into the sealed microchannels of either meandering or straight geometry. After thorough rinsing with buffer, microchannels were incubated with rhodamine-labeled streptavidin, then the surfaces were rinsed and visualized by fluorescence microscopy. Figure 1.4 shows microchannels that were coated with polymer and then subjected to the biotin/strepdavidin protocol. Homogeneous distribution throughout the entire microchannel was observed, indicating that functional groups were available throughout the entire coating area, for both amino-PPX and PPX-COCF$_3$. The deposition of reactive CVD coatings within confined microgeometries bridges a critical technological gap toward surface-modified microfluidic devices for use in "BioMEMS" applications.

1.3.3 Vapor-Assisted Micropatterning in Replica Structures

A related patterning approach utilizes vapor-assisted micropatterning in replica structures (VAMPIR). In this method, chemical and topological surface microstructures

can be obtained by masking certain areas of the substrate during chemical vapor deposition polymerization and then depositing the reactive coatings only within the exposed areas. Although conceptually simple, such an approach towards microstructured surfaces came with some challenges. For instance, in CVD polymerization, polymer deposition is transport-limited, and the feasibility of deposition within replica structures with micron-scale capillaries was unclear. However, the properties of polymers deposited are of a greater variety. While stencils and shadow masks have been applied for area-selective deposition using both rigid and elastomeric materials,[24, 77, 78] many of those pattern processes are limited to hydrophilic polymers that are soluble in polar solvents. However, the solvent-free process described here can be used for both hydrophilic and hydrophobic coatings.

In a recent study,[79] polydimethylsiloxane (PDMS) based replica structures (or stencils) designed to generate a desired surface pattern were reversibly sealed onto a silicon substrate (Figure 1.5). The masked substrate was then placed onto a temperature-controlled stage (15 °C) inside of the CVD polymerization chamber. 4-pentafluoropropionyl[2.2]paracyclophane underwent pyrolysis and polymerized into poly(4-pentafluoropropionyl-*p*-xylylene-co-*p*-xylylene). After completion of the CVD polymerization, the PDMS molds were removed, and hence a chemically and topologically structured surface was created. Surface features are defined by the deposited polymer footprints. In one instance, a substrate was masked with a PDMS membrane, which contained footprints shaped into the letters "UM" (Figure 1.5b). Subsequent CVD polymerization resulted in ultra-thin polymer films outside of the masked areas. Imaging X-ray photoelectron spectroscopy confirmed the presence of
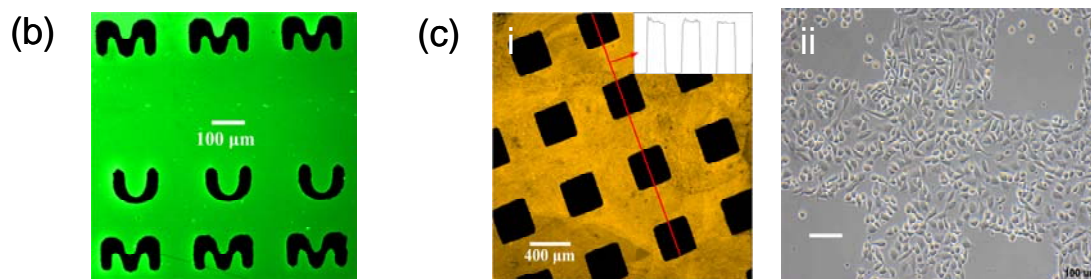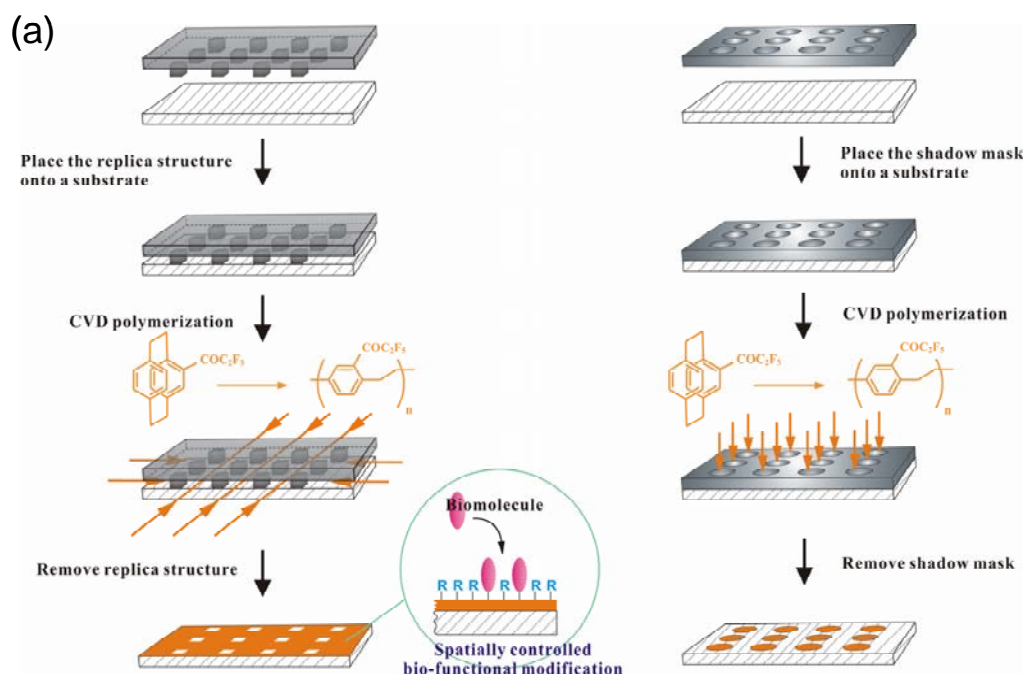
Figure 1.5. (a) Process of vapor-assisted microstructuring using replica structures (left column) as well as shadow masks (right column) during CVD polymerization. Fluorescently-tagged molecules are immobilized onto (b) poly(4-pentafluoropropionyl-*p*-xylylene-co-*p*-xylylene) and (c) poly(*p*-xylylene-4-methyl-2-bromoisobutyrate-*co*-*p*-xylylene). The latter was used to grow poly(OEGMA) within the squares, which inhibited the adsorption of fibrinogen (i) and attachment of NIH 3T3 fibroblasts (ii). Adapted from [79] and [81].

characteristic elements within their localized regions – i.e., fluorine was found only outside the "UM" footprint boundaries, whereas silicon was found within the footprint. PPX-COC_2F_5 has keto groups that can react with hydrazines or hydrazides in high yields.[80] Biotin hydrazide, a model ligand, was used for immobilization onto the functionalized polymer. In a subsequent step, the well-known interactions between biotin

14

and streptavidin are used for visualization of surface-immobilized biotin. To examine the immobilization of biotin ligands within the patterns, streptavidin conjugated with CdSe quantum dots (Qdot® 525) were allowed to bind to the biotin-modified surfaces. Binding was homogenous throughout the surface-modified areas. As anticipated, after biotin immobilization, the subsequently self-assembled quantum dots were resolved into a range of different pre-designed patterns.

In another instance,[81] poly(p-xylylene-4-methyl-2-bromoisobutyrate-*co-p*-xylylene) was patterned in the same manner as described for PPX-COC$_2$F$_5$. A PDMS structure with square holes was used during the deposition process. After patterned deposition of poly(p-xylylene-4-methyl-2-bromoisobutyrate-*co-p*-xylylene) onto PMMA surfaces (Figure 1.5c), the initiator contained within the functionalized coating was used to perform ATRP of poly(OEGMA). Fluorescently-labeled fibrinogen was found to adsorb selectively onto the bare PMMA substrate, whereas the poly(OEGMA)-modified
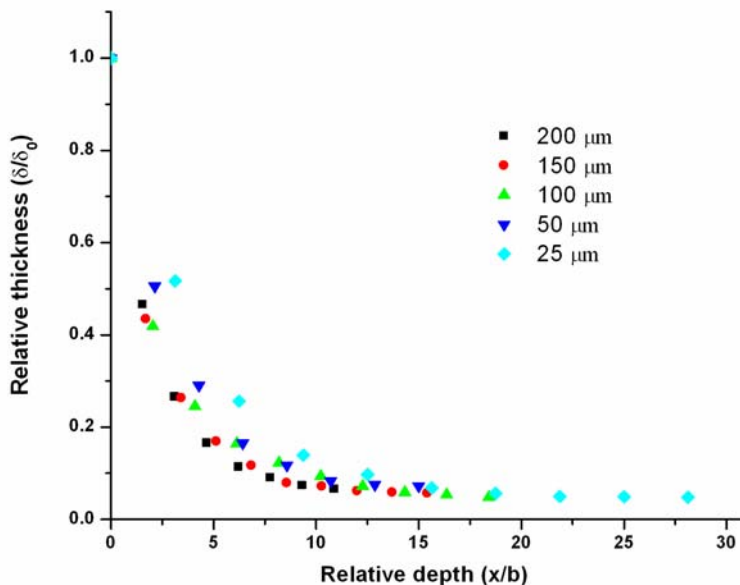
Figure 1.6. Plot of dimensionless thicknesses $\delta(x)/\delta_0$ vs. dimensionless width (x/b), where δ_0 is film thickness (nm) on an open area for an according dimension recorded by using imaging ellipsometry; b is the width (μm) of the dimension. Taken from [79].

15

squares inhibited protein adsorption (Figure 1.5c.i). The attachment and growth of NIH3T3 fibroblasts followed a similar trend (Figure 1.5c.ii).

The lower limit of VAMPIR feature sizes was also evaluated. A PDMS replica structure was prepared with varying distances between posts (150 μm, 100 μm, 50 μm, and 25 μm). Thicknesses of the deposited polymer coatings were measured in the center of each region. The thickness decreased from 49.6 nm measured for the area with 150 μm feature sizes, over 42 nm (100 μm) and 28.7 nm (50 μm), to 7.3 nm measured for the areas with 25 μm wide features. A relative coordinate system is used to express the coating thickness distribution for different feature sizes (Figure 1.6).[82, 83] Rearrangement of the thickness data in terms of dimensionless thicknesses $\delta(x)/\delta_0$ and width (x/b) reveals a surprisingly uniform behavior. $\delta(x)/\delta_0$ denotes the ratio of the absolute film thickness at the given point x to that at the open surface, and x/b is the ratio of depth over width of the feature. As indicated in Figure 1.6, the dimensionless thicknesses measured for feature sizes ranging from 25 μm to 200 μm fall onto a single trend line. Process parameters dominate over feature size, as predicted by Tolstopyatov et al. In his study, universal thickness distributions for the deposition of unfunctionalized poly-*p*-xylylene in microchannels were found.[82, 83] Given the theoretical and experimental findings done on vapor-deposition, vapor-assisted microstructuring in replica structures (VAMPIR) establishes a simple technique to create both chemical and topological surface patterns.

1.3.4 Projection Lithography of Photoreactive CVD Polymers

Another method of post-CVD micropatterning involves the projection of ultraviolet light micropatterns onto a photoreactive PPX coating. Recently, a

photodefinable polymer, poly(4-benzoyl-*p*-xylylene-co-*p*-xylylene) (benzoyl-PPX), was prepared by CVD polymerization and was used for fabrication of discontinuous surface patterns onto 3-dimensional microscale objects.[84, 85] Due to its structural analogy to benzophenone, the reactive coating provides light-reactive carbonyl groups that are readily activated at wavelengths of ~340 nm. The temporarily generated free radicals spontaneously react with adjunct molecules, mainly via C-H abstraction.[86] Suh et. al.[87] have demonstrated the ability of benzoyl-PPX to immobilize hydrogel elements, an important requirement in microfabrication processes. Capillary force lithography was
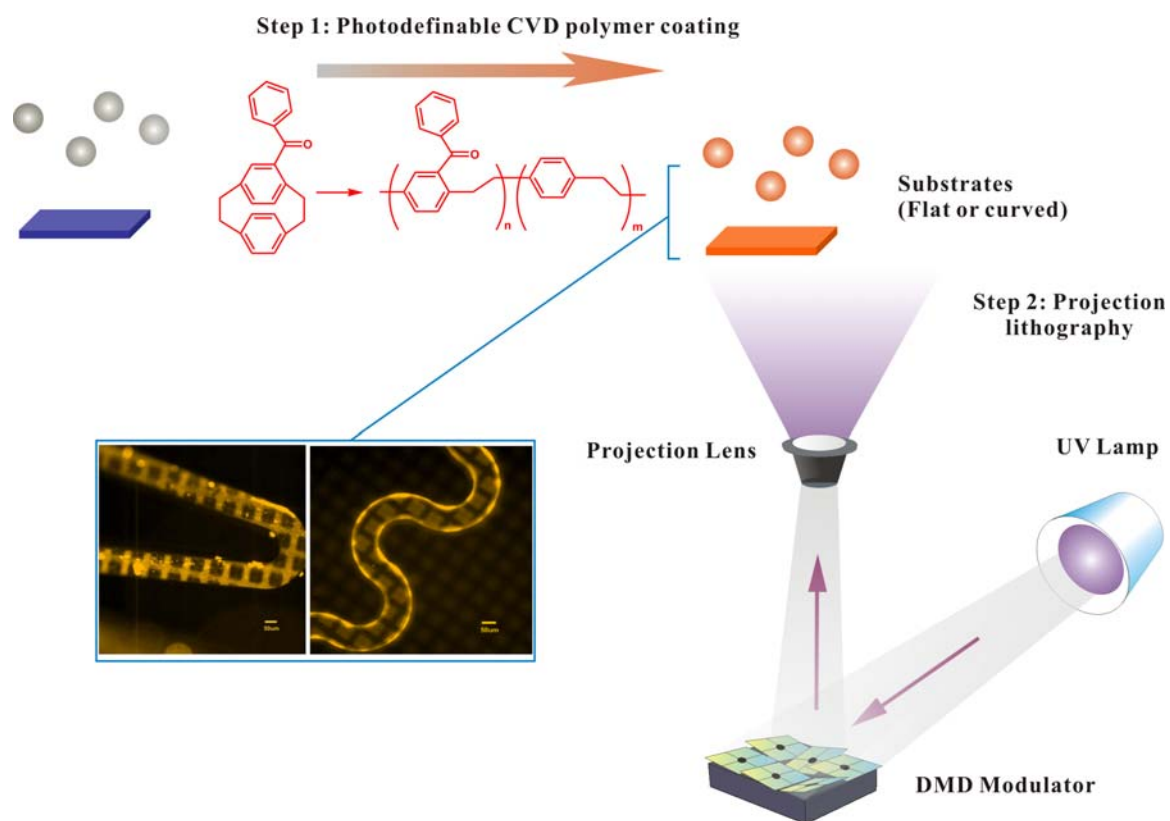
Figure 1.7. Schematic description of the 3D projection lithography technique. The method comprises two process steps: deposition of the photodefinable CVD coating (step 1) and subsequent projection lithographic rendering of the polymer-coated colloids (step 2). Inset shows an endovascular stent and a microfluidic pathway that are patterned using projection lithography. Adapted from [84] and [85].

17

combined with photoreactive patterning in order to fabricate an array of immobilized PEG hydrogels.

As shown in Fig. 1.7, microstructured stents and microchannels were recently fabricated by a two-step procedure: (i) coating of the objects with a photodefinable polymer, poly[4-benzoyl-*p*-xylylene-co-*p*-xylylene], via CVD polymerization[87, 88] and (ii) spatially controlled surface reaction of the photoreactive coatings using a highly parallel projection lithographic patterning step. Once the deposition of the photoreactive coatings on endovascular stents was demonstrated, spatially directed microstructuring became achievable. To obtain spatially controlled surface patches on stents, we selectively illuminated certain areas of previously coated stents with UV radiation at 365-400 nm by using a high-throughput projection technique that has been previously used for *in situ* synthesis of peptides and DNA on microarrays.[89-91]

After surface modification via CVD polymerization, the coated stents (Pulse Systems Inc.) were immersed in an aqueous solution of 4-arm star polyethylene glycol (star-PEO, 10.000 g/mol, 1 weight-%). For patterning, a digital micromirror device (DMD, Texas Instruments) was used as a dynamic mask.[92] UV radiation of about 365-400 nm wavelength was modulated by the dynamic mask. The corresponding patterns were then transferred onto the stents. DI-water was used to separate excess PEO. The stents were incubated with protein (Alexa Fluor 546-conjugated fibrinogen, Molecular Probes Inc.) solutions for 5 min. After incubation of, phosphate buffered saline (PBS) and DI-water were used to rinse off excess adsorbed proteins. After CVD coating, PDMS microchannels were immersed in an aqueous solution of biotin-PEO-LC-amine (10 mM, Pierce) in phosphate buffered saline (PBS, pH 7.4). The corresponding patterns were then

transferred onto the microchannels. After rinsing, samples were incubated with rhodamine (TRITC) conjugated streptavidin (50μg/ml, Pierce) in PBS containing 0.1% (w/v) bovine albumin and Tween 20 (0.02% (v/v)) for 60 min. The surface was rinsed several times with PBS containing 0.1% (w/v) bovine albumin and Tween 20 (0.02% (v/v)). Programmable patterns were created by using a 1,024- × 768-pixel digital micromirror device (DMD) (Fig. 1.7).

While the entire surface of the substrates was coated with the photoreactive coating during CVD polymerization, only the areas illuminated with the DMD underwent photochemical conversion of the carbon–oxygen double bond from the singlet ground state into the corresponding triplet state.[93] As seen in Figure 1.7, an endovascular stent and a microchannel were coated with the photoreactive benzoyl-PPX polymer and subsequently exposed to the DMD grid UV patterning. The PEO-free areas facilitated adsorption of fibrinogen, while the areas of PEO immobilization did not (inside squares). An identical pattern of immobilized streptavidin (inside the squares) was observed within microchannels. Despite the irregular shape and small dimensions of the objects, homogenous chemical micropatterns were obtained on the stent surface, making possible the progression of advanced surface architectures for medical devices.

1.3.5 Selective CVD on Metals

While the methods mentioned thus far rely on physical means to obtain spatially controlled surface modification, an even simpler approach would be to selectively inhibit CVD polymerization and deposition based on differences in the substrate chemistry. Jensen et al. first reported the selective inhibition of parylene™ N, parylene™ C, as well

as poly(*p*-phenylene vinylene) (PPV) by iron and iron salts[94] and used selective CVD

polymerization to create a wide range of patterns.[94] It was also shown that, in a similar

fashion, several transitional metals, metal salts, and organometallic complexes inhibit the

growth of parylene™ N and C.[95] Suh et al. have used selective CVD polymerization

within sub-micron scale polydimethylsiloxane (PDMS) channels to yield high aspect

ratio structures. Surface-coated PDMS channels of as little as 180 nm in width were

obtained by depositing iron on the bottom of microchannels and then selectively

depositing polymer only on the channel sidewalls.[96] Recently, the first selective CVD

polymerization of a functionalized poly-*p*-xylylene was reported.[97] The result is a simple

patterning process that relies on selective inhibition of polymer films that can act as

chemical anchors for further surface modification via covalent immobilization.

The study investigated selective inhibition of CVD polymerization by series of

metals. Based on IRRAS spectra, Ti appeared to be the only metal that effectively

inhibited the growth of poly(4-vinyl-*p*-xylylene-co-*p*-xylylene) (vinyl-PPX) during the

CVD polymerization process. Ti also inhibited CVD polymerization of poly(4-chloro-*p*-

xylylene). Next, a Ti-coated silicon wafer was prepared, and circles of Au were deposited

onto the Ti-coated silicon using a shadow mask. Following the protocol outlined in

Figure 1.8a, this bi-metal surface was CVD coated with vinyl-PPX and subsequently

subjected to olefin cross-metathesis reaction with fluorescein O-methacrylate. Only the

Au islands showed significant fluorescence signals (Figure 1.8b). In addition, a strong

contrast was observed between Au and the Ti surfaces providing further clarification on

the selective inhibition of chemical vapor deposition of vinyl-PPX. Moreover, Ti or Au

samples were coated with vinyl-PPX, and cross-metathesis reaction of poly(ethylene
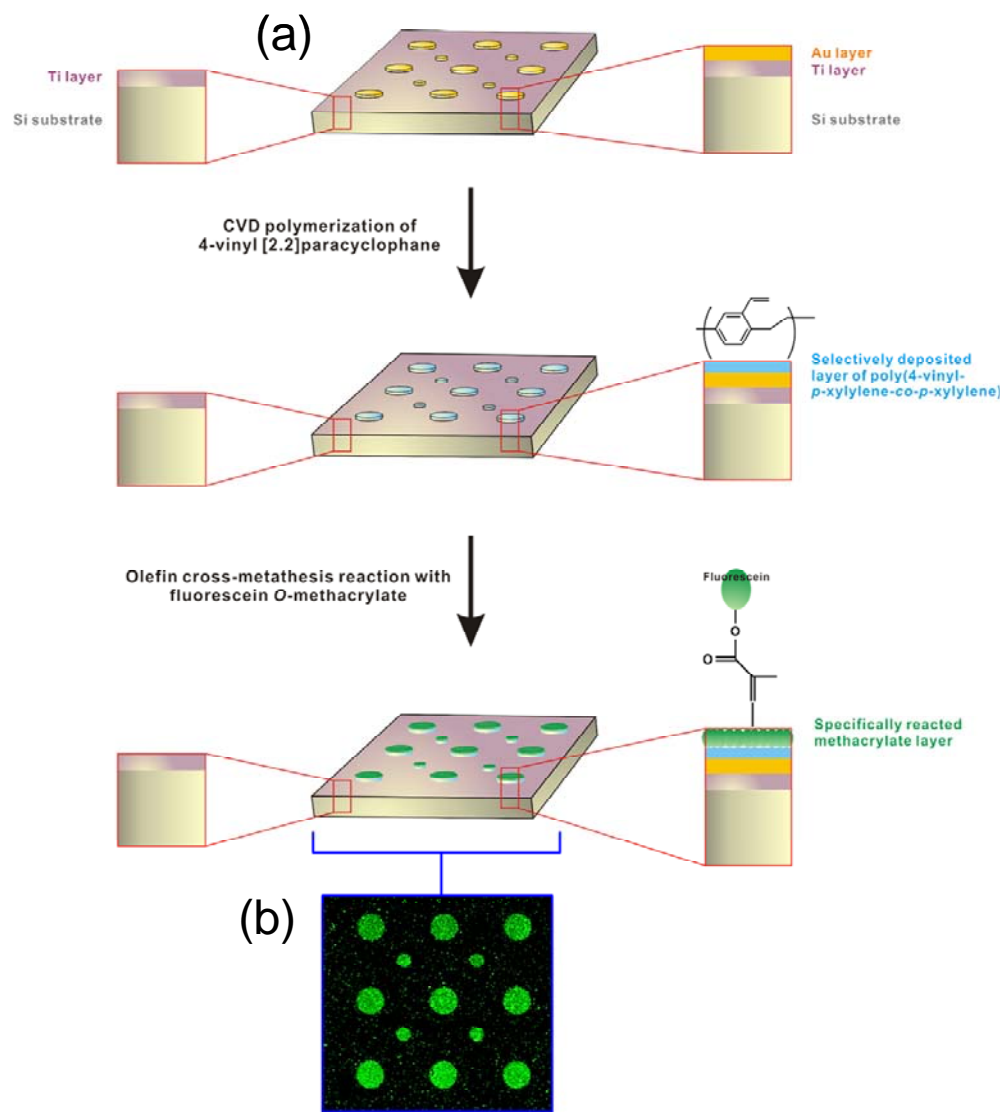
Figure 1.8. (a) Schematic illustration of the selective deposition of poly(4-vinyl-*p*-xylylene-co-*p*-xylylene) on patterned Ti/Au substrates. Au was deposited through a shadow mask onto a Ti-coated silicon wafer followed by polymer deposition *via* CVD polymerization. Olefin cross-metathesis reaction of fluorescein *O*-methacrylate was used to probe the selective deposited polymer on Au surface. (b) Fluorescence micrograph reveals that only the Au islands showed appreciable signals of fluorescence. Taken from [97].

glycol) methyl ether methacrylate (PEGMA) was conducted on both samples. For each modification step, IRRAS spectra were recorded. Absorption bands at 2866, 2924, and 3013 cm^{-1} due to C-H symmetric and asymmetric stretching bands can be clearly detected on the Au surface after deposition of vinyl-PPX. In addition, a strong, sharp band at 1717

cm^{-1} indicative of the C=O bond of the ester group, and a strong band at 1110 cm^{-1}, which is due to C–O–C stretches of the ester group appeared after olefin cross-metathesis reaction of OEGMA. At each modification step, no significant signal was detected on the Ti surface, providing strong evidence that vinyl-PPX was not deposited on Ti, which consequently prevented cross-metathesis reaction of OEGMA. The fact that the selectively deposited reactive coatings are equipped with functional groups for further surface modification provides a simple access route towards micro- and nanostructured surfaces.

1.4 Hypothesis and Specific Aims

Based upon the literature survey, reactive polymer coatings have primarily focused on controlling only one type of reaction pathway or surface property at a time. However, biological pathways are directly affected by more than one variable. By controlling multiple surface properties simultaneously, our goal is to improve the manipulation of biological environments via CVD coatings. This dissertation aims to develop reactive CVD coatings that are multifunctional in various aspects. 1) reactive homopolymer coatings, which can vary in both reactivity and hydrophobicity; 2) copolymer coatings, which are reactive towards multiple reaction pathways; 3) reactive CVD coatings, which exhibit preliminary biocompatibility and maintain their reactivities; 4) CVD coatings, which possess reactive surface composition gradients. Most of the chapters presented herein are either published or in press in various journals (*Advanced Materials, Chemical Vapor Deposition, Macromolecular Rapid Communications*).[64, 98, 99]

1.5 Overview

The current use of CVD polymerization towards surface engineering has been discussed. Specifically, this chapter outlined the adaptability of the CVD process towards microfabrication of polymer thin films. Two general fabrication methods were discussed. First, one may fabricate a biomolecular micropattern after the reactive poly(p-xylylene) has been coated. Microcontact printing and projection lithography are two approaches used for post-CVD surface modification. In microcontact printing, a patterned PDMS stamp is inked with the molecule of interest, then subsequently laid upon the CVD film. Projection lithography employs micromirrors in order to project UV light onto a photoreactive CVD polymer coating. Secondly, one may pattern a CVD polymer onto the substrate directly during the deposition process. Patterned replica structures mounted onto a substrate will mask deposition over specified areas. In addition, certain polymers have been known to deposit selectively on different metals. Thus, a patterned metal substrate would lead to patterned polymer deposition.

References

[1] A. Berg, W. Olthius, P. Bergveld, "Micro Total Analysis Systems" 2000, 1st edition, Kluwer, Dordrecht, The Netherlands 2000.

[2] P. Li, D. J. Harrison, Transport, *Anal. Chem.* **1997**, 69, 1564.

[3] H. Mao, T. Yang, P. S. Cremer, *Anal. Chem.* **2002**, 74, 379.

[4] S. H. Chen, W. C. Sung, G. B. Lee, Z. Y. Lin, P. W. Chen, P. C. Liao, *Electrophoresis* **2001**, 22, 3972.

[5] C. S. Effenhauser, J. M. Bruin, A. Paulus, M. Ehrat, *Anal. Chem.* **1997**, 69, 3451.

[6] J. Monahan, A. A. Gewirth, R. G. Nuzzo, *Electrophoresis* **2002**, 23, 2347.

[7] J.C. Love, L.A. Estroff, J.K. Kriebel, R.G. Nuzzo, G.M. Whitesides, *Chem. Rev.* **2005,** *105,* 4, 1103.

[8] D. Falconnet, G. Csucs, H.M. Grandin, M. Textor, *Biomaterials* **2006,** *27,* 16, 3044.

[9] D. S. Ginger, H. Zhang, C. A. Mirkin, *Angew. Chem. Int. Ed.* **2004**, *43*, 30.

[10] S. Kramer, R. R. Fuierer, C. B. Gorman, *Chem. Rev.* **2003**, *103*, 4367.

[11] S. Y. Chou, P. R. Krauss, P. J. Renstrom, *App. Phys. Lett.* **1995**, *67*, 3114.

[12] S. Y. Chou, P. R. Krauss, P. J. Renstrom, *Science* **1996**, *272*, 85.

[13] Y. N. Xia, G. M. Whitesides, *Ann. Rev. Mater. Sci.* **1998**, *28*, 153.

[14] A. Kumar, G. M. Whitesides, *App. Phys. Lett.* **1993**, *63*, 2002.

[15] J. L. Wilbur, A. Kumar, E. Kim, G. M. Whitesides, *Adv. Mater.* **1994**, *6*, 600.

[16] Y. N. Xia, E. Kim, X. M. Zhao, J. A. Rogers, M. Prentiss, G. M. Whitesides, *Science* **1996**, *273*, 347.

[17] X. M. Zhao, Y. N. Xia, G. M. Whitesides, *Adv. Mater.* **1996**, *8*, 837.

[18] E. Kim, Y. N. Xia, G. M. Whitesides, *Nature* **1995**, *376*, 581.

[19] E. Kim, Y. N. Xia, X. M. Zhao, G. M. Whitesides, *Adv. Mater.* **1997**, *9*, 651.

[20] K. Y. Suh, Y. S. Kim, H. H. Lee, *Adv. Mater.* **2001**, *13*, 1386.

[21] W. T. Tsang, A. Y. Cho, *App. Phys. Lett.* **1978**, *32*, 491.

[22] T. Schallenberg, T. Borzenko, G. Schmidt, M. Obert, G. Bacher, C. Schumacher, G. Karczewski, L. W. Molenkamp, S. Rodt, R. Heitz, D. Bimberg, *App. Phys. Lett.* **2003**, *82*, 4349.

[23] S. De Vusser, S. Steudel, K. Myny, J. Genoe, P. Heremans, *App. Phys. Lett.* **2006**, *88*, 103501.

[24] D. C. Duffy, R. J. Jackman, K. M. Vaeth, K. F. Jensen, G. M. Whitesides, *Adv. Mater*. **1999**, *11*, 546.

[25] N. Takano, L. M. Doeswijk, M. A. F. van den Boogaart, J. Auerswald, H. F. Knapp, O. Dubochet, T. Hessler, J. Brugger, *Journal of Micromechanics and Microengineering* **2006**, *16*, 1606.

[26] B. R. Ringeisen, J. Callahan, P. K. Wu, A. Pique, B. Spargo, R. A. McGill, M. Bucaro, H. Kim, D. M. Bubb, D. B. Chrisey, *Langmuir* **2001**, *17*, 3472.

[27] E. Ostuni, R. Kane, C. S. Chen, D. E. Ingber, G. M. Whitesides, *Langmuir* **2000**, *16*, 7811.

[28] R. Pal, K. E. Sung, M. A. Burns, *Langmuir* **2006**, *22*, 5392.

[29] D. G. Castner, B. D. Ratner, *Surf. Sci.* **2002**, *500*, 28.

[30] P. Rai-Choudhury, "Handbook of Microlithography, Micromachining, and Microfabrication. Volume 1: Microlithography", SPIE-The International Society for Optical Engineering, **1997**.

[31] F. Cerrina, *Journal of Physics D: Applied Physics* **2000**, *33*, R103.

[32] N. Yao, Z. L. Wang, *Handbook of Microscopy for Nanotechnology*, Springer, **2005**.

[33] A. A. Tseng, *Small* **2005**, *1*, 594.

[34] D. Meschede, H. Metcalf, *Journal of Physics D: Applied Physics* **2003**, *36*, R17.

[35] E. Delamarche, A. Bernard, H. Schmid, A. Bietsch, B. Michel, H. Biebuyck, *J. Am. Chem. Soc*. **1998**, 120, 500-508.

[36] S. Takayama, J.C. McDonald, E. Ostuni, M.N. Liang, P.J.A. Kenis, R.F. Ismagilov, G.M. Whitesides, *Proc. Natl. Acad. Sci. U.S.A*. **1999**, 96, 5545-5548.

[37] B. Regenberg, U. Kruehne, M. Beyer, L.H. Pedersen, M. Simon, O.R.T. Thomas, J. Nielsen, T. Ahl, *Lab Chip* **2004**, 4, 654-657.

[38] S. Takayama, E. Ostuni, P. LeDuc., K. Naruse, D.E. Ingber., G.M. Whitesides, *Nature* **2001**, 411, 1016.

[39] M. Schena, D. Shalon, R.W. Davis, P.O. Brown, *Science* **1995**, 270, 467-470.

[40] R.A. Heller, M. Schena, A. Chai, D. Shalon, T. Bedilion, J. Gilmore, D.E. Woolley, R.W. Davis, *Proc. Natl. Acad. Sci. U.S.A*. **1997**, 94, 2150-2155.

[41] D. Shalon, S.J. Smith, P.O. Brown, *Genome Res*. **1996**, 6, 639-645.

[42] M.F. Lopez, M.G. Pluskal, *J. Chromatogr., B* **2003**, 787, 19-27.

[43] A. Roda, M. Guardigli, C. Russo, P. Pasini, M. Baraldini, *Biotechniques* **2000**, 28, 492-496.

[44] A. Khademhosseini, K.Y. Suh, S. Jon, G. Eng, J. Yeh, G.J. Chen, R. Langer, *Anal. Chem.* **2004**, 76, 3675-3681.

[45] W. Zhan, G.H. Seong, R.M. Crooks, *Anal. Chem.* **2002**, 74, 4647-4652.

[46] D.J. Beebe, J.S. Moore, J.M. Bauer, Q. Yu, R.H. Liu, C. Devadoss, B.H. Jo, *Nature* **2000**, 404, 588-590.

[47] J. Heo, K.J. Thomas, G.H. Seong, R.M. Crooks, *Anal. Chem.* **2003**, 75, 22-26.

[48] M. Mrksich, L.E. Dike, J. Tien, D.E. Ingber, G.M. Whitesides, *Exp. Cell Res.* **1997**, 235, 305-313.

[49] S.W. Rhee, A.M. Taylor, C.H. Tu, D.H. Cribbs, C.W. Cotman, N.L. Jeon, *Lab Chip* **2005**, 5, 102-107.

[50] S.D. Senturia. "Microsystem Design", Kluwer Academic Publishers, **2000**.

[51] Y.C. Chang, C.W. Frank, *Langmuir* **1998**, 14, 326.

[52] N.H. Lee, C.W. Frank, *Langmuir* **2003**, 19, 1295.

[53] Y. Mao, K.K. Gleason, *Langmuir* **2004**, 20, 2484;

[54] T.P. Martin, K.K. Gleason, *Chem. Vap. Dep.* **2006**, 12, 685.

[55] W.F. Gorham, *J. Polym. Sci., Part A-1* **1966**, 4, 3027.

[56] J.B. Fortin, T.M. Lu, *Chem. Mater.* **2002**, 14, 1945-1949.

[57] [a] C.E. Morosanu, "Thin Films by Chemical Vapor Deposition", Elsevier, New York 1990 [b] M.L. Hitchman, K.F. Jensen, "Chemical Vapor Deposition", Academic Press, New York, 1993.

[58] W. F. Beach, *Macromolecules* **1978**, 11, 72.

[59] A. Zangwill, "The Physics at Surfaces" Cambridge University Press: Cambridge, 1988.

[60] J. Lahann, D. Klee, H. Hocker, *Macromol. Rapid Commun.* **1998**, 19, 441.

[61] J. Lahann, M. Balcells, T. Rodon, J. Lee, I.S. Choi, K.F. Jensen, R. Langer, *Langmuir* **2002**, 18, 3632.

[62] J. Lahann, R. Langer, *Macromolecules* **2002**, 35, 4380.

[63] J. Lahann, *Polym. Inter.* **2006**, 55, 1361.

[64] Y. Elkasabi, M. Yoshida, H. Nandivada, H.Y. Chen, J. Lahann, *Macromol. Rapid Comm*. **2008**, 29, 855-870.

[65] M. Morgen, S.H. Rhee, J.H. Zhao, I. Malik, T. Ryan, H.M. Ho, M.A. Plano, P. Ho, *Macromolecules* **1999**, 32, 7555.

[66] J.J. Senkevich, S.B. Desu, V. Simkovic, *Polymer* **2000**, 41, 2379.

[67] S.Y. Park, S.N. Chvalun, A.A. Nikolaev, K.A. Mailyan, A.V. Pebalk, I.E. Kardash, *Polymer* **2000**, 41, 2937.

[68] D. Klee, N. Weiss, J. Lahann, "Vapor-Based Polymerization of Functionalized [2.2]Paracyclophanes: A Unique Approach towards Surface-Engineered Microenvironments" Chapter 18, Modern Cyclophane Chemistry, Wiley-VCH, Weinheim 2004, p463.

[69] H. Nandivada, H.Y. Chen, J. Lahann, *Macromol. Rapid Comm*. **2005,** 26, 1794.

[70] G. T. Hermanson, "Bioconjugate Techniques", 1st edition, Academic, San Diego, CA 1996.

[71] D. N. Moothoo, J. H. Naismith, *Acta Crystallogr., Sect. D: Biol. Crystallogr.* **1999**, **D55**(1), 353.

[72] S. Thenevet, H.Y. Chen, J. Lahann, F. Stellacci, *Adv. Mater.* **2007**, 19, 4333.

[73] H. Nandivada, H.Y. Chen, L. Bondarenko, J. Lahann, *Angew. Chem. Int. Ed*. **2006**, 45, 3360.

[74] V. V. Rostovtsev, L. G. Green, V. V. Fokin, K. B. Sharpless, *Angew. Chem.* **2002**, 114, 2708-2711; *Angew. Chem. Int. Ed.* **2002**, 41, 2596-2599.

[75] H.Y. Chen, Y. Elkasabi, J. Lahann, *J. Amer. Chem. Soc*. **2006**, 128, 374.

[76] J.C. McDonald, G.M. Whitesides, *Acc. Chem. Res.* **2002**, *35*, 491-499.

[77] H. W. Gu, R. K. Zheng, X. X. Zhang, B. Xu, *Adv. Mater*. **2004**, *16*, 1356.

[78] M. Graff, S. K. Mohanty, E. Moss, A. B. Frazier, *Journal of Microelectromechanical Systems* **2004**, *13*, 956.

[79] H.Y. Chen, J. Lahann, *Adv. Mater.* **2007**, 19, 3801.

[80] G. T. Hermanson, *Bioconjugate Techniques*, Academic Press, **1996**.

[81] X. Jiang, H.Y. Chen, G. Galvan, M. Yoshida, J. Lahann, *Adv. Func. Mater*. **2008**, 18, 27.

[82] E. M. Tolstopyatov, *Journal of Physics D-Applied Physics* **2002**, *35*, 1516.

[83] E. M. Tolstopyatov, S. H. Yang, M. C. Kim, *Journal of Physics D-Applied Physics* **2002**, *35*, 2723.

[84] H.Y. Chen, J.M. Rouillard, E. Gulari, J. Lahann, *Proc. Nat. Acad. Sci*. **2007**, 104, 11173.

[85] H.Y. Chen, J.M. Rouillard, E. Gulari, J. Lahann, *PMSE Preprints* **2006**, 95, 125.

[86] W. W. Shen, S.G. Boxer, W. Knoll, C.W. Frank, *Biomacromol.* **2001**, *2*, 70-79.

[87] K.Y. Suh, R. Langer, J. Lahann, *Adv. Mater.* **2004**, 16, 1401.

[88] H.Y. Chen, J. Lahann, *Anal. Chem.* **2005**, 77, 6909.

[89] J. Tian, H Gong, N. Sheng, X. Zhou, E. Gulari, X. Gao, G. Church, *Nature* **2004**, 432, 1050.

[90] J.P. Pellois, X. Zhou, O. Srivannavit, T. Zhou, E. Gulari, X. Gao, *Nat. Biotech*. **2002**, 20, 922.

[91] X.L. Gao, X.C. Zhou, E. Gulari, *Proteomics* **2003**, 3, 2135.

[92] X. Gao, E. LeProust, H. Zhang, O. Srivannavit, E. Gulari, P. Yu, C. Nishiguchi, Q. Xiang, X. Zhou, *Nucleic Acids Research* **2001**, 29, 4744-4750.

[93] K.S. Taton, P.E. Guire, *Colloids Surf B* **2002**, 24, 123–132.

[94] K. M. Vaeth, K. F. Jensen, *Adv. Mater.* **1999**, *11*, 814.

[95] K. M. Vaeth, K. F. Jensen, *Chem. Mater.* **2000**, *12*, 1305.

[96] K. Y. Suh, R. Langer, J. Lahann, *App. Phys. Lett.* **2003**, *83*, 4250.

[97] H.Y. Chen, J.H. Lai, X. Jiang, J. Lahann, *Adv. Mater.* **2008**, 20, 3474.

[98] Y. Elkasabi, H.Y. Chen, J. Lahann, *Adv. Mater.* **2006**, 18, 1521.

[99] Y. Elkasabi, J. Lahann, *Macromol. Rapid Comm.* **2009**, 30, 57.

CHAPTER 2

MULTIFUNCTIONAL HOMOPOLYMER COATINGS

The materials in this chapter have been adapted with minor modifications from the following article: Y. Elkasabi, H. Nandivada, H.Y. Chen, S. Bhaskar, J. D'Arcy, L. Bondarenko, J. Lahann, "Partially Fluorinated Poly-*p*-xylylenes Synthesized by Chemical Vapor Deposition Polymerization", *Chemical Vapor Deposition* **2009**, in press.

2.1 Background and Motivations

Surface wettability is an important attribute of a coating, which determines the suitability of surfaces for a range of different applications. In this respect, fluorinated polymer coatings with low surface energy are particularly attractive due to their water-repellence, inertness, and low coefficient of friction.[1, 2] Fluorinated polymer films synthesized using CVD polymerization such as poly(octafluoro-*p*-xylylene) (also known as parylene-AF4) and poly(tetrafluoro-*p*-xylylene) (VT-4) have exhibited excellent optical properties, low dielectric constants and high thermal stability.[3, 4] Despite these interesting properties, these coatings typically lack reactive functional groups for further surface modification.

Several functionalized poly-*p*-xylyenes have been synthesized via CVD polymerization of substituted [2.2]paracyclophanes, creating a wide range of different reactive polymer coatings.[5, 6, 7] In order to incorporate the potential advantages of fluorinated polymers with the concept of reactive polymer coatings, fluorinated and reactive moieties can be

simultaneously introduced into [2.2]paracyclophanes, which are subsequently deposited via CVD polymerization. This can be achieved either through modification of the aliphatic bridges or by substitution at the aromatic rings.

Taking the aliphatic route, we intended to synthesize a fluorinated polymer coating, poly(4,12-dibromo-1,1,9,9-tetrafluoro-*p*-xylylene) (**2**) via CVD polymerization of precursor 4,12-dibromo-1,1,9,9-tetrafluoro[2.2]paracyclophane (**1**), which is partially fluorinated at the aliphatic bridge (Scheme 2.1). This polymer contains bromine at the aromatic ring, which may be further converted into reactive groups providing easy access for subsequent surface modification reactions. In fact, CVD polymerized brominated-PPX coatings are known to undergo dehydrohalogenation resulting in vinyl and ethynyl
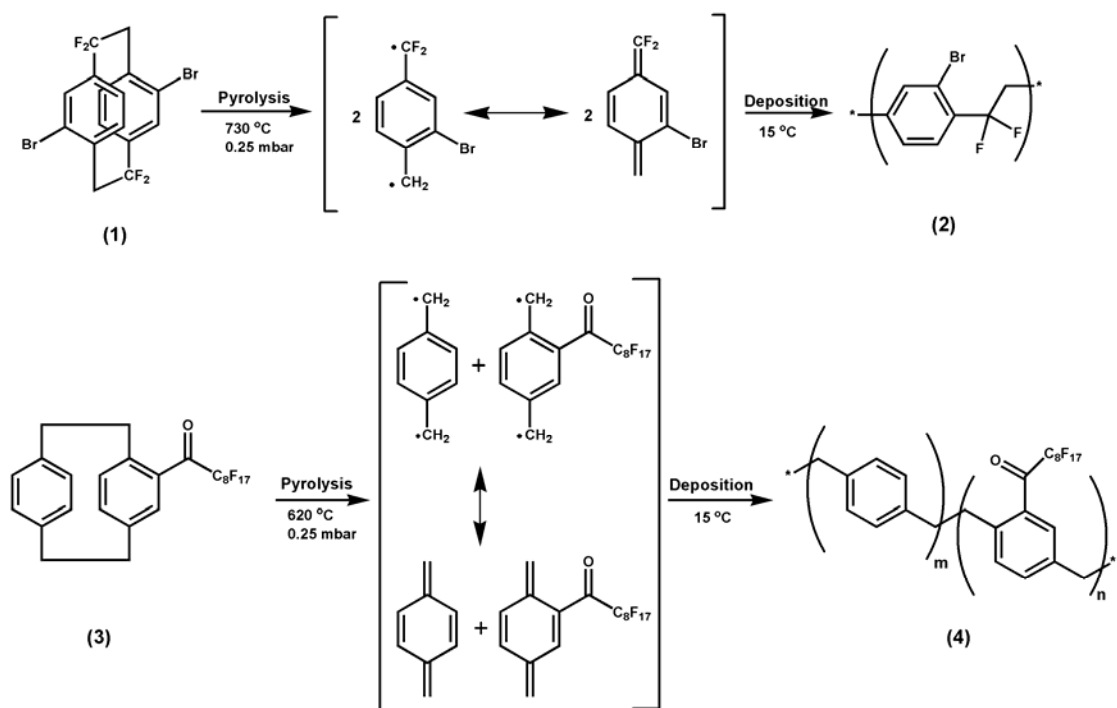
Scheme 2.1: Mechanism of CVD polymerization of partially fluorinated [2.2]paracyclophanes to yield the corresponding poly-*p*-xylylenes. Polymer **2** is fluorinated at the aliphatic bridge, whereas polymer **4** contains a fluorinated reactive group at the aromatic ring.

moieties.[8] However, post-polymerization modification of the brominated aromatic ring may require harsh chemical conditions. Hence, we alternatively explored incorporation of functional groups into the aromatic segments that may combine reactivity with high hydrophobicity. In the past, several poly-*p*-xylylenes have been synthesized with shorter fluorinated side chains resulting in relatively hydrophobic coatings.[5, 9-12] To further investigate this effect, we have now synthesized and CVD-polymerized a [2.2]paracyclophane with a long perfluorinated side chain. Specifically, 4-heptadecafluorononanoyl[2.2]paracyclophane (**3**) was synthesized and used to prepare ultrahydrophobic coatings of poly(4-heptadecafluorononanoyl-*p*-xylylene-co-*p*-xylylene) (**4**) which contained a carbonyl-functionalized derivative with an 8-carbon perfluorinated side chain (Scheme 2.1). Given the usefulness of non-functionalized as well as the perfluorinated PPX for coating applications,[3, 4, 13, 14] widening the scope of CVD polymerization by applying this technique to reactive, yet partially fluorinated paracyclophanes may significantly advance the field of low-surface energy coatings. Not only do new polymer coatings, such as polymer **4,** possess robust chemical properties, but their reactivity also allows for subsequent surface modifications.

2.2 Experimental Methods

Precursor synthesis Compound 4,12-dibromo-1,1,9,9-tetrafluoro[2.2]paracyclophane (**1**) was synthesized according to a previously-established synthesis chemistry.[15] Precursor, 4-heptadecafluorononanoyl[2.2]paracyclophane (**3**) was synthesized by Friedel-Crafts acylation of [2.2]paracyclophane with the corresponding acid chloride (heptadecafluorononanoyl chloride 98%, Apollo Scientific Ltd., Cheshire, UK).

Aluminum chloride (0.96 g) was dissolved in 30 mL of dichloromethane under inert conditions. The suspension was cooled down to -40 ^{o}C with constant stirring. The acid chloride (2.5 g, 5.2 mmol) was slowly added into this mixture using a syringe. Dichloromethane (10 mL) was further added to the suspension. After 20 min, [2.2]paracyclophane (1 g, 4.8 mmol) was slowly added to the suspension. The reaction continued with vigorous stirring at -40 ^{o}C for 45 min, and then the mixture was allowed to reach 0 ^{o}C over a period of 1 h. The reaction was quenched with aqueous HCl, and ethyl acetate was added to the organic phase to increase solubility of the heavy products. The organic layer was separated and subsequently washed with 10 mL each of DI H_2O, 0.5M Na_2CO_3, and 0.5M NaOH. After purification with column chromatography (1:40 ethyl acetate:hexane), the product was diluted with hexane. Hexane was then removed in volumetric increments using a rotovap. After each increment, the unreacted [2.2]paracyclophane was allowed to precipitate, with the final product still in solution. In the final increment, pure **3** (1.1 g) crystallized at the bottom of the flask.

CVD polymerization of precursors Starting materials **1** and **3** were sublimed at 80-90 ^{o}C under vacuum and pyrolyzed into the corresponding quinodimethanes, which spontaneously polymerized upon condensation onto the substrate surface (at 10-15 ^{o}C). A constant argon flow of 20 sccm was used as the carrier. Starting material **1** pyrolyzed at 720 °C, and compound **3** pyrolyzed at 620 ^{o}C. Subsequently, polymerization occurred on a rotating, cooled sample holder placed inside a stainless steel chamber with a wall temperature of 120 °C. The pressure was set at 0.3 mbar or lower.

Characterization ^{1}H, ^{13}C and ^{19}F NMR spectra were recorded using a Varian Inova 400, ^{1}H NMR (400 MHz), ^{13}C NMR (100.6 MHz), ^{19}F NMR (376 MHz) spectrometer. Chemical shifts (δ) are expressed in ppm downfield from tetramethylsilane using the residual non-deuterated solvent as internal standard (CDCl$_3$: ^{1}H: δ = 7.22; ^{13}C: δ = 77.00). Infrared spectroscopy was performed on a Nicolet 6700 spectrometer utilizing the grazing angle accessory (Smart SAGA) at a grazing angle of 85°. Mass spectra were recorded using a VG (Waters) 70-250-S Magnetic sector mass spectrometer (EI, 70 eV) on a DCI desorption probe. The instrument was scanned from m/z 1000 to m/z 35 and was calibrated with perfluorokerosene-H. X-ray photoelectron spectroscopy (XPS) data were recorded on an Axis Ultra X-ray photoelectron spectrometer (Kratos Analyticals, UK) equipped with a monochromatized Al K$_\alpha$ X-ray source. In these experiments, pass energy was set to 160.0 eV with an X-ray power of 150 kW, and the aperture was 600 μm x 600 μm. Thickness measurements were recorded at a wavelength of 532 nm using an EP^3-SW ellipsometry (Nanofilm Technologie GmbH, Germany). Nulling experiments were performed at an angle of incidence of 60°, and an anisotropic Cauchy model was used to model the ellipsometric parameters psi and delta. Surface morphology was examined by scanning electron microscopy (Philips XL30 ESEM, high vacuum mode).

Polymer **2**: XPS (atomic ratios): Br$_{3p}$/C$_{1s}$: 11.3% (calc: 12.5%), C-Br/C-C: 13.9% (calc: 16.7%), F$_{1s}$/C$_{1s}$: 17.7% (calc: 25.0%), C-F/C-C: 14.0% (calc: 16.7%); FTIR (grazing angle 85°): ν (cm^{-1}) = 842, 886, 1056, 1089, 1132, 1157, 1245, 1326, 1392, 1430, 1493, 1563, 1609, 1811, 2848, 2939, 3037, 3072.

Precursor **3**: ^{1}H NMR (400 MHz, CDCl$_3$): δ = 2.9-3.3 (7H, CH2), 3.6 (1H, CH$_2$), 6.3 (1H, CH), 6.5 (4H, CH), 6.75 (1H, CH), 7.0 (1H, CH). ^{13}C NMR (100 MHz, CDCl$_3$): δ = 34.90, 34.92, 34.99, 35.85, 107.50, 110.22, 110.52, 110.69, 111.18, 112.93, 115.66, 118.52, 130.87, 131.04, 132.45, 132.70, 132.85, 133.43, 136.61, 138.54, 139.37, 139.79, 139.93, 144.38, 184.84. ^{19}F NMR (376 MHz, CDCl$_3$): δ = -80.8, -110.9, -111.9, -112.5, -113.6, -120.6, -120.9, -121.8, -122.7, -126.1. EI (70 eV): *m/z* (%) = 654.2 (43.8) [M+], 550.1 (7.4) [C$_8$H$_7$COC$_8$F$_{17}$+], 235 (4.7) [C$_{16}$H$_{15}$CO+], 131.1 (14.8) [C$_8$H$_7$CO+], 104.1 (100) [C$_8$H$_8$+]. FTIR (grazing angle 85°): ν (cm^{-1}) = 2931, 2852, 1707, 1591, 1549, 1500, 1371, 1329, 1248, 1198, 1146, 1116, 1070, 997, 960, 935, 843.

Polymer **4**: XPS (atomic ratios): F$_{1s}$/C$_{1s}$: 86.4 (calc. 85.6%), O$_{1s}$/C$_{1s}$: 5.9% (calc. 5.0%). FTIR (grazing angle 85°): ν (cm^{-1}) = 2934, 1714, 1568, 1498, 1458, 1416, 1370, 1330, 1251, 1222, 1154, 1061, 1005, 943, 880, 811.

Contact angle measurements A microsyringe was used to place a 5 µl droplet on the substrate, and picture of the droplet was captured using a digital camera (Canon EOS 20D) after 5 s. An image processing software (Image J) was used to analyze the droplet images and calculate the contact angle.

Immobilization of biotinamidocaproyl hydrazide PDMS stamps were fabricated as described in literature. The PDMS stamp consisted of square-shaped indentations (400 µm on a side) with 50 µm gaps between the square edges. The PDMS stamp was treated with UV-ozone for 25 min (UV-Ozone Cleaner; Model no. 342, Jelight company Inc.),

then inked with a 10 mM solution of biotinamidocaproyl hydrazide (Pierce Biotechnology, IL) in ethanol at a pH of 5-6. The inked surface was then stamped onto a surface coated with polymer **4**. The stamp was kept in contact with the substrate for 1 min and then the patterned substrate was incubated with rhodamine-labeled streptavidin (50 µg/ml, Pierce Biotechnology, IL) or streptavidin labeled with Alexa Fluor 633 (50 µg/ml, Invitrogen, CA) in an aqueous phosphate buffer solution (pH 7.4, Sigma, MO) consisting of bovine serum albumin (0.1% w/v, Sigma, MO) and Tween 20 (0.02% v/v, Sigma, MO) for 1 h. The substrate was washed three times with the incubating buffer and rinsed with DI-water. The micropatterns on the substrate were visualized using a Nikon TE200 fluorescence microscope and confocal laser scanning microscope (CLSM) (Olympus FluoView 500, USA).

2.3 Results and Discussion

2.3.1 Precursor Synthesis and Characterization

4,12-Dibromo-1,1,9,9-tetrafluoro[2.2]paracyclophane, **1**, was synthesized and characterized as previously described.[15] In principle, presence of bromine may allow subsequent modifications of the polymer, albeit harsh conditions may have to be employed. On the other hand, 4-heptadecafluorononanoyl[2.2]paracyclophane, **3**, was synthesized as described previously for similar compounds[10, 16] using Friedel-Crafts acylation of the commercially available [2.2]paracyclophane with heptadecafluorononanoyl chloride in the presence of $AlCl_3$. To control the reaction, the synthesis was carried out at low temperatures (-40 to -30 ^oC) in dichloromethane. Even slightly elevated temperatures close to 0 ^oC caused an uncontrollable reaction and

resulted in loss of the paracyclophane and in-solution polymerization, which resulted in insoluble byproducts.

The chemical structure of compound **3** was analyzed using nuclear magnetic resonance (NMR) spectroscopy and mass spectrometry (MS). Both ^{1}H-NMR and ^{13}C-NMR confirmed the expected structure of paracyclophane **3**. Mass spectrometry conducted during CVD polymerization further confirmed the structure of compound **3** revealing a mass peak at 654 Da (M+) and characteristic peaks at 550 Da and 104 Da corresponding to the two quinodimethanes ($C_8H_7COC_8F_{17}+$, C_8H_8+), respectively.

2.3.2 CVD Polymerization and Characterization

Once the synthesis of functionalized fluorinated [2.2]parcyclophanes was achieved, we addressed the question of whether they would lend themselves to CVD polymerization without loss of the functional groups. For CVD polymerization, precursor **1** was sublimated under a reduced pressure of 0.2 mbar and a temperature of 80 °C. The argon carrier gas transported the vaporized **1** into the pyrolysis zone, which was heated to 720 °C to ensure cleavage of the C-C bonds of the bridge, resulting in the corresponding quinodimethanes (monomers). Finally, these monomers were adsorbed on the substrate, which was maintained at 10-15 °C, where they spontaneously polymerized. This process resulted in transparent and topologically uniform films of polymer **2** with thicknesses between 20 and 50 nm, as determined by ellipsometry. These polymer films were amorphous, as confirmed by X-ray diffraction (XRD) studies. Moreover, polymer **2** was deposited on a wide range of materials, including polymers (polyethylene, polystyrene),

metals (stainless steel, gold), glass, and silicon. Grazing angle Fourier transform infrared (FTIR) spectrum of polymer **2** showed characteristic bands of the C-F stretches from 1056 cm^{-1} to 1132 cm^{-1} (Figure 2.1).[17] In addition, the spectrum showed characteristic signals from 2939 cm^{-1} to 3072 cm^{-1} indicative of aliphatic and aromatic C-C groups.
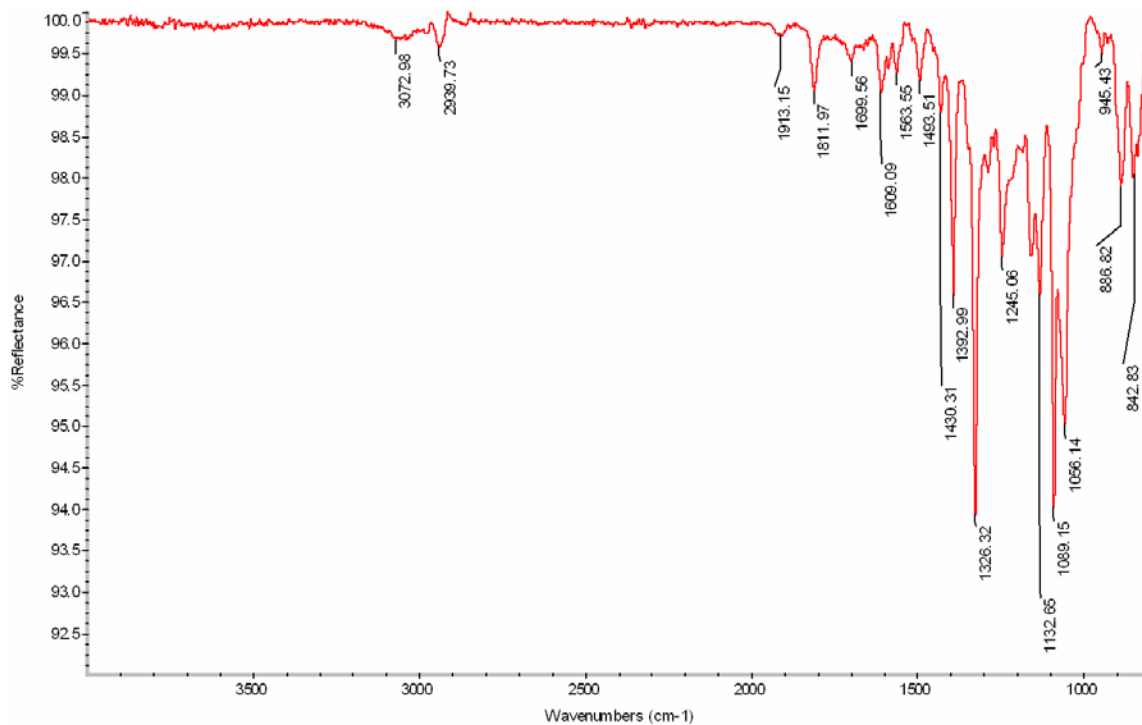
Figure 2.1. Grazing angle FTIR spectrum of polymer **2** deposited on a gold substrate.

X-ray photoelectron spectroscopy (XPS) was used to ascertain the elemental composition of polymer **2**. The following atomic ratios were calculated from the survey spectrum and high-resolution C$_{1s}$ spectrum: Br$_{3p}$/C$_{1s}$: 11.3% (calc: 12.5%), C-Br/C-C: 13.9% (calc: 16.7%), F$_{1s}$/C$_{1s}$: 17.7% (calc: 25.0%), C-F/C-C: 14.0% (calc: 16.7%) (Table 2.1 and Figure 2.2). These values compare well with theoretical (calc.) values calculated based on the chemical structure of the corresponding paracyclophanes. The high-resolution C$_{1s}$ spectrum further revealed characteristic signals for aliphatic and aromatic carbon atoms
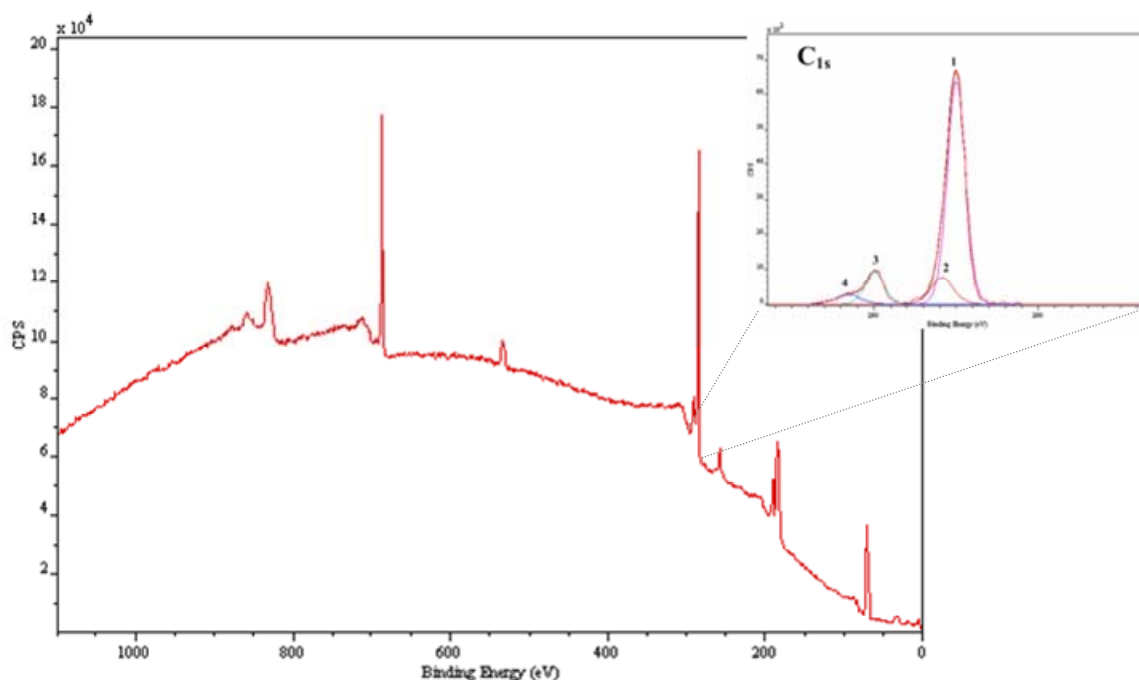
Figure 2.2: XPS survey spectrum of polymer **2**; inset shows the high-resolution C_{1s} spectrum.

(<u>C</u>-C, <u>C</u>-H) (normalized to 285.0 eV), carbon attached to bromine (<u>C</u>-Br) at 285.9 eV, carbon-fluorine (<u>C</u>-F) at 289.9 eV, and a signal indicating $\pi \rightarrow \pi^*$ transitions at 291.6 eV. The latter is a characteristic of aromatic molecules and has been previously reported for similar poly-*p*-xylylenes.[5] The XPS data in conjunction with FTIR spectrum strongly suggests that the chemical structure of the synthesized CVD polymer film **2** was as expected (shown in Scheme 2.1).

	Polymer **2**			Polymer **4**		
	BE (eV)	Expt. (%)	Calc. (%)	BE (eV)	Expt. (%)	Calc. (%)
C-C	285.0	74.1	75.0	285.3	42.6	49.63
C-Br	285.9	10.7	12.5	--	--	--
C-C=O	--	--	--	286.9	3.7	5.04
C=O	--	--	--	288.8	5.7	5.04
C-F	289.9	11.0	12.5	--	--	--
$\pi \rightarrow \pi^*$	291.6	4.2	--	291.1	4.1	--
CF_2	--	--	--	292.0	38.2	35.25
CF_3	--	--	--	294.2	5.7	5.04

Table 2.1: High resolution C_{1s} XPS data for polymers **2** and **4**.

40

Polymer **4** was synthesized by CVD polymerization of precursor **3** under conditions similar to that used for preparation of polymer **2**. Owing to the long fluorinated side chain, precursor **3** possessed a higher molecular weight compared to other functionalized [2.2]paracyclophanes previously reported.[5] Therefore, sublimation temperature between 90-100 ^{o}C and lower optimum pyrolysis temperature of 630 ^{o}C were used. Characterization of polymer **4** using FTIR spectroscopy showed a strong peak at 1713 cm^{-1} indicating carbonyl (C=O) stretches confirming the presence of the functional group after CVD polymerization. Also, characteristic signals at 1329, 1251, 1222, and 1154 cm^{-1} signified C-F vibrations (Figure 2.3).
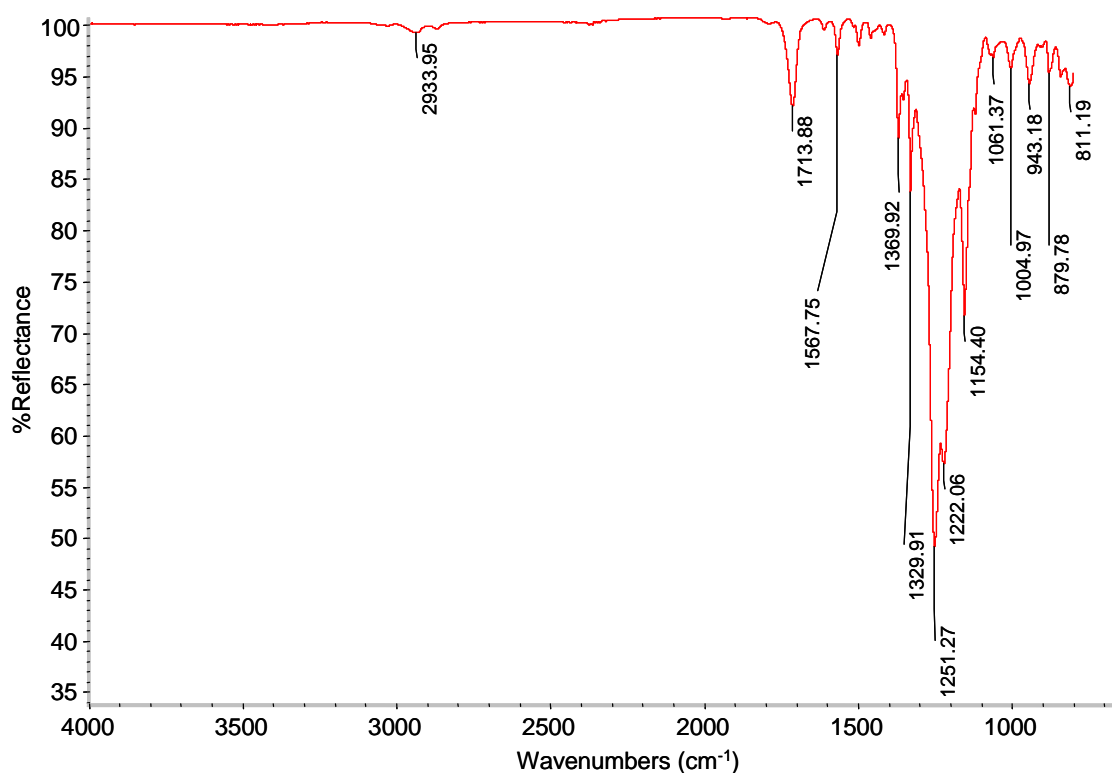
Figure 2.3: FTIR spectrum of polymer **4** deposited on a gold surface.

Polymer **4** was synthesized by CVD polymerization of precursor **3** under conditions similar to that used for preparation of polymer **1**. Owing to the long fluorinated side

chain, precursor **3** possessed a higher molecular weight compared to other functionalized

[2.2]paracyclophanes.[5] Therefore, a sublimation temperature between 90-100 $^\circ$C and

lower optimum pyrolysis temperature of 630 $^\circ$C were used. Characterization of polymer **4**

using FTIR spectroscopy showed a strong peak at 1713 cm^{-1} indicating carbonyl (C=O)

stretches confirming the presence of the functional group after CVD polymerization.

Also, the vibration band at 1329, 1251, 1222, and 1154 cm^{-1} signified the presence of C-F

bonds.

Similar to polymer **2**, the XPS-based atomic ratios for polymer **4** were in good agreement

with theoretical calculations (Table 2.1). Figure 2.4 shows the survey and high-resolution

C$_{1s}$ XPS spectra for polymer **4**. In the high-resolution C$_{1s}$ spectrum, a binding energy of
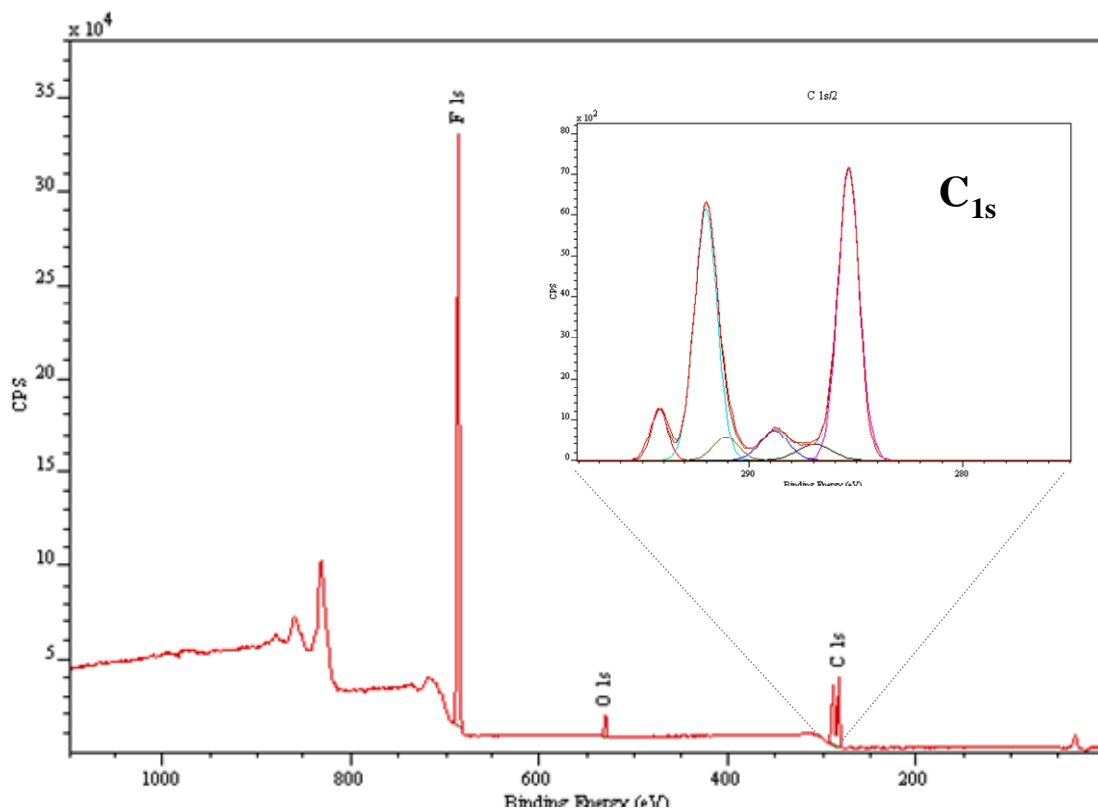
Figure 2.4: XPS survey spectrum of polymer **4**; inset shows the high-resolution C$_{1s}$ spectrum.

288.8 eV indicated the carbonyl carbon ($\underline{C}$=O). Furthermore, the ratio of $\underline{C}$-F$_3$ to $\underline{C}$-F$_2$ carbons equals 0.143, which agreed well with the calculated value of 0.149, indicating preservation of the fluorinated ketone. Overall, the high-resolution XPS spectrum confirmed the FTIR results.

Water contact angle measurements of the polymers provided an insight into the degree of hydrophobicity of the polymers. Polymers **2** and **4** were compared to non-functionalized PPX films and two previously reported poly-*p*-xylylenes with shorter fluorinated side groups namely, poly(4-trifluoroacetyl-*p*-xylylene-co-*p*-xylylene) (PPX-COCF$_3$) and poly(4-pentafluoropropionyl-*p*-xylylene-co-*p*-xylylene) (PPX-COC$_2$F$_5$).[9,10,12] Differences in the functionalities and chain lengths influenced the contact angles in such a manner that a greater degree of fluorination increased the contact angle (Figure 2.5).
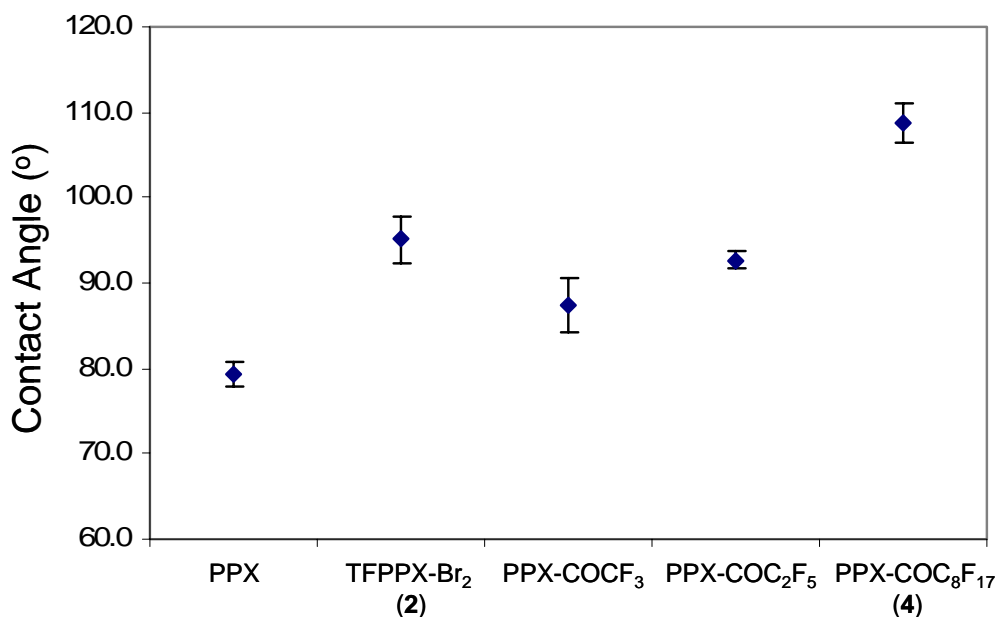
Figure 2.5: Comparing contact angles of non-functionalized PPX, polymer **2**, PPX-COCF$_3$, PPX-COC$_2$F$_5$ and polymer **4**.

Polymers **2** and **4** were also deposited on a variety of different substrates such as gold, silicon, glass, and PDMS on which they showed good adhesion. To ascertain the adhesiveness of the polymers, a piece of scotch tape was first pressed onto the film and then released by peeling it off.[18] The robustness of the film was examined visually (Figure 2.6) and FTIR was used for further confirmation. The films also remained stable after ultrasonication in water for 15-20 min. Moreover, polymers **2** and **4** were stable in aqueous solutions and several organic solvents such as ethanol, acetone, methanol,
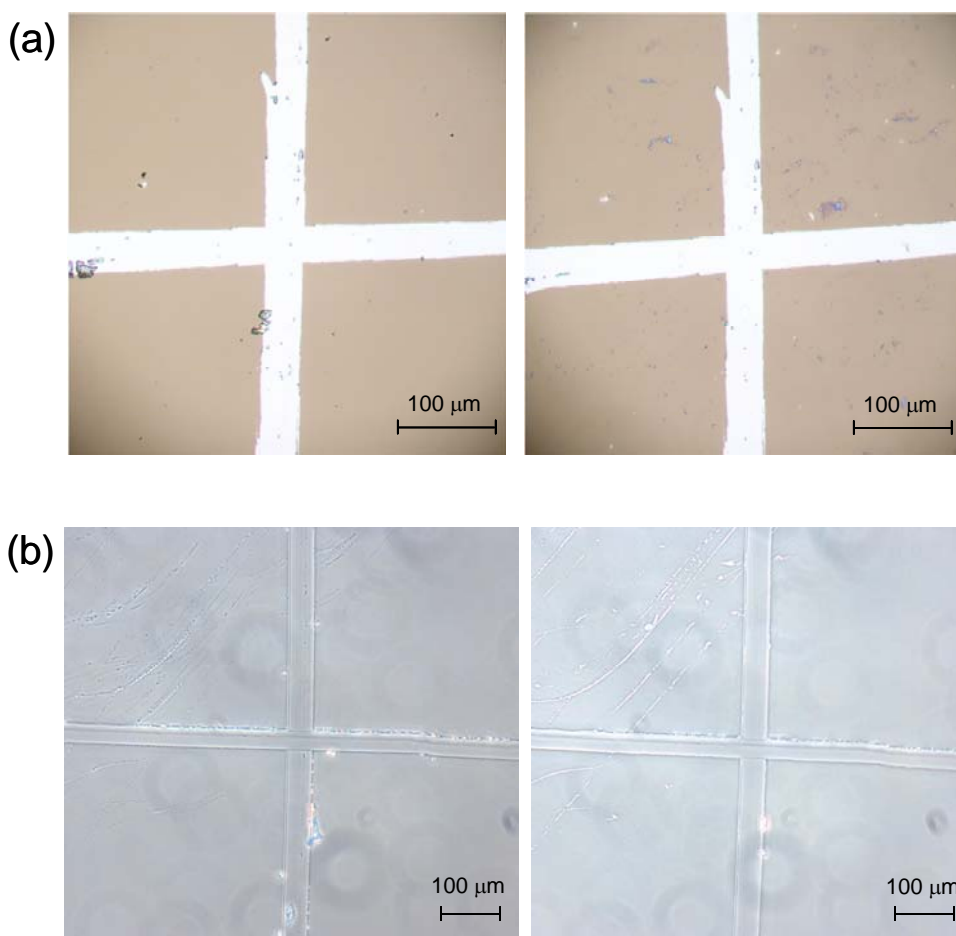
Figure 2.6: Adhesion tests of (a) polymer **2** and (b) polymer **4.** The polymer surface was first marked using a sharp object and then scotch tape was pressed onto the surface. The surface was observed before and after peeling off the tape. Optical micrographs before and after testing are shown on the left and right panels, respectively. IR spectra remained identical before and after testing.

dichloromethane, chloroform, dimethylformamide, and toluene. This is an important property of the polymer which differentiates it from the precursor as well as other oligomers and low molecular weight polymers, thus indicating the formation of a high-molecular weight polymer. However, it was observed that higher pyrolysis temperatures for polymer **4** resulted in coatings, which were stable in ethanol but soluble in other organic solvents.

2.3.3 Surface Modification

The ability to pattern the surface of low surface energy coatings is an important requirement for surface engineering. The presence of a reactive keto group in polymer **4** provides an opportunity for surface modification. Accessibility of the functional groups was evaluated by using a reaction between the keto group and hydrazide-containing ligands to form hydrazones. The surface reaction between biotinyl hydrazide was conducted using microcontact printing as previously described.[18] Briefly, an oxidized PDMS stamp was inked with a biotinamidocaproyl hydrazide solution, which was then brought into contact with a substrate coated with polymer **4** (Figure 2.7a). The biotin-patterned substrate was then visualized by incubating the substrate with rhodamine-labeled streptavidin, which bound specifically to the biotinylated regions on the substrates (Figure 2.7 b). Fluorescence signal from the fluorescently labeled streptavidin was observed predominantly in the regions, where the PDMS stamp was brought in contact with the coating. This demonstrates the availability of keto groups on the polymer surface for surface reaction with hydrazide functionalized moieties.
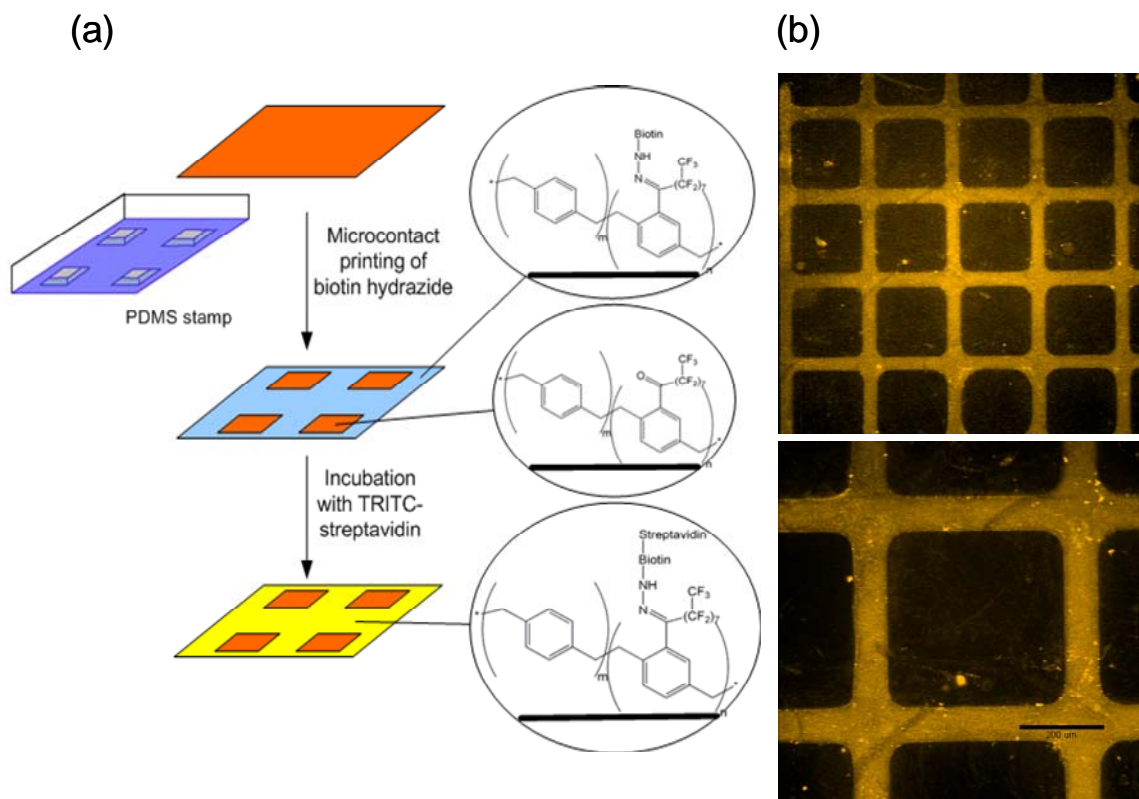
Figure 2.7: (a) Schematic of the microcontact printing process used to verify the reactivity of polymer **4** towards hydrazides. (b) Fluorescence micrographs of TRITC-labeled streptavidin immobilized onto patterned biotin hydrazide substrates.

2.3.4 Combination of Superhydrophobicity and Reactivity

Superhydrophobicity of a surface is often created by the combination of low surface energy materials in conjunction with a complex hierarchical surface architecture. Typically superhydrophobic surfaces do not possess any reactivity and therefore cannot be used for further surface modifications. This is because most functional groups tend to render a surface more hydrophilic. If coating **4** is applied to a substrate with rough topography, the properties of a low surface energy reactive polymer coating will be further enhanced and a reactive-superhydrophobic coating can be prepared. Reactive polymer coating **4** was deposited onto a poly(acrylic acid-co-acrylamide) (P(AA-co-

AAm)) surface displaying a rough morphology, which was fabricated using electrohydrodynamic jetting and stabilized by thermal imidization.[19, 20] Briefly, a layer of interconnected P(AA-co-AAm)particles was deposited onto a solid substrate using electrohydrodynamic jetting. After curing the particles for 6 hours at 175 ^{o}C, a thin film of **4** was coated onto these particles. Scanning electron micrographs (SEM) of the surface (with and without the CVD polymer layer) revealed that the surface morphology consisted of a random distribution of particles with a diameter of 1-2 μm (Figures 2.8 a,b). Previously, electrohydrodynamic jetting has been used to enhance the surface roughness by creating a network of microparticles and nanofibers on flat substrates.[21, 22] Contact angle measurements showed that this combined film rendered a superhydrophobic character to the solid surface with a contact angle of > 153° (Inset of Figure 2.8b). This angle is much higher than the contact angle of the hydrophilic P(AA-co-AAm) surface (~15°; Inset of Figure 2.8a) or a smooth surface coated with polymer **4** (108.7^o ± 2.3). Moreover, the water droplet freely rolled off the surface suggesting that the surface has a very low hysteresis, one of the key characteristics of superhydrophobic
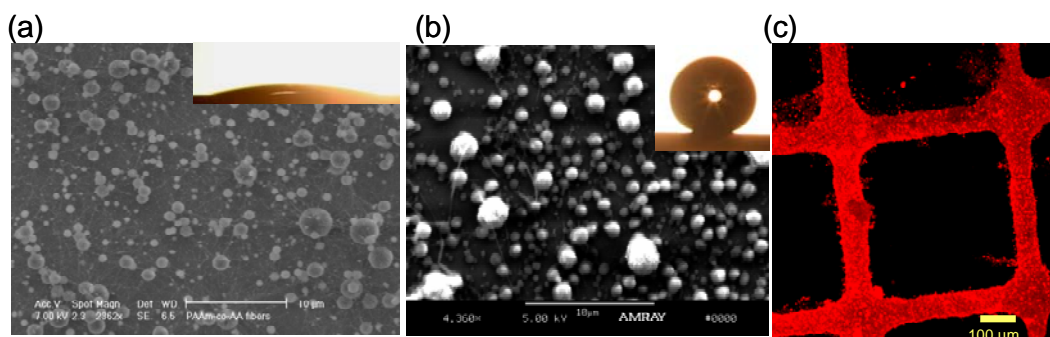
Figure 2.8: SEM of the surface (a) before CVD coating (b) after CVD coating. Insets show the corresponding water contact angles. (c) Confocal image showing binding of fluorescently-labeled streptavidin to biotinylated, micropatterned surfaces.

surfaces.[23-25] Finally to demonstrate the reactivity of polymer **4**, the surface was reacted with biotinamidocaproyl hydrazide (as previously described in Section 2.2.3) and incubated with Alexa Fluor 633 Streptavidin. Analysis with confocal scanning laser microscopy confirmed the reactivity of this superhydrophobic surface towards hydrazide-containing ligands (Figure 2.8c).

2.4 Conclusions

In summary, we have synthesized and polymerized two partially fluorinated [2.2]paracyclophane precursors with aliphatic or aromatic functionalization. Precursor **1** is fluorinated at the aliphatic bridge and may allow for further functionalization of the aromatic rings because of the presence of bromine groups. Precursor **3** contained a highly fluorinated keto group at the aromatic ring. Deposition of these polymers using CVD yielded coatings **3** and **4** that were stable in a range of different organic solvents and aqueous solutions. Polymer **4** was also shown to be reactive towards hydrazide-functionalized biotin, which then linked readily with fluorescently-labeled streptavidin. Finally, polymer coating **4** was applied towards the fabrication of reactive-superhydrophobic coatings. This class of functionalized, fluorinated poly-*p*-xylylenes could be of great interest as low energy reactive vapor-based coatings for biomedical applications, automotive industries, and anti-fouling coatings.

References

[1] T. Imae, *Current Opinion in Colloid & Interface Science* **2003**, *8*, 307-314.

[2] L. R. Hutchings, A. P. Narrianen, R. L. Thompson, N. Clarke and L. Ansari, *Polymer International* **2008**, *57*, 163-170.

[3] W. R. Dolbier and W. F. Beach, *Journal of Fluorine Chemistry* **2003**, *122*, 97-104.

[4] J. J. Senkevich and S. B. Desu, *Applied Physics Letters* **1998**, *72*, 258-260.

[5] J. Lahann and R. Langer, *Macromolecules* **2002**, *35*, 4380-4386.

[6] M. Yoshida, R. Langer, A. Lendlein and J. Lahann, *Polymer Reviews* **2006**, *46*, 347-375.

[7] S. Thévenet, H.-Y. Chen, J. Lahann, F. Stellacci, *Advanced Materials* **2007**, *19*, 4333-4337.

[8] J. J. Senkevich, B. W. Woods, B. P. Carrow, R. D. Geil and B. R. Rogers, *Chemical Vapor Deposition* **2006**, *12*, 285-289.

[9] Y. Elkasabi, M. Yoshida, H. Nandivada, H. Y. Chen and J. Lahann, *Macromolecular Rapid Communications* **2008**, *29*, 855-870.

[10] J. Lahann, D. Klee and H. Hocker, *Macromolecular Rapid Communications* **1998**, *19*, 441-444.

[11] Y. Elkasabi, H. Y. Chen and J. Lahann, *Advanced Materials* **2006**, *18*, 1521-1526.

[12] H. Y. Chen, Y. Elkasabi and J. Lahann, *Journal of the American Chemical Society* **2006**, *128*, 374-380.

[13] J. Lahann, *Polymer International* **2006**, *55*, 1361-1370.

[14] J. Lahann, *Chemical Engineering Communications* **2006**, *193*, 1457-1468.

[15] L. Bondarenko, J. W. Kampf and J. Lahann, *European Journal of Organic Chemistry* **2006**, 5499-5504.

[16] K. Y. Suh, R. Langer and J. Lahann, *Advanced Materials* **2004**, *16*, 1401-1405.

[17] D. Lin-Vien, N. B. Colthup, W. G. Fateley and J. G. Grasselli, *The Handbook of Infrared and Raman Characteristic Frequencies of Organic Molecules*, Academic Press, Boston, **1991**, p.

[18] H. Nandivada, H. Y. Chen and J. Lahann, *Macromolecular Rapid Communications* **2005**, *26*, 1794-1799.

[19] K. H. Roh, D. C. Martin and J. Lahann, *Nature Materials* **2005**, *4*, 759-763.

[20] K. H. Roh, M. Yoshida and J. Lahann, *Langmuir* **2007**, *23*, 5683-5688.

[21] F. Xia and L. Jiang, *Advanced Materials* **2008**, *20*, 2842-2858.

[22] K. Acatay, E. Simsek, C. Ow-Yang and Y. Z. Menceloglu, *Angewandte Chemie, International Edition* **2004**, *43*, 5210-5213.

[23] A. B. D. Cassie, S. Baxter, *Transactions, Faraday Society* **1944**, *40*, 546-551.

[24] A. B. D. Cassie, *Discussions of the Faraday Society* **1948**, *3*, 11-16.

[25] R.M. Jisr, H.H. Rmaile, J.B. Schlenoff, *Angewandte Chemie International Edition* **2004**, *44*, 782-785.

CHAPTER 3

MULTIPOTENT COPOLYMER COATINGS

The materials in this chapter have been adapted with minor modifications from the following published articles: Y. Elkasabi, H.Y. Chen, J. Lahann, *Advanced Materials* **2006,** 18, 1521-1526; Y. Elkasabi, M. Yoshida, H. Nandivada, H.Y. Chen, J. Lahann, *Macromolecular Rapid Communications* **2008**, 29, 855-870.

3.1 Background and Motivations

The controlled and stable immobilization of one or multiple types of (bio)molecules to a surface has been identified as one of the critical challenge in several emerging research fields, such as the regulation of cell shapes,[1] the development of advanced biological assays,[2,3] scaffolds for regenerative medicine,[4,5] or the fabrication of increasingly complex micro-total analytical systems (μTAS).[6,7] This is partly motivated by the need for defined surface architectures simultaneously presenting multiple biological entities in controlled ratios. While a range of methods has been developed for the immobilization of a single type of biomolecules to artificial substrates, fewer concepts are available for the precious immobilization of multiple biomolecules in a controllable fashion.[8] Recently, we established a suite of surface modification techniques based on chemical vapor deposition (CVD) polymerization of substituted [2.2]paracyclophanes.[9-11] This novel coating technology resulted in a diverse class of functionalized poly-*p*-

xylylenes presenting a wide variety of functional groups, such as amines,[12] esters,[13,14] aldehydes,[15] and alcohols.[16] The resulting polymers provide a flexible solution to surface engineering challenges, as they decouple surface design from bulk properties.[17] In essence, the CVD technology is a one-step coating procedure to generate functionalized surfaces without the need of further post-treatments once the films are deposited.[18] In a significant extension of previous work, we describe the use of CVD polymerization to fabricate multi-potent and modular coatings. The term "multi-potent coating" refers in that context to a reactive coating that is compatible with the simultaneous presentation of multiple biomolecules in controllable ratios.

3.2 Experimental Methods

CVD Copolymerization – 4-Trifluoroacetyl[2,2]paracyclophane (**1**) was synthesized via Friedel-Crafts acylation of [2,2]paracyclophane.[10] 4-Aminomethyl[2,2]paracyclophane (**2**) was synthesized from [2.2]paracyclophane (Aldrich) in a two-step synthesis as described elsewhere.[19] CVD co-polymerization was performed using molar mixtures of **1** and **2** to produce poly[(4-trifluoroacetyl-*p*-xylylene)-co-(4-aminomethyl-*p*-xylylene)-co-*p*-xylylene] (**3**). To independently control each source independently, the two species were kept in separate feed dishes within the sublimation zone. A pressure of 0.56 mbar and a temperature between 90 and 100 ^{o}C were employed for CVD copolymerization. Under these conditions, the species sublimated and were transferred in a stream of argon carrier gas (20 sccm) to the pyrolysis zone (670 ^{o}C). Following pyrolysis, the diradicals were transferred into the deposition chamber, where polymerization occurred. While the wall temperature was adjusted to 120 ^{o}C, the silicon, gold, or glass substrates were cooled

to 10 $^{\circ}$C to optimize the deposition onto the substrate and to avoid loss of starting material due to wall deposition. Moreover, rotation of the sample holder ensured uniform film deposition. For copolymerization of varying molar feed ratios, all reaction conditions were maintained with the exception of the adjusted ratio of the two starting materials (for the 1:1 feed ratio, we used 38.0 μmol each). XPS composition of a co-polymer with a 1:1 molar feed ratio: C_{1s}: 83.26% (calc. 84.76%), N_{1s}: 2.84% (calc. 3.05%), F_{1s}: 8.54% (calc. 9.15%), O_{1s}: 5.35% (calc. 3.05%); IR (grazing angle 85°): 3361.5, 3301.1, 3007.9, 2926.1, 2860.4, 1715.7, 1641.2, 1499.9, 1454.3, 1227.2, 1202.0, 1152.4, 976.9, 837.8 cm^{-1}.

X-ray Diffraction – To assess the crystallinity of functionalized poly(p-xylylene) films, silicon substrates coated with the polymer of interest were examined by wide-angle X-ray diffraction, using a Rigaku 12 kW high intensity rotary anode generator. All CVD films were examined both as deposited and after annealing. The polymer films were annealed for 14 hours in an oven at a temperature of 120 $^{\circ}$C, unless specified otherwise.

Surface Characterization – X-ray photoelectron spectroscopy (XPS) data were recorded on an Axis Ultra X-ray photoelectron spectrometer (Kratos Analyticals, UK) equipped with a monochromatized AlKα X-ray source. All spectra were calibrated with respect to the non-functionalized aliphatic carbon with a binding energy of 285.0 eV. For XPS imaging, the lens mode was in hybrid, pass energy was set to 160.0 eV, and the aperture was 600 μm x 600 μm for all imaging acquisitions. Thicknesses were recorded at a wavelength of 532 nm using an EP^3-SW imaging ellipsometry (Nanofilm Technologie

GmbH, Germany). Both, nulling (four zones) and mapping experiments were performed at an angle of incident of 60°, and an anisotropic Cauchy model was used to model the ellipsometric parameters psi and delta. Infrared spectroscopy was performed on a Nicolet 6700 spectrometer utilizing the grazing angle accessory (Smart SAGA) at a grazing angle of 85°.

Surface Reaction – Biotin hydrazide and rhodamine-linked streptavidin were purchased from Pierce Inc., and Atto 655 NHS ester was purchased from Sigma Aldrich. All surface reaction experiments were performed on glass substrates for poly(4-trifluoroacetyl-*p*-xylylene-co-*p*-xylylene) (**4**) and poly(4-aminomethyl-*p*-xylylene-co-*p*-xylylene) (**5**) homopolymers, as well as on different ratios of copolymer **3**. As a control, amine and ketone-reactive ligands were applied separately to each polymer. For surface reaction, 1.7 μL of reaction buffer was dispensed onto the film, incubated, and rinsed several times. For the copolymers, consecutive surface reactions were conducted. Fluorescence images and intensities were acquired using a GenePix 4000B scanner with 532 nm (17 mW) and 635 nm (10 mW) lasers. Both excitation wavelengths are scanned simultaneously at 20 μm spatial resolution. Colors shown in the scanning images are not true colors, but were set for better resolution.

Ligand 1: 0.5 ml of anhydrous dimethylformamide was added to 1 mg Atto 655 NHS ester. From this, 3.6 μl were diluted with 2 ml 0.1 M sodium bicarbonate buffer (pH 8.3), containing 0.02% (v/v) Tween 20. NHS esters are time-sensitive in aqueous solution, so the buffer was applied to the film immediately upon dilution. The solution was incubated

for 1 hour at room temperature, after which the surface was rinsed with ethanol for 5 minutes and with PBS/Tween solution for 30 minutes.

Ligand 2: Biotin hydrazide was diluted to 10 mM in phosphate buffered saline (PBS pH 7.4). The solution was gently heated and acid-catalyzed prior to surface application. Incubation time lasted 5 to 7 minutes, which was followed by a wash of PBS containing 0.02% (v/v) Tween 20. The area was then applied with rhodamine-linked streptavidin solution (0.075 mg/ml in PBS; 0.02% (v/v) Tween 20; 0.1% (w/v) bovine serum albumin) for 10 minutes. Finally, the entire glass slide was immersed for 1 hour in a PBS/Tween/BSA solution.

3.3 Results and Discussion

3.3.1 CVD Copolymerization

Prior to CVD co-polymerization, 4-trifluoroacetyl [2.2]paracyclophane (**1**) and 4-aminomethyl [2.2]paracyclophane (**2**) had to be synthesized from commercially available
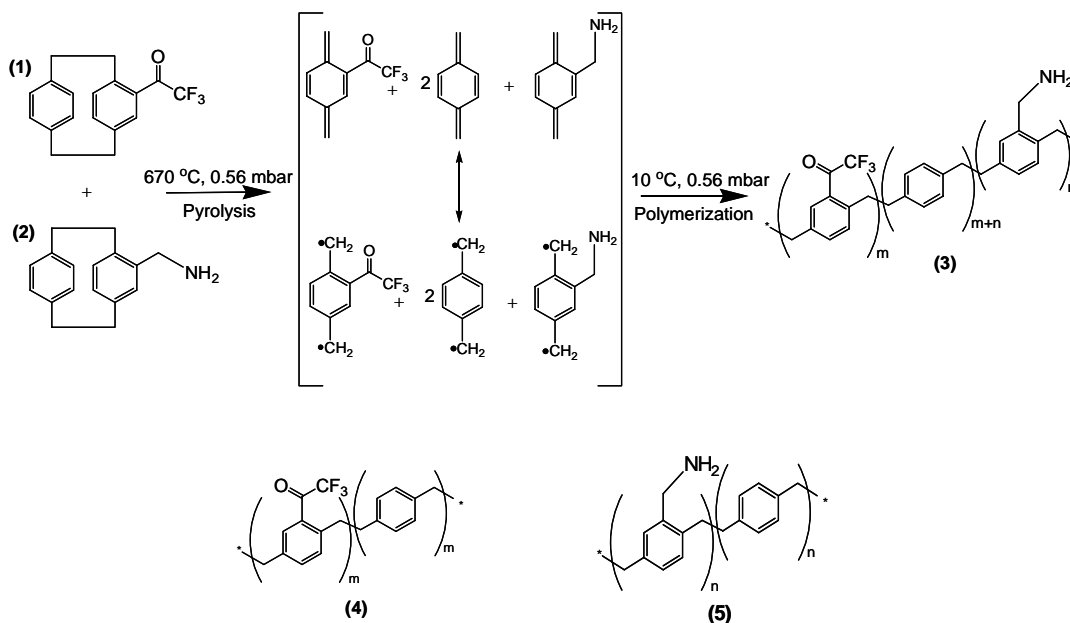
Figure 3.1. The multifunctional polymer (**3**) accessible by CVD copolymerization of [2.2]paracyclophanes (**1**) and (**2**); the structures of the individual polymers **4** and **5** are shown for comparison.

[2.2]paracyclophane following established synthesis routes.[10,19] CVD copolymerization of **1** and **2** was then conducted and resulted in a vacuum-deposited film of copolymer **3** on the substrate (Figure 3.1).

For CVD copolymerization, mixtures of carefully purified dimers **1** and **2** were initially sublimated under a reduced pressure of 0.56 mbar at temperatures between 90 and 100 °C. The sublimation temperatures of **1** and **2** were sufficiently similar to ensure that the compounds were exposed to comparable sublimation conditions by placing them in proximity to each other within the CVD system. Sublimated **1** and **2** were then transferred to the pyrolysis zone, which was heated to 670 °C to ensure cleavage of the C-C bonds resulting in the corresponding quinodimethanes (monomers). In the last step, monomers were adsorbed on the substrate at temperatures around 10 °C and spontaneously polymerized. CVD copolymerization of **1** and **2** resulted in transparent and topologically uniform polymer films (Figure 3.2) with thicknesses between 50 and 200 nm. The film thickness is mainly determined by the total amount of

(a) (b)
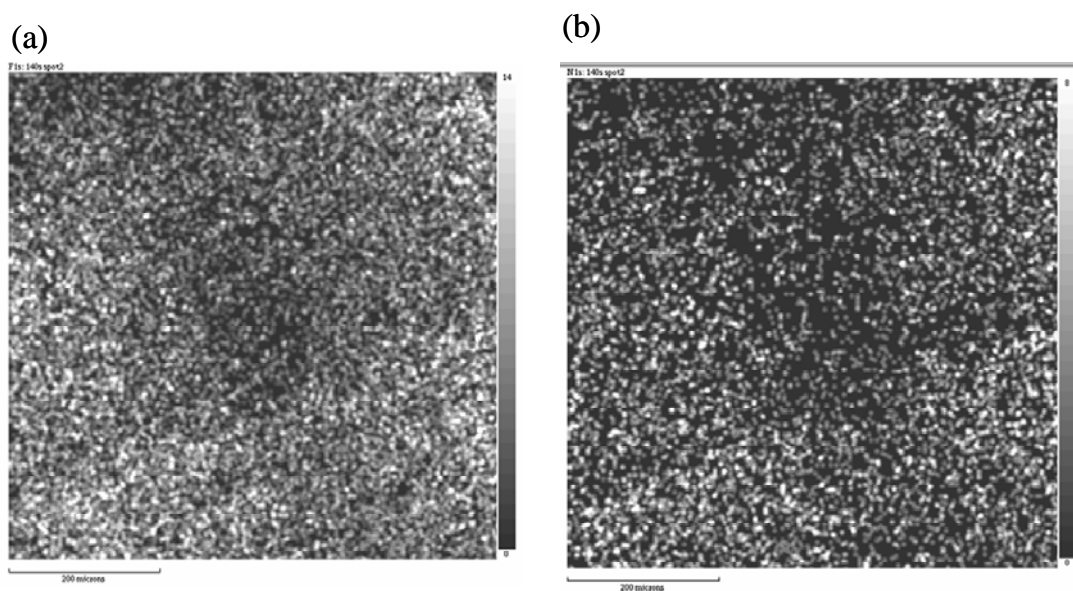
Figure 3.2 – XPS elemental imaging maps of (a) fluorine and (b) nitrogen, for copolymer **3** prepared with a 1:1 feed ratio

[2.2]paracyclophanes used for polymerization. For instance, the thickness of a film produced by the deposition of 20 mg of equimolar amounts of **1** and **2** was determined by means of imaging ellipsometry to be (115 ± 15) nm. Moreover, the multi-functional coatings showed excellent chemical stability in a dry air environment. No significant change in composition or chemical behavior was found for samples stored in a dry air atmosphere for several weeks as compared to freshly prepared samples. All copolymers as well as the two individual polymers **4** and **5** remained intact after rinsing with standard solvents, such as water, chloroform, acetone, and ethanol.

The elemental composition of the copolymer poly[4-aminomethyl-*p*-xylylene-*co*-4-trifluoroacetyl-*p*-xylylene-*co-p*-xylylene] (**3**) was studied by X-ray photoelectron spectroscopy (XPS). XPS is capable of detecting atomic composition within a depth of about 10 nm.[20] The co-polymer **3** was compared to the individual polymers, poly[4-trifluoroacetyl-*p*-xylylene-*co-p*-xylylene] (**4**) and poly[4-aminomethyl-*p*-xylylene-*co-p*-xylylene] (**5**, see Table 3.1).

	C–C	C–N	C=O	$\pi \rightarrow \pi^*$	C–F
BE/eV	285.0	286.8	288.4	291.2	292.9
Calculated/% (**3**)	89.2	3.6	3.6	–	3.6
Experimental/%[a]	89.5	3.1	3.3	4.3[b]	4.1
Calculated/% (**4**)	81.48	0	9.26	--	9.26
Experimental/%	80.17	0	9.29	4.2	10.54
Calculated/% (**5**)	94.12	5.88	0	--	0
Experimental/%	94.27	5.73	0	5.8	0

[a] Percentage of total without $\pi \rightarrow \pi^*$; applies to all experimental values
[b] Actual value obtained; applies to all $\pi \rightarrow \pi^*$ values.

Table 3.1. High-resolution C_{1s} XPS results for poly[(4-aminomethyl-*p*-xylylene)-*co*-(4-trifluoroacetyl-*p*-xylylene)-*co-p*-xylylene] (**3**) prepared with a 1:1 feed ratio compared to the individual polymers **4** and **5**.

Characteristic chemical elements detected for the individual polymers **4** and **5**, such as oxygen (polymer **4**), fluorine (polymer **4**), and nitrogen (polymer **5**) were simultaneously detected in the copolymer, indicating the presence of both functional groups on the surface. Because nitrogen is only present in the aminomethyl group of polymer **5**, while fluorine is a characteristic element for the ketone of polymer **4**, the ratio
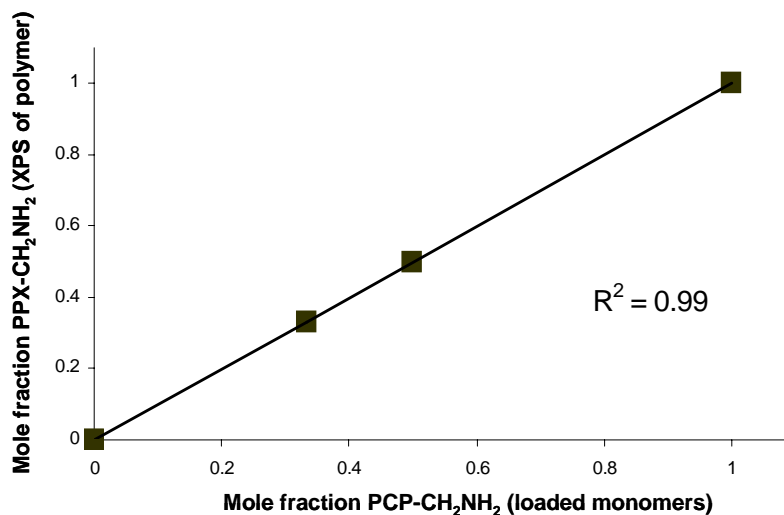
Figure 3.3 Graph of copolymer ratios of CH_2NH_2:$COCF_3$ plotted against their monomer loading ratios.

of the elemental composition of nitrogen and fluorine is a good indicator for the chemical quality of the copolymer films. Using XPS, we found a N/F ratio of 0.332, which is in good accordance with the theoretically expected ratio of 0.333. Accordingly, side reactions, such as decomposition of the functional groups, were negligible, when pyrolysis temperatures under 670 °C and working pressures between 0.4 and 0.6 mbar were chosen. Furthermore, XPS revealed no signs of cross-reaction of the aminomethyl and keto groups under the conditions of CVD polymerization. Table 3.1 shows the experimental results of the 1:1 co-polymer high-resolution C_{1s} XPS to be in good agreement with theoretical values.[9,21] Furthermore, Figure 3.3 shows a tight

correspondence between the loaded monomer ratio and the actual composition of the copolymer as indicated by the N/F ratio measured by XPS. Copolymer composition can also be correlated to the monomer sublimation rates, which were controlled by the sublimation temperatures. Compositions were determined using XPS, and the sublimation temperatures of both monomers were recorded in situ using a thermocouple. Table 3.2 details the results of this study.

mole fraction CH_2NH_2	$T\_CH_2NH_2$ (^{o}C)	T_COCF_3 (^{o}C)	total growth rate (A/s)
0	88.0	95.0	0.7
0.18	93.6	73.8	0.6
0.26	95.8	64.8	0.6
0.4	104.3	58.3	0.7
0.49	110.6	51	0.7
0.62	115.8	40.7	0.7
0.73	137.6	40	0.7
0.91	142	35	0.7

Table 3.2. XPS composition of co-polymer (PPX-CH_2NH_2/-$COCF_3$), deposited using various monomer sublimation temperatures. Monomer loading ratio of 1:1 was used for all depositions.

To further support the XPS data, we used grazing angle FTIR spectroscopy to assess the structure of copolymers deposited onto a gold substrate. Figure 3.4 displays IR spectra of polymer films made by co-polymerization of **1** and **2** using varying feed ratios. The spectra are ranging from 100% of compound **2** (a) to 100% of compound **1** (g). All spectra were normalized based on the C-H band intensity (2926.1 cm^{-1}), because the C-H group is present in each polymer. If the feed ratio changed, the peak intensities of side groups were changed accordingly. Due to potential differences in film thickness, we restrained ourselves to qualitative analysis only: The carbonyl stretches at 1715 cm^{-1} being characteristic for $COCF_3$ groups were compared to the C-H band at 2926.1 cm^{-1}. The carbonyl stretch at 1715 cm^{-1} is absent in spectrum (a). For spectra (b) to (g), the
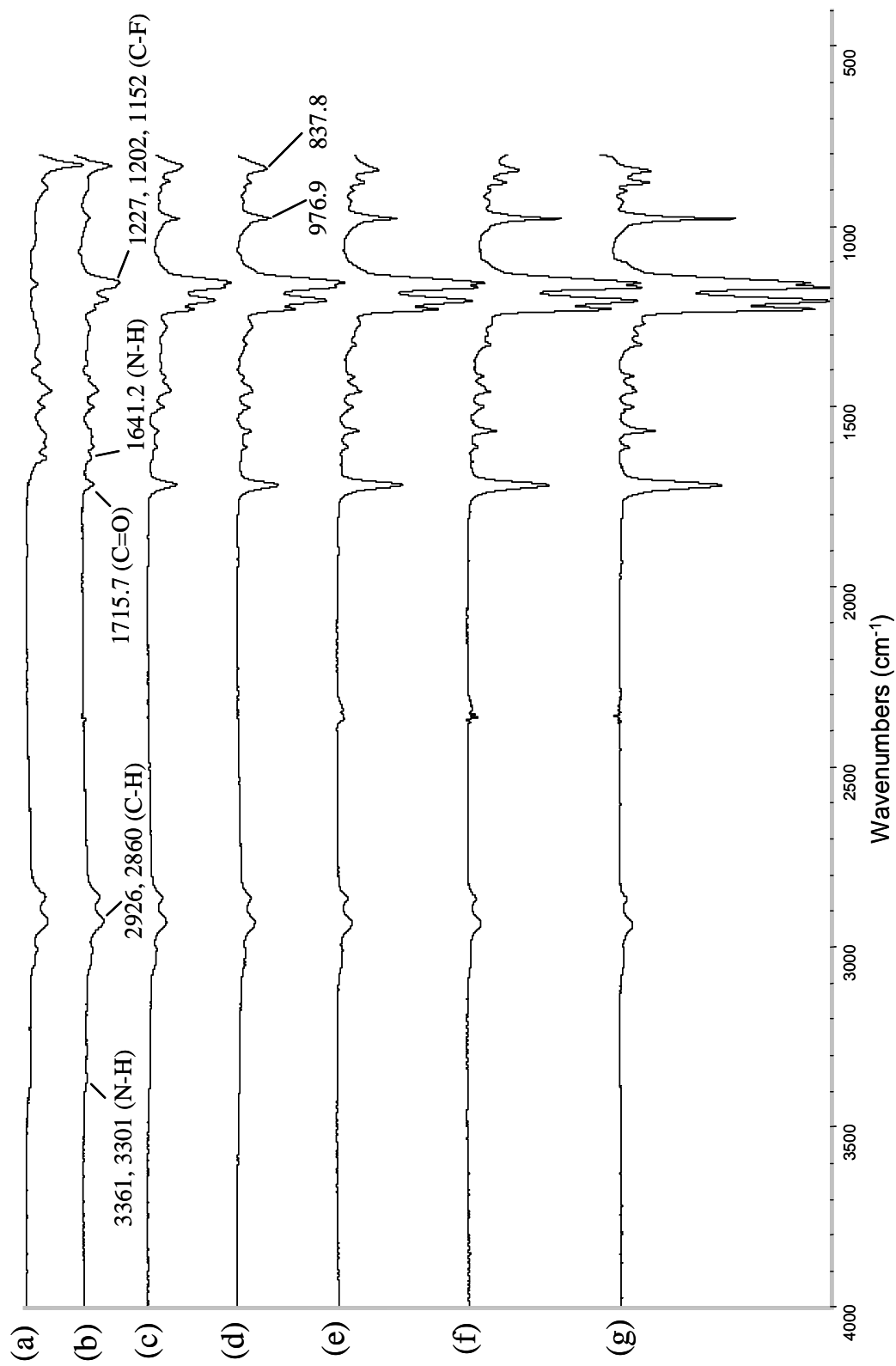
Figure 3.4. FTIR spectra of (**3**) with varying molar ratios of CH_2NH_2:$COCF_3$. (a) pure CH_2NH_2 (b) 5:1 (c) 2:1 (d) 1:1 (e) 1:2 (f) 1:5 (g) pure $COCF_3$.

carbonyl stretch grows until maximum intensity is attained for spectrum (g). The same trend can be observed for the C-F stretches at 1227, 1202, and 1152 cm^{-1}. Similarly, the signal at 976 cm^{-1} increases with increasing contribution of the ketone to become a strong signal for the pure polymer **4**. This band has been previously reported for similar polymers.[22]

In many cases, homogeneous deposition of coatings is an important technological requirement. The deposition chamber used in this study is large enough for temperature gradients within the chamber and/or on the sample holder to form. Such differences, if they exist, may impede accurate deposition of defined co-polymer ratios. To assess potential inhomogeneities created during CVD co-polymerization due to temperature differences, co-polymer PPX-CH$_2$NH$_2$/-COCF$_3$ (1:1 monomer ratio) was deposited on 9 different samples, each located at various positions within the sample holder (Figure 3.5). The experimental conditions were maintained as described for other CVD co-polymerization procedures, with the exception that the sample holder was not rotated and the substrate temperature was systematically varied. FTIR was used to obtain the ratio of C-N to C=O bands, which served as an indicator of co-polymer ratios. For each temperature, sample #2 (Figure 3.5a) was used as a reference; all sample peak ratios were normalized by the peak ratio of sample #2. As shown in Figure 3.5b, average ratio of two functional groups remained relatively constant across all deposition temperatures, suggesting no significant compositional differences on the sample holder, even at different substrate temperatures.

Once the fundamental concept of CVD co-polymerization of [2.2]paracyclophanes with different functional groups was established, the structural properties of the resulting
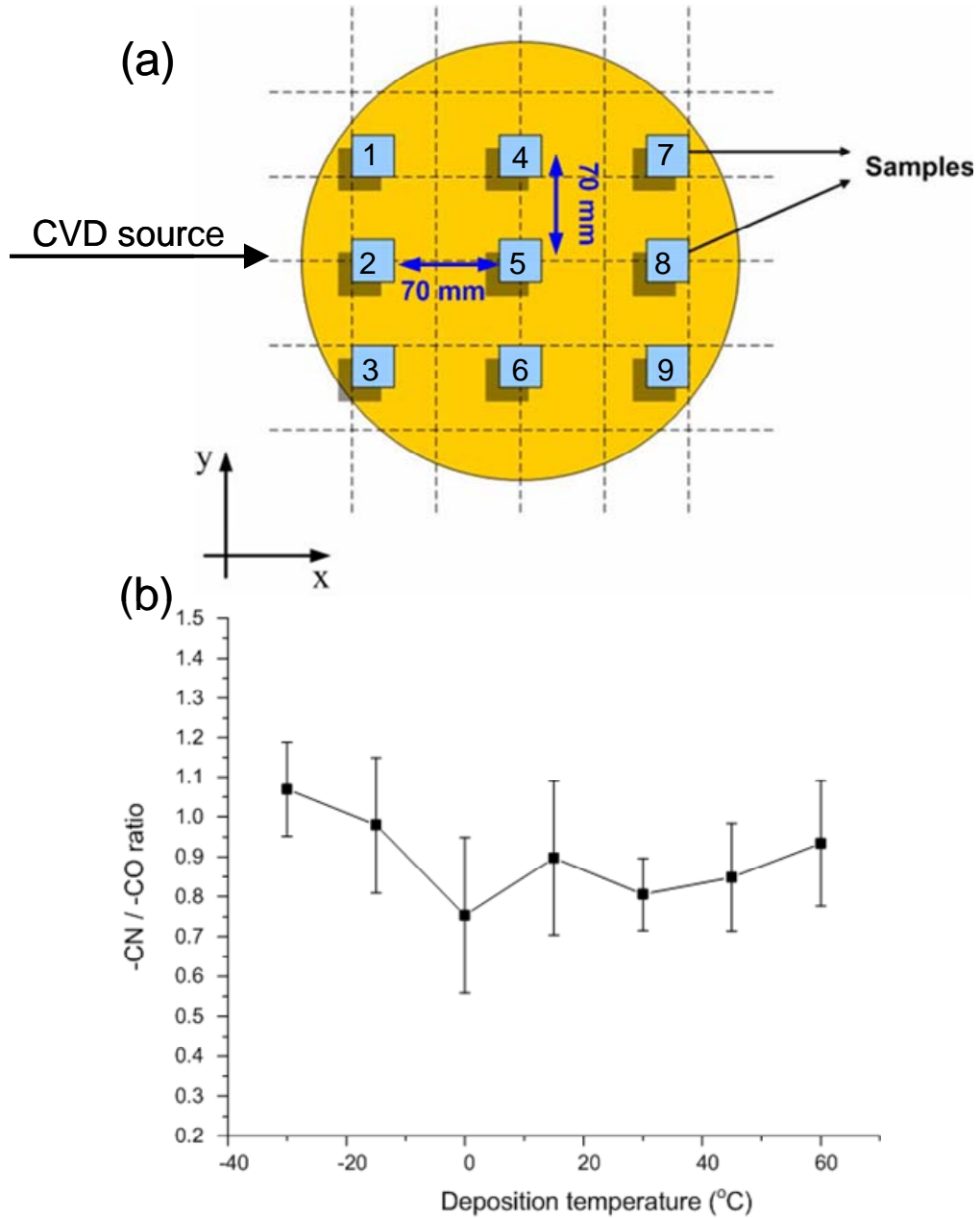
Figure 3.5 (a) Schematic representation of substrate positions arranged on the CVD sample holder. (b) Plot of FTIR peak ratios (CN:C=O), with respect to substrate temperature.

co-polymers needed to be elucidated in further details. In principle, CVD co-polymerization could result in a true co-polymer - with properties distinct from individual polymers **4** and **5** - or could result in a layered blend of the two polymers.

We used X-ray diffraction (XRD) measurements of thin CVD films before and after annealing to address this question.[23] This approach takes advantage of the fact, that poly(*p*-xylylenes) are often semi-crystalline polymers with characteristic features in the XRD spectra.[24,25] Since XRD data for polymers **4** and **5** had not yet been reported, we studied the individual CVD polymers first. Prior to annealing, no diffraction patterns were obtained for either **4** or **5**, indicating that both films were largely amorphous in the as-deposited state.[26]

After annealing for 14 hrs at 120 ºC, however, the trifluoroacetyl-functionalized polymer **4** showed characteristic diffraction patterns, which likely correspond to (020) and (110) planes, and a d-spacing greater than that reported for the monoclinic poly(*p*-xylylene).[27] In contrast, the aminomethyl-functionalized polymer **5** remained amorphous. Figure 3.6 compares diffraction patterns before and after annealing for the individual polymers **4** and **5** and the co-polymers. Exposing the films to a high-temperature environment allows for realignment of functional groups to form crystalline domains.[20] Next, we assessed the structural properties of polymer **3** made by co-polymerization of an equimolar feed ratio of **1** and **2**. Based on the FTIR study, we expect this co-polymer to contain both components in about the same ratio. If the co-polymerization would result in a layered blend of individual polymers **4** and **5**, the resulting diffraction pattern should essentially be the superposition of the diffraction patterns of the individual polymers. If however the CVD co-polymerization results in a

true co-polymer, a new polymer with distinct, presumable amorphous structure will be prepared. As shown in Figure 3.6, no diffraction patterns were detected for the co-polymer, independent of the annealing. This observation also holds for the co-polymer made from [2.2]paracyclophanes **1** and **2** in a feed ratio of 1:2. If a large excess of the ketone is used (feed ratio: 1:5), a smaller diffraction pattern can be detected after
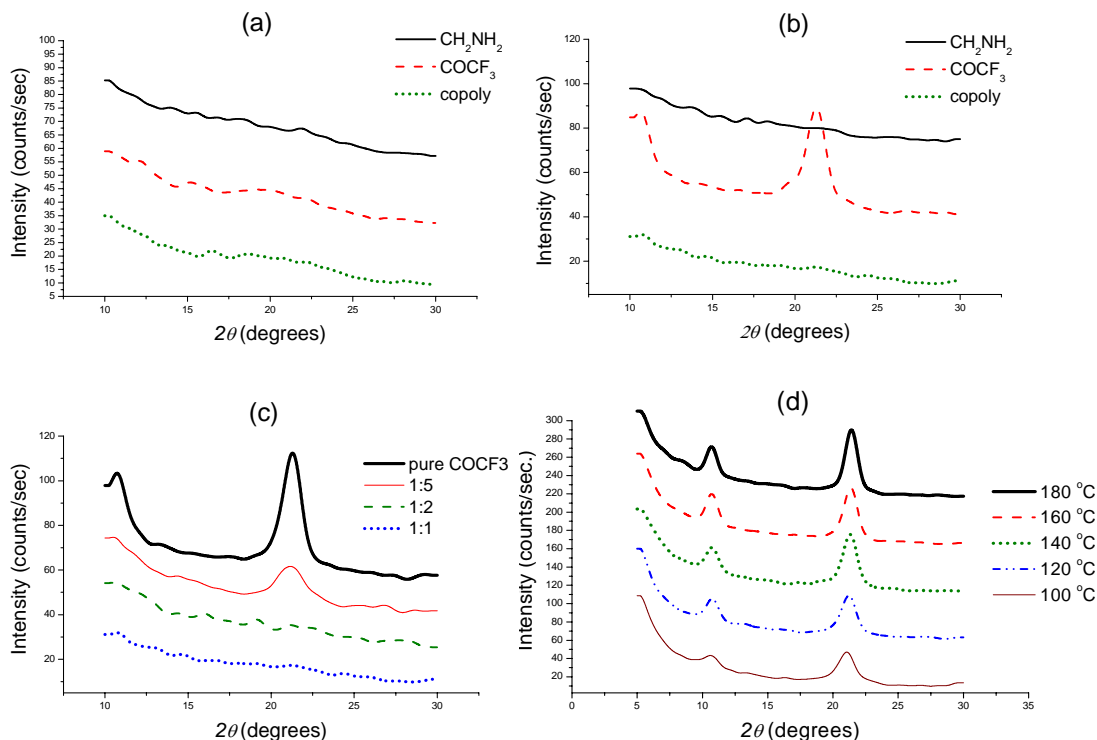
Figure 3.6. X-ray diffraction patterns of the individual polymers **4** and **5** and the co-polymer **3** (a) before and (b) after annealing at 120 ^{o}C. Only the polymer **4** exhibits crystallinity after annealing. (c) X-ray diffraction of co-polymers with varying ratios. (d) X-ray diffraction of **4** at various annealing temperatures.

annealing indicating the onset of a semi-crystalline structure. We concluded based on the XRD data that the CVD co-polymerization results in true copolymers with distinct structural properties, rather than layered blends of the individual polymers **4** and **5**.

3.3.2 Surface Reactions

Finally, we verified that both functional groups contained in co-polymer **3** are available for further surface modification. The availability of the functional groups for further surface reaction is essential for immobilization of two different types of (bio)molecules. In a proof of concept experiment using the approach shown in Figure 3.7, the copolymer surface (**3**) was reacted with two fluorescent dyes, which exhibited
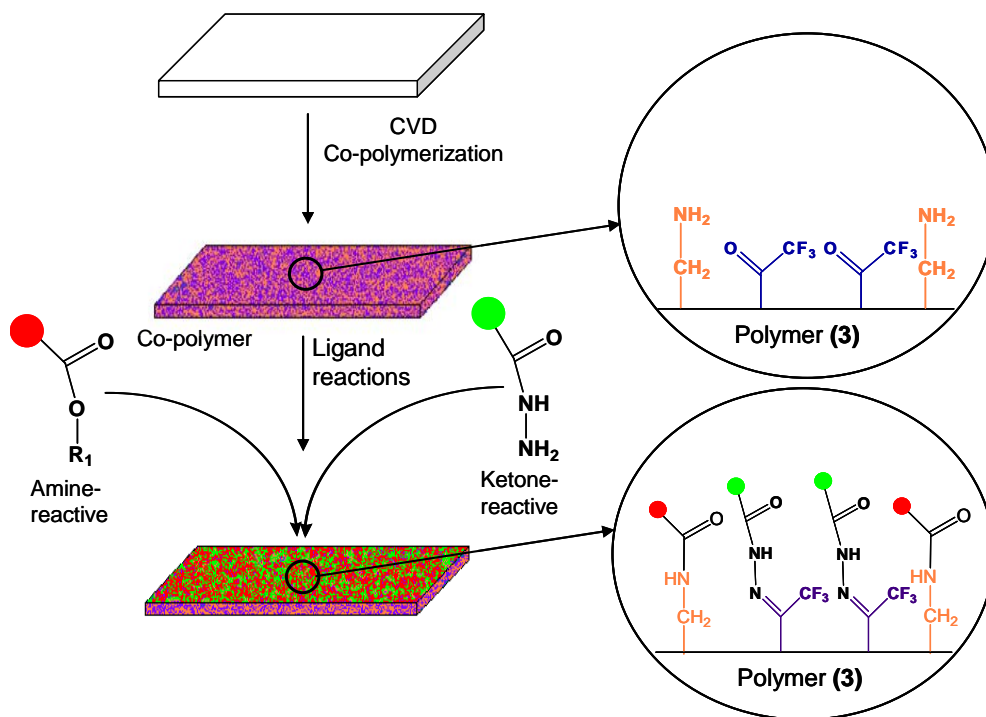
Figure 3.7. Schematic outlining the selective reactivity of the multivalent surface. The activated ester will only react with the aminomethyl group, while the hydrazide group shows selective reactivity towards ketones.

orthogonal reactivity. The purpose of this experiment was to assess whether or not each functional group remains active and able to specifically react with the assigned ligands. Fluorescence scanning was used to examine the presence of surface-bound ligands. Figure 3.8 shows the results of the surface reaction of polymer **3** with Atto 655 as well as biotin-streptavidin. To avoid reaction of the Atto 655 ligand with the amino groups of

strepdavidin, a conceutive immobilization scheme was employed: The Atto 655 ligand was immobilized first followed by the biotin ligand.
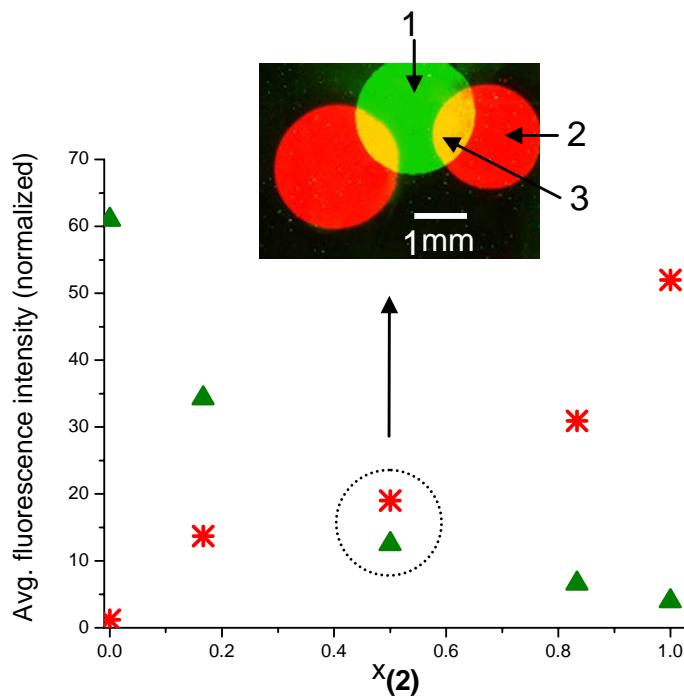
Figure 3.8. Fluorescence intensities detected on the co-polymers versus $x_{(2)}$, the relative feed concentration of [2.2]paracyclophane **2** used for CVD copolymerization. The trends demonstrate ligand immobilization occurs in controlled ratios as a function of increasing relative ratio of the [2.2]paracyclophanes. Inlet: Fluorescence micrograph of areas that were reacted with biotin ligand (1), Atto 655 ligand (2), or both (3).

We found Atto 655 to bind strongly to the aminomethyl-containing polymer **5**. In contrast, only negligible amounts of Atto bound to polymer **4**. When reacting the two individual polymers **4** and **5** with the second ligand, a biotin hydrazide derivative, the biotin ligand was found to bind strongly to polymer **4**, but not to **5**. Fluorescence-labeled streptavidin, a specific binding partner of biotin, was than used to visualize the biotin ligands and confirmed selective binding to biotin-modified coating **4**. In contrast, streptavidin applied to the polymer **4** that was not modified with the biotin ligand did not

give any appreciable fluorescence signal. When performing the same procedure on co-polymer **3**, both fluorescence signals were observed simultaneously (Figure 3.8). By varying the feed ratios of [2.2]paracyclophanes **1** and **2** in the CVD polymerization, the relative ratio of ligands bound to the surface was varied. The relative increase of starting material **2** resulted in surfaces with increased amounts of Atto-labled ligands (red color), while a relative increase of compound **1** used for CVD polymerization resulted in an increased fluorescence signal indicating more stepdavidin/biotin pair bound to the surface. Based on the FTIR spectra (Figure 3.4), these trends can be explained by the controlled variation of binding sides available for the two ligands on the surface, which corresponds to the feed ratio of staring materials used during CVD copolymerization. For the 1:1 ratio, the fluorescence micrographs of different reaction areas are shown in the inlet of Figure 3.8. Area 1 shows copolymer **3**, which reacted only to the biotin ligand (green color), while area 2 is characterized by red fluorescence, which is due to surface-immobilization of the Atto-labeled ligand. Where both ligands were allowed to react with the copolymer **3** (area 3), yellow color is observed indicating the parallel immobilization of the two ligands.

3.4 Conclusions

The herein proposed concept of CVD polymerization of functionalized [2.2]paracyclophanes establishes a general, but simple protocol for preparation of multi-reactive polymer films. Applicability of the reactive coating to various substrates, such as polymers, metals, or composites generates a fairly universal platform without relying on broad chemical alteration of the bulk material.[28-30] Although multipotent biointerfaces

could in principle be prepared by simultaneously immobilizing mixtures of two different biomolecules through the same functional groups, the exploration of reactive coatings with two orthogonal functional groups bears several potential advantages: (1) Surface ratios can be controlled with high precision, because the ligand immobilization reactions can be conducted independently. (2) Substantially different biomolecules can be co-immobilized, even so their transport to the surface is substantially different. (3) The ability to immobilize biomolecules in a sequence allows for combinations of biomolecules that would otherwise cross-react with each other. For applications, where substantially different biomolecules need to be immobilized in precisely defined ratios, the CVD co-polymerization may provide a simple access route. Moreover, this study presents a first step towards the establishment of a modular coating design, where the properties of a coating can simply be dialed-in by selecting the right combination of building blocks for CVD polymerization. Copolymer compositions are directly related to the monomer sublimation temperatures, where changing the sublimation temperature(s) affected relative sublimation rates. Such a modular surface design may be of great value for future biomedical devices, high-throughput screening platforms, microfluidic analysis devices, or diagnostic platforms.

References

[1] C.S. Chen, J.L. Alonso, E. Ostuni, G.M. Whitesides, D.E. Ingber, *Biochem. Biophys. Res. Comm*. **2003,** *307,* 355.

[2] H, Tani, K. Maehana, T. Kamidate, *Anal. Chem*. **2004,** *76*, 6693.

[3] K. Kato, H. Sato, H. Iwata, *Langmuir* **2005,** *21*, 7071.

[4] X. Liu, Y. Won, P. X. Ma, *J. Biomed. Mater. Res*. **2005**, *74A*, 84.

[5] M.H. Ho, D.M. Wang, H.J. Hsieh, H.C. Liu, T.Y. Hsien, J.Y. Lai, L.T. Hou, *Biomaterials* **2005,** *26*, 3197.

[6] D.R. Reyes, D. Iossifidis, P.A. Auroux, A. Manz, *Anal. Chem*. **2002,** *74*, 2623.

[7] P.A. Auroux, D. Iossifidis, D.R. Reyes, A. Manz, *Anal. Chem*. **2002** ,*74*, 2637.

[8] D.G. Castner, B.D. Ratner, *Surface Science* **2002,** *500*, 28.

[9] J. Lahann, R. Langer, *Macromolecules* **2002,** *35*, 4380.

[10] J. Lahann, D. Klee, H. Höcker, *Macromol. Rapid Commun.* **1998**, *19*, 441.

[11] J. Lahann, R. Langer, *Macromol. Rapid Commun.* **2001**, *22*, 968.

[12] J. Lahann, H. Hocker, R. Langer, *Angew. Chem. Int. Ed.* **2001,** *40*, 726.

[13] J. Lahann, I.S. Choi, J. Lee, K. Jensen, R. Langer, *Angew. Chem., Int. Ed.* **2001**, 40, 3166.

[14] J. Lahann, M. Balcells, T. Rodon, J. Lee, I. Choi, K. Jensen, R. Langer, *Langmuir* **2002**, *18*, 3632.

[15] H. Nandivada, H.Y. Chen, J. Lahann, *Macromol. Rapid Commun*. **2005,** *26*, 1794.

[16] K. Schürmann, J. Lahann, J. Meyer, H. Klosterhalfen, D. Vorwerk, D. Klee, R.W. Günther, *Radiology* **2004**, *230*, 151.

[17] A. Greiner, *Trends Polym. Sci.* **1997**, *5*, 12.

[18] D. Klee, N. Weiss, J. Lahann, "Vapor-Based Polymerization Of Functionalized [2.2]Paracyclophanes: A Unique Approach Towards Surface-Engineered Microenvironments" in *Paracyclophanes*, H. Hopf (ed.), VCH Weinheim, **2004**.

[19] V.I. Rozenberg, T.I. Danilova, E.V. Sergeeva, I.A. Shouklov, Z.A. Starikova, H. Hopf, K. Kuhlein*, Eur. J. Org. Chem*. **2003,** 432.

[20] B.D. Ratner, A.S. Hoffman, F.J. Schoen, J.E. Lemons, "Biomaterials Science". **1996,** Elsevier Science, USA.

[21] D. Briggs, G. Beamson, *Anal. Chem*. **1992**, *64*, 1729.

[22] C.H. Cheng, E.M. Pearch, *J. Poly. Sci: Poly. Chem. Ed*. **1980**, 18, 1883.

[23] B.D. Cullity, S.R. Stock, "Elements of X-ray Diffraction." 3rd Ed. **2001,** Prentice-Hall, Inc.

[24] S. Isoda, M. Tsuji, M. Ohara, A. Kawaguchi, *Polymer* **1983,** *24*, 1155.

[25] W.D. Niegisch, *J.Appl. Phys.* **1966,** *37*, 4001.

[26] All films were deposited at 10 ºC.

[27] J.J. Senkevich, S.B. Desu, V. Simkovic, *Polymer* **1999,** *41*, 2379.

[28] K.-Y. Suh, R. Langer, J. Lahann, *Adv. Mater.* **2004,** *16*, 1401.

[29] H.Y. Chen, J. Lahann, *Anal. Chem.* **2005**, *77*, 6909.

[30] J. Lahann, M. Balcells, H. Lu, T. Rodon, K.F. Jensen, R. Langer, *Anal. Chem.* **2003**, *75*, 2117.

CHAPTER 4

PRELIMINARY BIOCOMPATIBILITY OF COPOLYMER COATINGS

The materials in this chapter have been adapted with minor modifications from the following published article: Y. Elkasabi, M. Yoshida, H. Nandivada, H.Y. Chen, J. Lahann, *Macromolecular Rapid Communications* **2008**, 29, 855-870.

4.1 Background and Motivations

The fields of materials engineering and biointerface science are witnessing an increasing merger of concepts and applications.[1] While these two fields remained quite exclusive from each other only 40 to 50 years ago,[2] recent progress in biotechnological and medical applications has expedited and necessitated their fusion. Examples include, but are not limited to, the study of cell/matrix interactions,[3] micro total analytical systems (μTAS),[4] and scaffolds for tissue engineering.[5] More specifically, these applications require materials with sufficient mechanical integrity, while providing adequate contact properties within biologically-relevant environments. To date, many of the currently employed biomaterials still induce unfavorable responses, such as chronic inflammation[6] or blood coagulation.[7,8] One way of addressing these shortcomings is controlled surface modification, because interactions of the biomaterial surface with proteins and cells are among the key factors that govern these biological responses.[8,9] Methods such as plasma polymerization,[10] self-assembly of monolayers,[11] and spray coating[12] have been extensively used in the past to design materials which exhibit

defined surface chemistries; however, many of these methods fall short when devices with materials that diverge from well-defined model systems and non-planar geometry are used.[13] Although widely used, solution-based surface modification methods bear the risk of introducing coating non-uniformities and impurities.[14]

In this chapter, we focus on the synthesis and characterization of carbonyl-functionalized copolymers and elucidate important aspects of these coatings for future biomedical applications. We also assessed preliminary biocompatibility of these coatings in short-term experiments, using human umbilical vein endothelial cells and 3T3 murine fibroblasts.

4.2 Experimental Methods

Monomer Synthesis 4-Aminomethyl-[2.2]paracyclophane was purchased from Uniglobe Kisco, Inc. (White Plains, NY). 4-Amino-[2.2]paracyclophane was synthesized from [2.2]paracyclophane using an established synthesis route.[15] All carbonyl-functionalized PCPs were synthesized by Friedel-Crafts acylation of commercially available [2.2]paracyclophane (Uniglobe Kisco) as described previously.[16] All synthesized monomers were purified by column chromatography prior to CVD polymerization, and characterized by nuclear magnetic resonance spectroscopy (NMR), mass spectrometry (MS) and Fourier Transform infrared spectroscopy (FTIR).

CVD Polymerization All polymer coatings were synthesized using a custom-built CVD system.[17] For CVD polymerization, a total of 20-30 mg of either one or two different

functionalized [2.2]paracyclophane(s) was used. For co-polymerization, the molar ratios of amino-functionalized (-NH_2, -CH_2NH_2) and carbonyl-functionalized (-COC_6H_5, -COC_2H_5, -COC_2F_5, -$COCF_3$) PCPs (refer to Scheme 4.2) were varied to yield a previously specified target ratio of functional groups of the CVD coatings. To account for differences in the sublimation temperatures of different PCPs, charges of starting material were loaded individually into magnetically movable glass dishes. For CVD co-polymerization, the working pressure was 0.28 Torr and sublimation temperatures varied between 90 and 100 $^{\circ}$C. For different functionalized PCPs, the pyrolysis temperature changed with various functionalities. PCP-COC_6H_5 was activated at a pyrolysis temperature of 800°C in order for polymerization to occur, whereas all other monomers were cleaved at 670°C. Preparation of co-polymers (-COC_6H_5/-NH_2 and - COC_6H_5/-CH_2NH_2 required a pyrolysis temperature of 730°C. All other copolymers utilized a pyrolysis temperature of 670°C. Silicon, gold, stainless steel, or glass substrates were placed on a cooled sample holder (15°C; unless stated otherwise) for polymer deposition. Sample holder was rotated to ensured more uniform film deposition. For co-polymerization of varying molar feed ratios within one subgroup, all reaction conditions were maintained with the exception of the adjusted ratio of the two starting materials.

Surface Characterization X-ray photoelectron spectroscopy (XPS) data were recorded on an Axis Ultra X-ray photoelectron spectrometer (Kratos Analyticals, UK) equipped with a monochromatized AlKα X-ray source. All spectra were calibrated with respect to the non-functionalized aliphatic carbon with a binding energy of 285.0 eV. Coating thicknesses were recorded using EP^3-SW imaging ellipsometry (Nanofilm Technologie

GmbH, Germany) at a wavelength of 532 nm. Both nulling (four zones) and mapping experiments were performed at an angle of incident of 60°, and an anisotropic Cauchy model was used to model the ellipsometric parameters psi and delta. FTIR was performed on a Nicolet 6700 spectrometer utilizing the grazing angle accessory (Smart SAGA, Thermo) at a grazing angle of 85°.

X-ray Diffraction (XRD) To assess the crystallinity of functionalized PPX films, silicon substrates coated with the polymer of interest were examined by wide-angle XRD, using a Rigaku 12 kW high intensity rotary anode generator. All CVD films were examined both as deposited and after annealing. Prior to analysis, the polymer films were annealed for 14 hrs in an oven at a temperature of 120^oC.

Enzyme Linked Immunosorbent Assay (ELISA) Nunc 96 well plates and CVD-coated stainless steel disks placed in 24 well plates were coated with varying concentrations of human fibrinogen (Calbiochem) diluted in Dulbecco's PBS overnight at 4^oC. Surfaces were blocked (1% BSA in Dulbecco's PBS 25^oC, 1 hr), incubated with primary antibody (rabbit anti-human fibrinogen, Calbiochem, San Diego, CA; 1:8,000) in wash buffer (0.5% Tween20 in Dulbecco's PBS) for 1 hr at 25^oC, washed, and incubated with secondary antibody (goat anti-rabbit IgG H&L chain, peroxidase conjugate, Calbiochem, 1:10,000) in wash buffer for 1 hr at 25^oC. Upon washing, the surfaces were incubated with 2,2'-azino-bis-(3-ethylbenzthiazoline-6-sulfonic acid) (ABTS) for 20 min at 25^oC. The enzymatic reaction was terminated with a 0.5M H_2SO_4 stop solution and analyzed by absorbance measurement at 405 nm.

Growth of HUVECs and NIH3T3s on CVD-coated surfaces Human umbilical vein endothelial cells (HUVECs) (Cambrex, Walkersville, MD) or murine fibroblasts (NIH 3T3s) (ATCC, Manassas, VA) were cultured in tissue culture-treated polystyrene (TCPS) flasks (Corning, Lowell, MA), maintained at 37°C in a humidified atmosphere of 5% CO_2, and media replaced every other day until ~80% confluency was reached.

Functionalized PPX polymers and co-polymers were deposited on 18 mm, No. 1 glass cover slips. Polymer-coated cover slips were placed in sterile 12-well plates and incubated in Endothelial Growth Medium (Cambrex) prior to addition of cells. HUVECs were suspended at a density of $1x10^5$/ml, and added at 1 ml/well. Phase contrast micrographs were taken at 2 hrs and 24 hrs post-seeding. At 24 hrs post-seeding, substrates with adherent cells were processed for immunocytochemistry. Samples were fixed and permeabilized (4% paraformaldehyde, 0.5% TritonX-100 in Dulbecco's PBS) for 15 min, blocked (1% BSA) for 30 min, and stained with a primary antibody (1:400 anti-vinculin, Sigma, 1:400). Upon washing, cells were blocked (5% normal goat serum, (Zymed, Carlsbad, CA)) then stained with secondary antibody (Alexa Fluor 488-conjugated goat anti-mouse IgG1 (Invitrogen, Carlsbad, CA)), followed by rhodamine-conjugated phalloidin (Invitrogen). Finally, samples were mounted with Prolong Gold with DAPI (Invitrogen) for analysis by confocal microscopy.

NIH3T3s were grown on CVD-coated stainless steel disks or PVC films at a density of $7.5x10^4$/ml in 24 well plates. All substrates were UV-sterilized for 30 min prior to addition of cells. After 24 hrs in culture, substrates were fixed, permeabilized, then stained with rhodamine-conjugated phalloidin and Hoechst 33342 (Invitrogen).

Substrates were mounted on cover slips with Prolong Gold, and imaged by confocal microscopy. All fluorescently-labeled cells were visualized using Zeiss LSM 510 confocal microscope at the Microscopy & Image Analysis Laboratory of the University of Michigan.

Glucose 6-phosphatase Dehydrogenase (G6PD) Release Upon culturing NIH3T3 cells on bare or CVD-coated stainless steel disks for 24 hrs, cell culture media was collected and cleared by centrifugation at 1200 rpm for 5 min. Growth media alone or media from cells grown on TCPS, or that from lysed cells (0.1% TritonX-100 for 5 min) were used as controls. Cleared media were analyzed for G6PD content by Vybrant Cytotoxicity Assay Kit (Molecular Probes) per manufacturer's directions. Fluorescence values (ex/em: 544/590) were recorded every 5 min after addition of 2x resazurin reaction mixture to the well at 37°C. For statistical analysis, results from all surfaces were compared to those of live cells grown on TCPS, using $p<0.01$.

Statistical Analysis Statistical analysis was performed using a general linear model ANOVA with Minitab software (Version 13.20, Minitab, State College, PA, USA). Unless otherwise indicated, p-values of 0.05 were considered significant. Experiments were repeated as indicated.

NMR Studies Carbonyl-functionalized p-xylenes were synthesized following an approach slightly modified from the synthetic procedures described for the corresponding PCPs. Model reactions of the carbonyl groups with hexanoic hydrazide were performed

in an NMR tube and sequence of ^{1}H NMR (Varian Inova, 400 MHz) spectra was collected in real-time. Prior to starting the reaction, a base ^{1}H NMR spectrum was taken as a reference. A slight excess of hexanoic hydrazide (1.1 equivalents) was dissolved in deuterated ethyl alcohol, and the functionalized *p*-xylene was added. Next, acetic acid was added to initiate the reaction, and data acquisition was started immediately after the sample was placed in the NMR spectrometer. NMR spectra were acquired every 7 minutes for two hours, and a final measurement was taken after 12 hrs.

r-Hirudin Immobilization and Binding Assay. CVD-coated surfaces were incubated with hexamethylene diisocyanate (HDI) (1:10 w/w in absolute diethyl ether) for 24 hrs in argon atmosphere. The surfaces were then washed via Soxhlet extraction in absolute diethyl ether for 6 hrs and dried under vacuum. Hirudin was immobilized by incubating the surfaces with an N-terminal protected hirudin (500 nmol/ml in water) at 4°C for 24 hrs.[18] The surfaces were washed extensively using wash buffer (PBS containing 0.1% Tween-20). The protecting group was cleaved by exposing the surface to piperidine solution (10% in deionized (DI) water) at 0°C for 3 hrs, and substrates were washed rigorously.

Hirudin binding was measured via an amidolytic assay (chromogenic assay) for thrombin. The surfaces were incubated with thrombin solution (20 U/ml in PBS, pH 7.4, Sigma-Aldrich, MO) for 30 min at 25°C, to which thrombin-active chromogenic substrate (S-2238, 1 mmol/L in DI-water; DiaPharma Group Inc., OH) was added. The reaction was stopped after 120 s with acetic acid (20 %), and the resulting colored solution was transferred to cuvettes for UV absorption reading at 405 nm.

Heparin Immobilization and Binding Assay. CVD-coated substrates were incubated with a 500 mM solution of adipic acid dihydrazide (Sigma-Aldrich, MO) in PBS for 24 h. The substrates were then washed with wash buffer (PBS with 0.1% Tween20). These hydrazide-functionalized substrates were immersed in heparin solution (1 mg/ml in water, Sigma-Aldrich, MO) overnight at 50°C, washed with the wash buffer and finally rinsed with water. To quantify heparin immobilization, 1 ml of Toluidine blue (0.0005%, Sigma-Aldrich, MO) was placed with the heparin-modified surface and shaken vigorously, to which 1 mL of n-hexane was added. After the organic layer (containing the heparin-toluidine blue complex) was removed, the absorbance of the aqueous layer was measured by UV spectrophotometry at 631nm.

4.3 Results and Discussion

4.3.1 Mono-Functionalized CVD Coatings

CVD-based PPXs offer a high degree of flexibility for functional groups that can be introduced and therefore provide a very versatile chemical modification platform. Such a strategy, however, requires synthesis of the appropriate PCPs and subsequent vapor deposition of well-defined reactive coatings (Scheme 4.1), while maintaining the integrity of the functional groups under the conditions of CVD polymerization. Among the many reactive coatings that have been synthesized,[19] carbonyl-functionalized polymers are of particular interest because of their favorable deposition properties and their selectivity towards hydrazide-functionalized ligands.[20] When conducting CVD polymerization of functionalized PCPs ($-COC_6H_5$, $-COC_2H_5$, $-COC_2F_5$, $-COCF_3$),
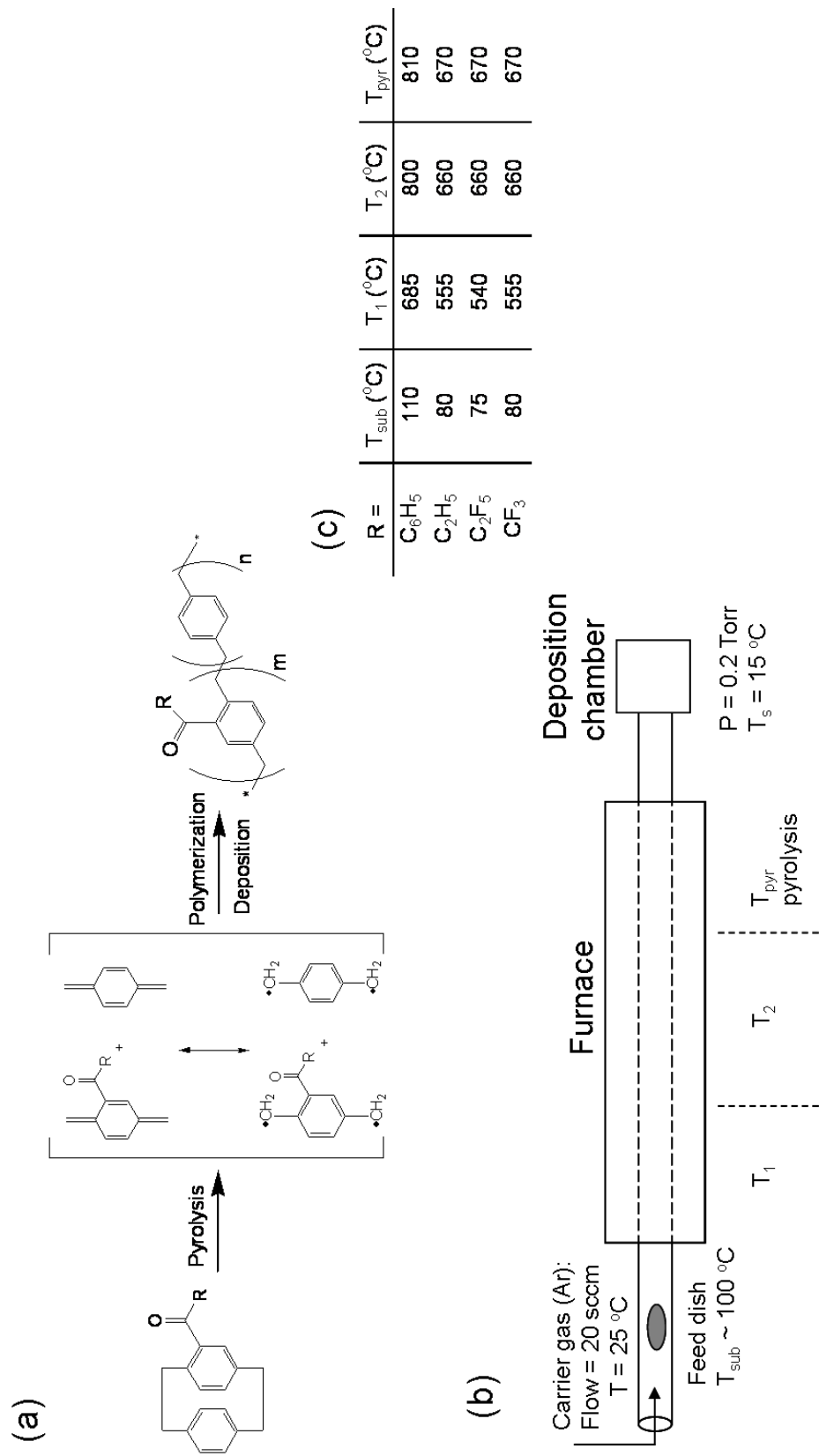
Scheme 4.1. (a) Mechanism for the CVD polymerization of carbonyl-functionalized PCPs to produce corresponding PPXs. (b) Schematic diagram of CVD process. (c) CVD process conditions required for PPX deposition.

R =	T_{sub} (°C)	T_1 (°C)	T_2 (°C)	T_{pyr} (°C)
C_6H_5	110	685	800	810
C_2H_5	80	555	660	670
C_2F_5	75	540	660	670
CF_3	80	555	660	670

transparent polymer films with excellent adhesion were obtained for silicon, gold, stainless steel, and glass substrates. While the substrates used in this study were flat, we have recently demonstrated that the CVD process is also amenable to the coating of microspheres.[21] In addition, a range of complex patterns can be created using masking techniques during CVD polymerization.[22] FTIR spectra of the polymers are shown in Figure 4.1 and correspond well with the expected polymer structures.[23,24] Strong carbonyl stretches were present in the range of 1720 – 1660 cm^{-1} in all spectra. Characteristic C-H stretches which are due to aromatic hydrogen atoms were present between 3050 – 2910 cm^{-1}. In addition, the spectrum of PPX-COC$_2$H$_5$ revealed a higher intensity band at 2930 cm^{-1}, indicative of aliphatic hydrogen atoms. Strong FTIR bands between 1204 and 1170 cm^{-1} are due to the fluorinated alkyl groups present in polymers PPX-COC$_2$F$_5$ and PPX-COCF$_3$. Collectively, the FTIR spectra shown in Figure 4.1 confirm the expected structures of carbonyl-functionalized polymers.

It has been previously observed that PPX derivatives with different functional groups can either be semi-crystalline or amorphous.[25,26] In fact, even subtle differences in the side group structure can influence the crystallinity of the polymer films. Therefore, XRD was used to assess the differences amongst the four different carbonyl-functionalized polymers, and the results were compared to unfunctionalized PPX (parylene N). Upon deposition, XRD spectra of all polymers except for the unfunctionalized PPX were void of any detectable signals indicating that these polymers were amorphous (data not shown). After annealing at 120°C for 14 hrs, however, the fluoroalkyl-containing polymers (PPX-COC$_2$F$_5$ and PPX-COCF$_3$) underwent significant chain remodeling as indicated by the appearance of sharp signals at 10.7° and 21.2°
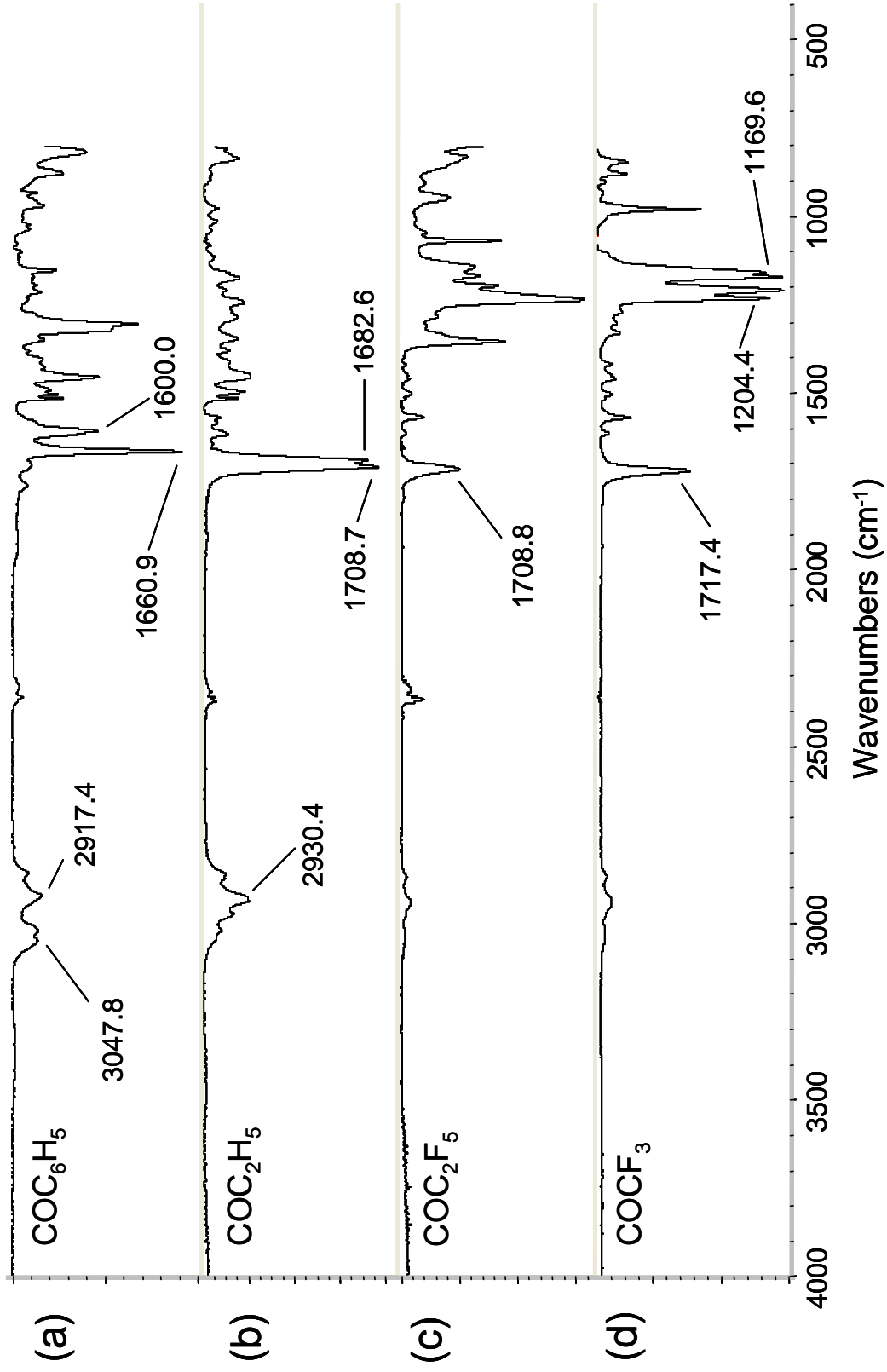
Figure 4.1 FTIR spectra of PPX polymers containing the following functional modifications: (a) COC_6H_5, (b) COC_2H_5, (c) COC_2F_5, and (d) $COCF_3$.

(PPX-COCF$_3$), as well as 18.4^o (PPX-COC$_2$F$_5$) (Figure 4.2). In fact, these polymers underwent a transition from an amorphous polymer to become semi-crystalline. In contrast, -COC$_6$H$_5$ - and -COC$_2$H$_5$-functionalized PPX coatings remained amorphous (Figure 4.2), even after exposure to identical annealing conditions.
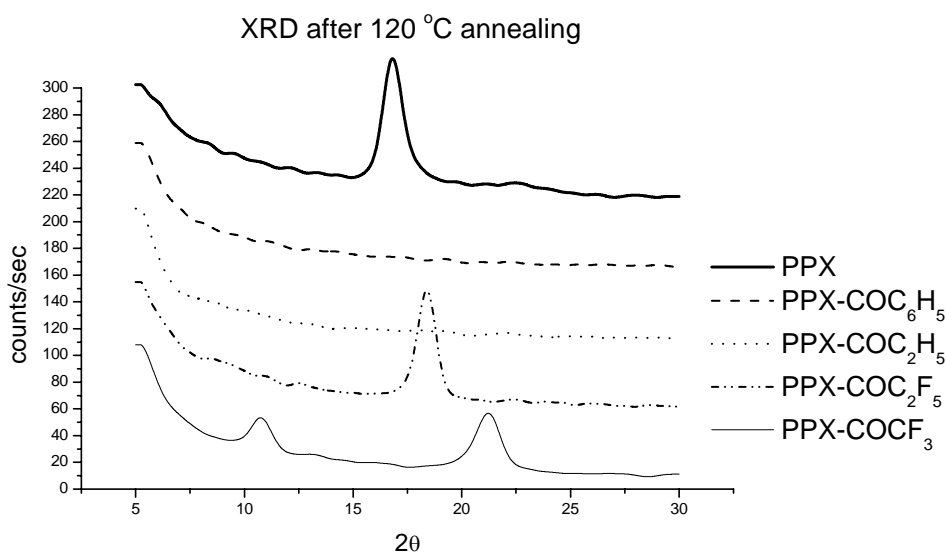
Figure 4.2 XRD of carbonyl-functionalized polymers upon annealing at 120°C for 14 hours.

Next, short-term cell adhesion on these polymers was examined by culturing human umbilical vein endothelial cells (HUVECs). As these experiments were intended to serve as baseline assessment of studies with the copolymers described later in this chapter, we included four carbonyl-functionalized PPXs along with two amine-functionalized coatings (poly(4-aminomethyl-*p*-xylylene-*co*-*p*-xylylene) and poly(4-amino-*p*-xylylene-*co*-*p*-xylylene)). In addition, a poly(L-lysine) (PLL)-coated surface and cytotoxic poly(vinyl chloride) (PVC) were used as positive and negative controls, respectively. As shown in Figure 4.3a, HUVECs grown on PLL are spread out and present extensive actin cytoskeletal network, suggestive of growth-conducive interactions

with the substrate. Interestingly, HUVECs cultured on the two amino-functionalized PPXs (Figure 4.3b and c) showed cell morphology similar to those cultured on PLL-coated glass substrate. In contrast, HUVECs grown on carbonyl-functionalized PPXs
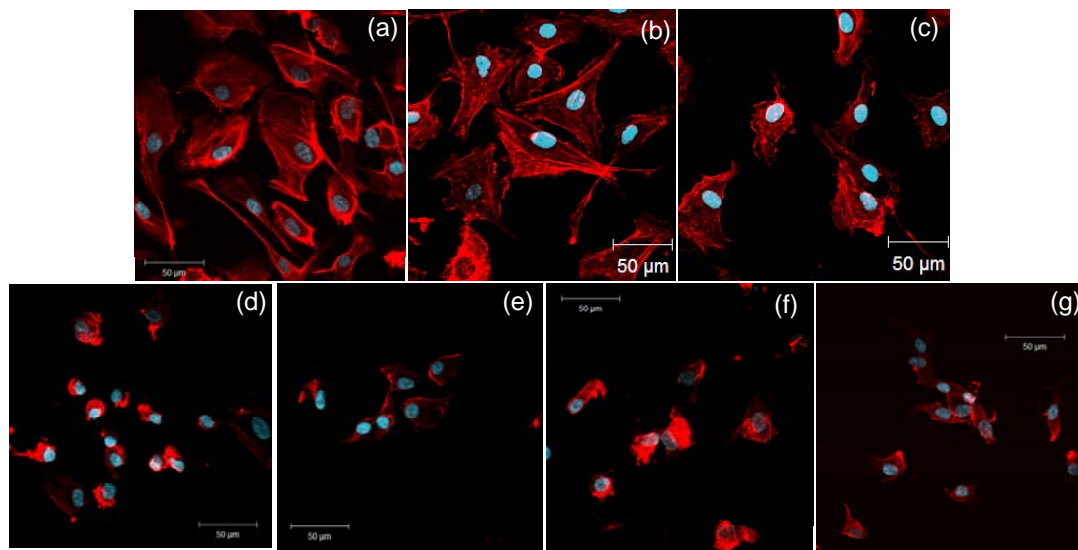
Figure 4.3 Confocal microscopy images of HUVECs grown on (a) poly(L-lysine) coated cover slip, (b) PPX-CH$_2$NH$_2$, (c) PPX-NH$_2$, (d) PPX-COC$_6$H$_5$, (e) PPX-COC$_2$H$_5$, (f) PPX-COC$_2$F$_5$, and (g) PPX-COCF$_3$ surfaces. Red: actin cytoskeleton (rhodamine-phalloidin), blue: nucleus (DAPI). n=3, representative images shown. All scale bars are 50 μm.

presented different morphologies, as shown in Figure 4.3d – g; these cells appeared smaller and were less spreadout, to various extent, as compared to those grown on PLL-coated cover slips or on amino-functionalized PPX. In addition, fewer cells adhered on these surfaces as observed by phase contrast micrographs of cells in culture up to 24 hrs (data not shown). These findings suggest that the carbonyl-functionalized PPX may be less conducive to cell adhesion as compared to amino-functionalized PPX, as HUVECs minimize contact with these polymer surfaces. In addition, presence of vinculin was evaluated for these cells by immunocytochemistry. Vinculin is a membrane/ cytoskeletal protein, and a component of focal adhesion protein complex, which binds actin

cytoskeleton to link cells to its substrate via adhesion molecules.[27] Immunostaining revealed increased numbers of punctuate vinculin staining on cells cultured on PLL- and amino-functionalized PPX-coated surfaces relative to those cultured on carbonyl-functionalized PPX coatings (data not shown). These results corroborate the findings of more spreadout morphology of cells on PLL and amino-functionalized PPX surfaces in that cell adhesion on these substrates is likely stronger than that of cells on carbonyl-functionalized PPX. Together, results from this preliminary study suggest that differences in the functional side groups of carbonyl-functionalized PPXs can result in polymer coatings, with a wide range of different biological responses.

4.3.2 Multi-Functionalized CVD Coatings

Studies described thus far evaluated surfaces coated with a single type of PPX. In next set of experiments, multifunctional coatings which simultaneously present multiple chemical functional groups on the surfaces, were prepared by copolymerizing an amino-functionalized PCP ($-NH_2$ or $-CH_2NH_2$) with a carbonyl-functionalized PCP ($-COC_6H_5$, $-COC_2H_5$, $-COC_2F_5$, or $-COCF_3$), as outlined in Scheme 4.2. In these experiments, the relative ratio of amino- versus carbonyl- groups was varied by altering the ratio of starting amounts of different PCPs used for CVD polymerization. For a given copolymer combination, all other process parameters, including total amount of starting materials, pressure, and sublimation, pyrolysis, and deposition temperatures were kept constant.

By adjusting the ratio of monomers loaded into the CVD sublimation zone, different molar ratios were prepared for each polymer combination, resulting in a variety of co-polymers. For this approach to be successful, special care was taken to ensure that

amines	A	B
$X_1 =$	NH_2	NH_2

ketones	1	2	3	4
$X_2 =$	O C_6H_5	O C_2H_5	O C_2F_5	O CF_3
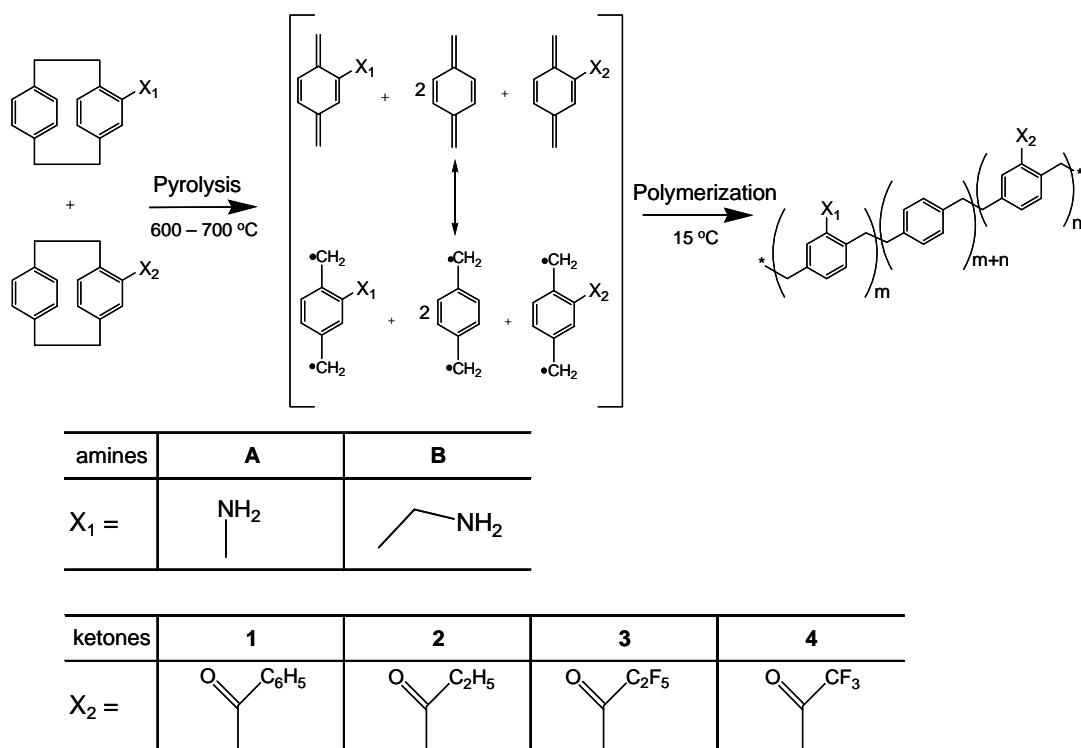
Scheme 4.2 Mechanism for CVD copolymerization of two different PCPs

the deposition rates of both PCPs were similar. To illustrate generalized trends, selected

FTIR spectra are shown in Figures 4.4 and 4.5. Figure 4.4 shows FTIR spectra for co-

polymer PPX-NH$_2$/-COC$_2$F$_5$ deposited in 5 different ratios as well as spectra of the

mono-functional polymers PPX-NH$_2$ and PPX-COC$_2$F$_5$ as references. FTIR bands of

characteristic of N-H bond occur at 3461.5 and 3380.7 cm^{-1}, whereas stretches

characteristic of COC$_2$F$_5$ occur at 1711.2 cm^{-1} (C=O), 1351.3 cm^{-1}, and 1231.0 cm^{-1} (C-

F). Even for ratios with low carbonyl content, C-F stretches was clearly distinguished. As

the amount of PPX-COC$_2$F$_5$ was increased, ratios of peaks characteristic to NH$_2$ stretches

and COC$_2$F$_5$ changed accordingly. A characteristic band at 1625.9 cm^{-1} was detected in

all amino-containing polymers. Likewise, PPX-CH$_2$NH$_2$/-COC$_2$H$_5$ co-polymers showed

similar trends in the FTIR spectra as the ratio of amount of starting material was varied
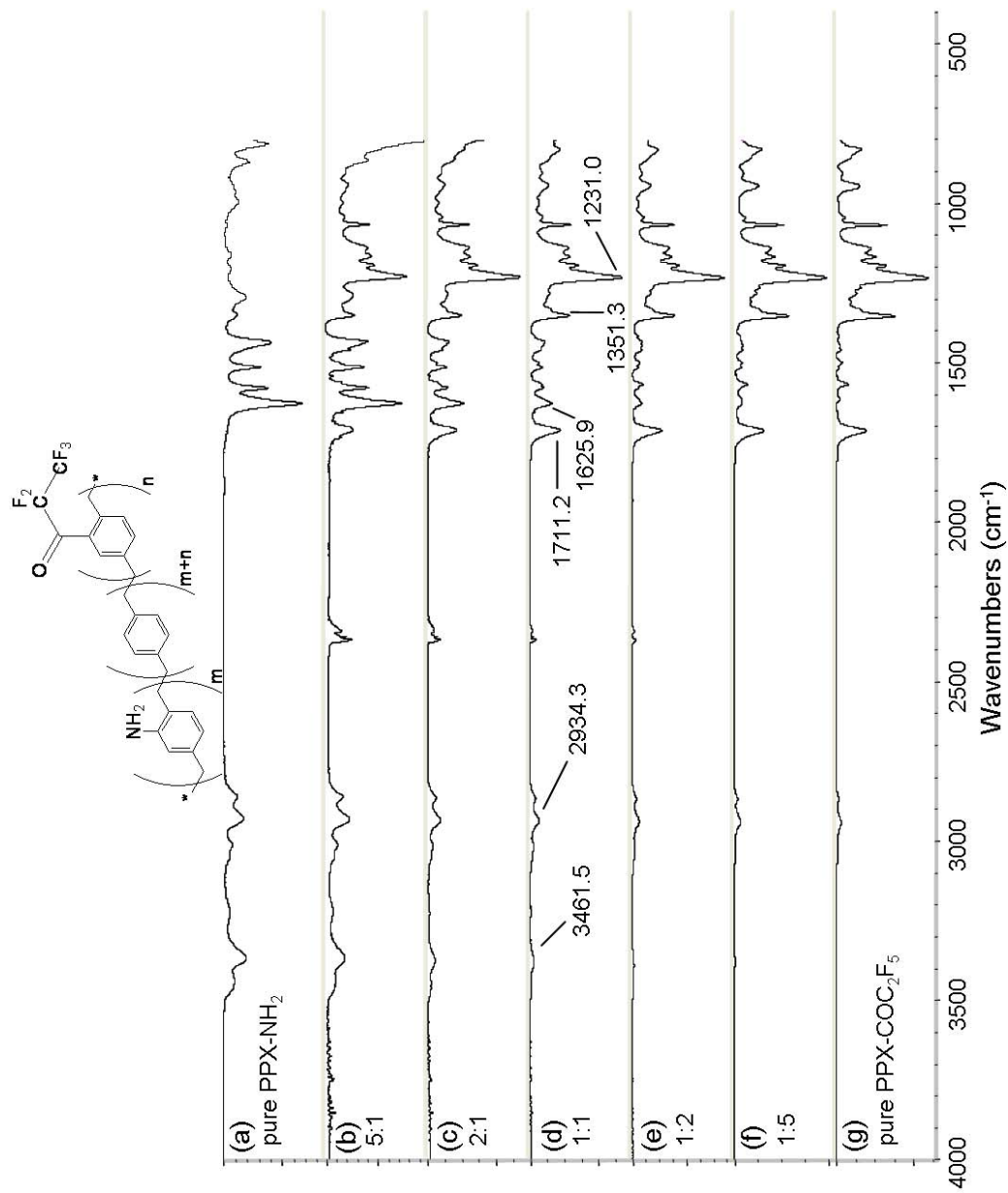
Figure 4.4 FTIR spectra of CVD copolymer (-NH$_2$/-COC$_2$F$_5$), co-polymerized in different molar ratios of PPX-NH$_2$: PPX-COC$_2$F$_5$. (a) pure PPX-NH$_2$ (b) 5:1 (c) 2:1 (d) 1:1 (e) 1:2 (f) 1:5 (g) pure PPX-COC$_2$F$_5$.
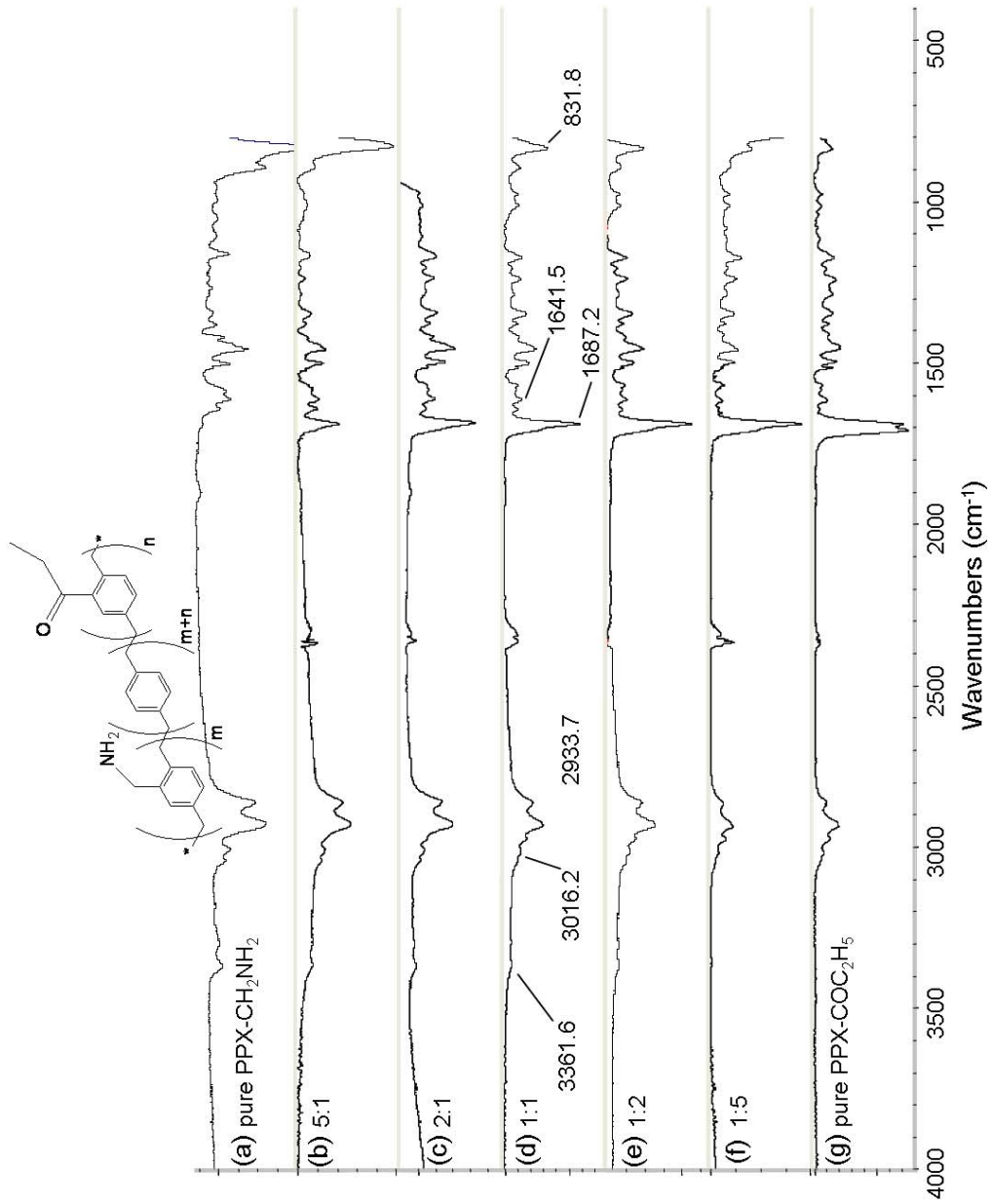
Figure 4.5 FTIR spectra of CVD copolymer ($-CH_2NH_2/-COC_2H_5$) co-polymerized to different molar ratios of PPX-CH_2NH_2: PPX-COC_2F_5. (a) pure PPX-CH_2NH_2 (b) 5:1 (c) 2:1 (d) 1:1 (e) 1:2 (f) 1:5 (g) pure PPX-COC_2H_5.

systematically (Figure 4.5). For example, bands at 3361.6 and 1641.5 cm^{-1} were distinct until ratio of 1:2 was reached. Vibration at 1641.5 cm^{-1} is characteristic of NH$_2$ scissoring stretches, while vibration at 3361.6 cm^{-1} indicates N-H stretches. As the concentration of PPX**-**COC$_2$H$_5$ increased, these vibrations gradually disappeared. Other subtle changes in FTIR spectra include a change in C-H bands with respect to their relative intensities; with increasing content of PPX-CH$_2$NH$_2$ in the co-polymer, an increase in the aliphatic C-H bands due to the COC$_2$H$_5$ group was observed. There appears to be no evidence of cross-reaction between the amine and carbonyl functional groups, as indicated by imine stretch (1655 cm^{-1}) (Figures 4.4 and 4.5). In addition, for each co-polymer spectrum, all FTIR bands can be accounted for based on the spectra of the constituting mono-functional polymers (Figure 4.1).

Although FTIR spectra indicated agreement of the bulk co-polymer composition with the loaded monomer ratio, this method has limited surface sensitivity and provides averaged information of the entire polymer films. To assess the actual surface composition of the co-polymer films, surfaces were analyzed by XPS, which can detect the atomistic composition of a surface, usually within 5-10 nm. This technique can provide a survey spectrum of all atoms present, as well as a high-resolution scan that provide information about the binding state of a particular element. Table 4.1 summarizes the chemical composition of all 1:1 ratios of the entire group of amino/carbonyl co-polymers. Experimental data are compared to theoretical values obtained on the basis of the starting materials assuming a 1:1 ratio of the two PCPs. Generally, all co-polymers demonstrated good agreement between experimental values and theoretical compositions. All high-resolution C$_{1s}$ spectra revealed $\pi \rightarrow \pi^*$ transitions, which are characteristic of

	COC$_6$H$_5$ (1)		COC$_2$H$_5$ (2)		COC$_2$F$_5$ (3)		COCF$_3$ (4)	
	X$_2$							
	exper	theor	exper	theor	exper	theor	exper	theor

NH$_2$ series (A)

	exper	theor	exper	theor	exper	theor	exper	theor
F	---	---	---	---	15.35	14.37	11.8	9.43
O	1.69	2.04	5.04	2.70	4.56	2.87	5.42	3.14
N	2.01	2.04	2.66	2.70	2.61	2.87	3.71	3.14
C (total)	96.3	95.92	92.29	94.59	77.48	79.89	79.06	84.28
C-C	84.01	87.76	76.26	83.78	60.53	68.39	66.02	74.85
C-N	2.33	2.04	2.33	2.70	2.54	2.88	2.17	3.14
C-C=O	3.8	4.08	4.58	5.41	---	---	---	---
C=O	1.91	2.04	4.37	2.70	3.39	2.88	4.25	3.14
π → π*	4.25	---	4.76	---	4.04	---	3.07	---
CF$_3$	---	---	---	---	3.49	2.88	3.56	3.14
CF$_2$	---	---	---	---	3.49	2.88	---	---

CH$_2$NH$_2$ series (B)

	exper	theor	exper	theor	exper	theor	exper	theor
F	---	---	---	---	17.18	13.97	8.54	9.15
O	1.9	2.00	2.63	4.49	4.84	2.79	5.35	3.05
N	1.23	2.00	2.63	2.36	1.90	2.79	2.84	3.05
C (total)	96.87	96.00	94.74	93.15	76.08	80.45	83.26	84.76
C-C	86.46	88.00	79.40	82.80	59.14	69.28	71.40	75.61
C-N	1.30	2.00	2.55	2.59	2.41	2.79	2.50	3.05
C-C=O	3.65	4.00	5.36	5.18	---	---	---	---
C=O	1.88	2.00	3.77	2.59	3.67	2.79	2.67	3.05
π → π*	3.58	---	3.66	---	2.94	---	3.43	---
CF$_3$	---	---	---	---	3.96	2.79	3.25	3.05
CF$_2$	---	---	---	---	3.96	2.79	---	---

Table 4.1. Elemental compositions of CVD co-polymers containing 1:1 ratios of (a) (PPX-NH$_2$):(PPX-R) (b) (PPX-CH$_2$NH$_2$):(PPX-R), as determined by XPS. Atomic composition results are shown on the top half of each table, while high resolution C$_{1s}$ spectra results are shown on the bottom. Theoretical calculations are based upon ideal deposition of the copolymer ratio.

aromatic polymers.[28] Nevertheless, discrepancies existed between experimental results and theoretically calculated values. Even though a 1:1 monomer loading ratio is used, fluctuations in ratios can occur during monomer sublimation.

4.3.3 Biocompatibility Studies

In order for such a polymer to function as an advanced biointerface, its compatibility with cells must be assessed. We have demonstrated the ability of co-polymer PPX-CH_2NH_2/-$COCF_3$ to immobilize multiple ligands in defined ratios,[26] but its short-term biocompatibility has not yet been tested. As shown in Figure 4.3, general differences among the homopolymers existed with regard to HUVEC attachment and morphology. To study the biocompatibility of co-polymers, we investigated several cellular responses upon culture on CVD films. Initially, protein adsorption on these CVD polymer coatings was evaluated using fibrinogen as a model protein. Fibrinogen was chosen as a model protein due to its role in blood coagulation.[29] As many biologically relevant devices contact blood upon implantation, fibrinogen adsorption behavior may be
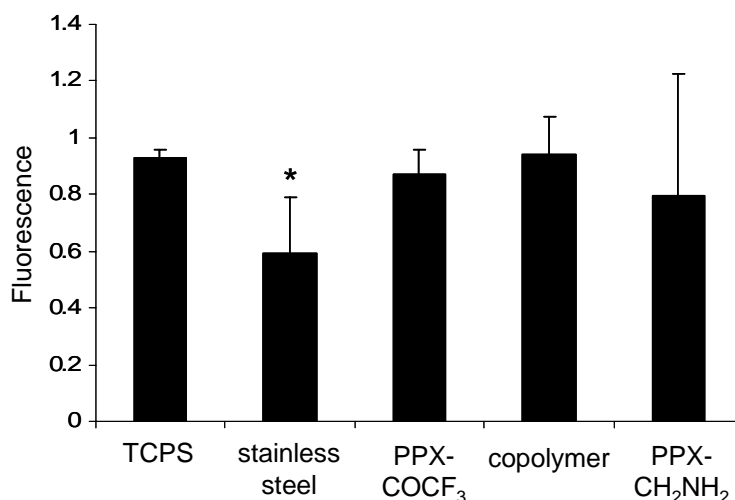
Figure 4.6 Fibrinogen adsorption on various substrates. Normalized fluorescence values are reported. Results were compared to TCPS. n=3, *: $p<0.05$.

an important indicator for potential pro-thrombotic activity. As shown in Figure 4.6, adsorption of fibrinogen on CVD surfaces evaluated (mono-functional polymers PPX-CH_2NH_2 and PPX-$COCF_3$ and PPX-CH_2NH_2/-$COCF_3$ at 1:1 ratio) was not significantly different from that of TCPS, but higher than on stainless steel.

As cell attachment onto CVD surfaces supports potential biomedical applications of CVD polymer coatings, biocompatibility of these coatings was assessed using NIH3T3 fibroblasts. These cells were cultured and grown on various CVD surfaces and their release of glucose-6-phosphate dehydrogenase (G6PD) was measured. This enzyme is normally intracellular but upon compromise in cell membrane integrity or lysis, is
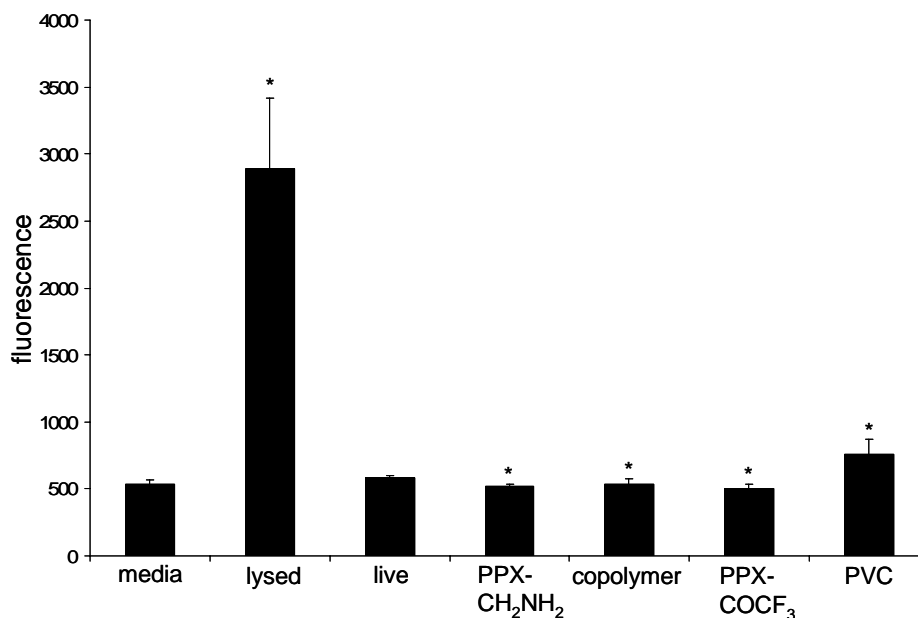
Figure 4.7 G6PD release from NIH 3T3s grown on various substrates. Fluorescence values are reported. Results are compared G6PD measured in media supporting live cells. n=3, *: $p < 0.05$.

released into the surrounding media.[30] Thus, the amount of G6PD detected in cell culture media may be indicative of surface cytotoxicity. As compared to media of live cells, significantly higher amounts of G6PD were detected in media of lysed cells and

those grown on PVC (Figure 4.7). In contrast, lower G6PD release was observed from cells grown on PPX-CH$_2$NH$_2$, the 1:1 co-polymer ratio, and PPX-COCF$_3$ as compared to live cells, suggesting that CVD surfaces may not cause cell death or lysis above that of cells cultured on TCPS at the time point evaluated.

Morphologies of NIH3T3 fibroblasts grown on CVD homopolymers and copolymer PPX-CH$_2$NH$_2$/-COCF$_3$ were evaluated (Figure 4.8). As expected, murine fibroblasts showed reduced growth on PVC disks, as many of the initially seeded cells did not adhere or were detached during washing steps. Cells that remained adherent were small in size and round in shape, suggesting lack of spreading and contact with the surface. NIH3T3s grown on surfaces PPX-CH$_2$NH$_2$ and PPX-CH$_2$NH$_2$/-COCF$_3$ showed morphologies comparable to those grown on PLL cover slip, with cell spreading as
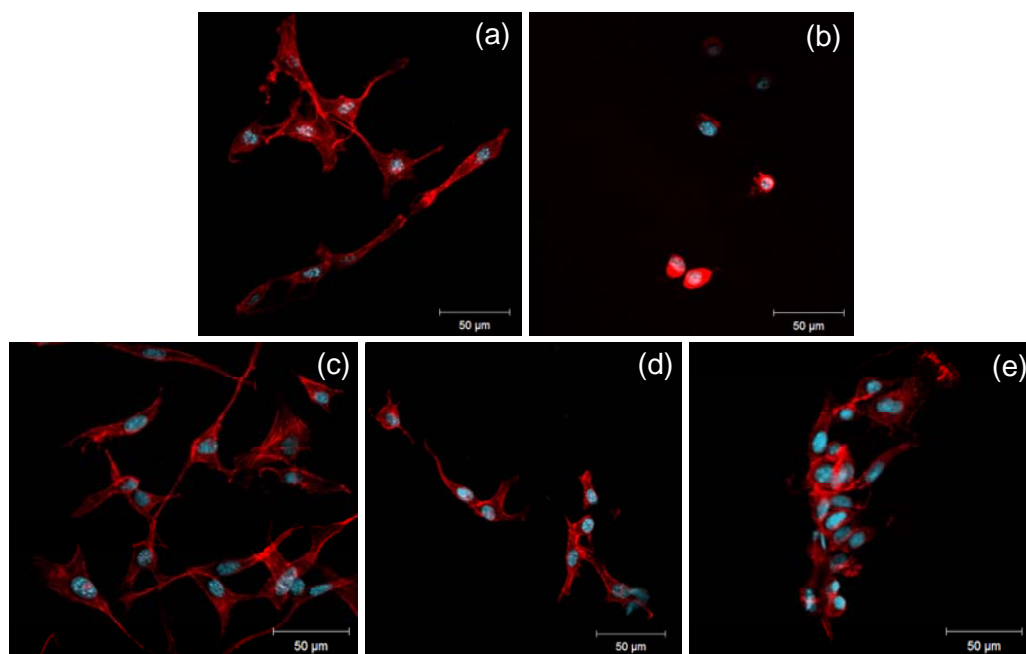
Figure 4.8 Confocal microscopy images of NIH 3T3 murine fibroblasts grown on (a) poly(L-lysine) coated cover slip, (b) polyvinyl chloride film, (c) PPX-CH$_2$NH$_2$, (d) 1:1 ratio of PPX-CH$_2$NH$_2$ and PPX-COCF$_3$, (e) PPX-COCF$_3$ surfaces. Red: actin cytoskeleton (rhodamine-phalloidin), blue: nucleus (DAPI). n=3, representative images shown. All scale bars are 50 μm.

indicated by actin filaments. On PPX-COCF$_3$, cells mostly aggregated, although more cells remained adherent on this surface and more spreading was observed than on PVC. In this set of experiments, introduction of polymer PPX-CH$_2$NH$_2$ to polymer PPX-COCF$_3$, as copolymer PPX-CH$_2$NH$_2$/-COCF$_3$, improved NIH3T3 adhesion to the polymer coating.

4.3.4 Reactivity Study

An ultimate goal of developing carbonyl-functionalized co-polymers is to simultaneously immobilize multiple ligands. For the purpose of having orthogonal reactivity under physiological conditions, it is necessary to understand the relative chemical reactivity of the different carbonyl groups towards target molecules (hydrazides). In this context, we analyzed the reaction kinetics of these different carbonyl functionalities using *in situ* ^{1}H NMR. Rather than reacting functionalized PCP monomers, we chose to synthesize correspondingly functionalized *p*-xylenes, because the constrained ring system of PCPs significantly alters the chemical reactivity of PCPs and disqualify them as model reactants for PPXs. Functionalized *p*-xylenes may be considered as the smallest repetition unit of the polymer coatings, and therefore more closely resembles the PPX chain.

By integrating two specific peaks on the NMR spectra, one characteristic of the reactants (-C<u>H</u>) and the other one indicating the product (-C=N-N<u>H</u>), the percent yield of product was evaluated. Measurement frequency was decreased when the percent yield reached a plateau. The percent yields were plotted as a function of time for the different reactions with functionalized *p*-xylene derivatives. Figure 4.9 shows kinetic curves fitted

to the experimental data. For most *p*-xylenes, NMR peaks characteristic of the product were evident within 15-20 minutes of initiating the reaction. NMR spectra for benzoyl-functionalized *p*-xylene showed no signals that were characteristic of the product over reaction durations as long as 15 hrs. The fluorinated keto group was more reactive than non-fluorinated groups. Of the functional groups, $COCF_3$ was the most reactive, followed by COC_2F_5, COC_2H_5, and COC_6H_5 in order of decreasing reactivity. Benzoyl (COC_6H_5) group yielded essentially no product within the evaluated reaction times. On the basis of these experiments, the trifluoroacetyl ($COCF_3$) group was selected for further multifunctional surface immobilization.
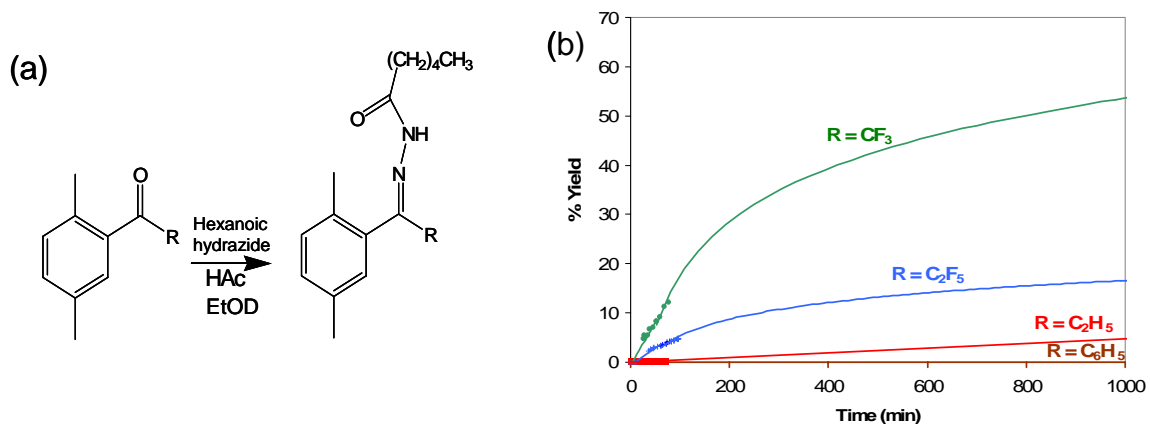
Figure 4.9 (a) Protocol used to determine the reaction kinetics of different carbonyl-PPXs, using functionalized *p*-xylenes as test molecules. (b) Percent yield of carbonyl reactions with respect to time, based upon ^{1}H NMR of characteristic reactant/product peaks.

For surface immobilization, we used r-hirudin, a recombinant protein which deactivates thrombin. Thrombin plays a central role in blood coagulation and mediates restenosis.[31] Thus, the immobilization of hirudin may be one remediation approach for blood-contacting devices, such as cardiovascular stents. In addition, heparin, a highly-sulfated glycosaminoglycan anticoagulant, was utilized for immobilization. Hirudin and

94

heparin are expected to be immobilized onto copolymer coating of -CH_2NH_2/-$COCF_3$ through aminomethyl group via a diisocyanate linker[32] and carbonyl groups via adipic acid dihydrazide,[20] respectively.

For r-hirudin immobilization, the substrates were incubated with hexamethylene diisocyanate, which is reactive towards amine groups.[18] FTIR spectroscopy confirmed the presence of isocyanate (NCO) group on the amine and the copolymer surfaces with a stretch at 2275 cm^{-1}, which was absent in the FTIR spectra of the ketone surfaces. After immobilization, r-hirudin was deprotected to restore biomolecular activity, and its binding capacity was measured via a chromogenic substrate (S-2238) for thrombin.[18] In this assay, surface-bound hirudin complexes thrombin, whereas free thrombin cleaves the chromogenic substrate. As shown in Figure 4.10a , the absorbance was lower for amine-containing homopolymer PPX-CH_2NH_2 and the co-polymer PPX-CH_2NH_2/-$COCF_3$, as compared to control surface of stainless steel, indicating a higher amount of surface-bound hirudin on the surfaces of PPX-CH_2NH_2 or PPX-CH_2NH_2/-$COCF_3$. Immobilized heparin was photometrically quantified using toluidine blue test.[33] As the activity of surface-bound heparin increases, more dye is surface-bound, leaving less dye in the solution, yielding a lower UV-absorbance. Figure 4.10b shows that the absorbance/cm^2 was lowest for PPX-$COCF_3$ compared to the co-polymer PPX-CH_2NH_2/-$COCF_3$ and the stainless steel control, indicating a higher amount of heparin bound to PPX-$COCF_3$.

While these results demonstrate successful reactivity of the co-polymer towards both molecules, precise control of number of molecules immobilized to the surface poses a challenge. Theoretically, the co-polymer contains half the number of active immobilization sites compared to the homopolymer. However, this preliminary study

suggests that not all groups are used for r-hirudin immobilization. This may be due to steric hindrances, whereby immobilization of r-hirudin onto CH_2NH_2 groups results in masking of other CH_2NH_2 sites available for immobilization. As such, appropriate choice of spacers for the successful control of the ratio of immobilized agents will be among the future challenges.
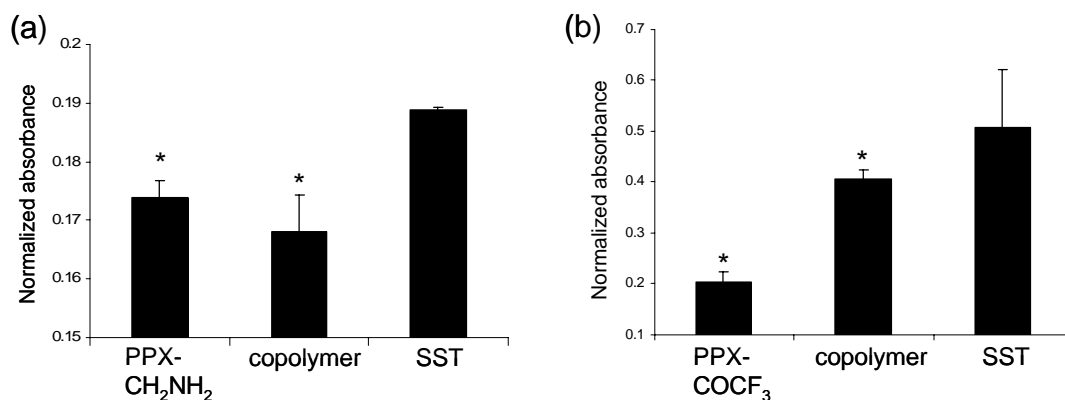
Figure 4.10 (a) Hirudin binding as measured by chromogenic assay. Normalized absorbance at 405 nm are reported. n=3, *: $p<0.05$ compared to stainless steel. (b) Heparin binding as measured by Toluidine Blue absorbance. Normalized absorbance at 631 nm are reported. n=3, *: $p<0.05$ compared to stainless steel.

4.4 Conclusions

We have demonstrated versatility and activity of carbonyl-functionalized PPXs polymerized from functionalized PCPs. Compositions of these polymers, both within the bulk coating and at the surface, were verified by FTIR and XPS. The carbonyl-functionalized polymers also exhibit drastic differences in crystallinity, which can be attributed to compositional changes of the functional group. These subtle changes also resulted in altered cellular morphologies on surfaces coated with CVD polymers.

In addition, we also copolymerized carbonyl-functionalized paracyclophanes with amine-functionalized molecules. The resulting copolymers possessed mechanical integrity and were dually-reactive through the presence of amine and carbonyl groups. FTIR spectra illustrated control of copolymer compositions, which were relatively homogeneous over several inches. These copolymers showed potential use as biomedical coatings as determined by protein adsorption, cell adhesion, cytotoxicity assay, and immobilization of antithrombotic drugs.

References

[1] A. Chilkoti, J.A. Hubbell, *MRS Bulletin* **2005**, 30, 175.

[2] R. Langer, D.A. Tirrell, *Nature* **2004**, 428, 487.

[3] M. Mrksich, *MRS Bulletin* **2005**, 30, 180.

[4] [4a] P.S. Dittrich, K. Tachikawa, A. Manz, *Anal. Chem.* **2006**, 78, 3887; [4b] D.R. Reyes, D. Iossifidis, P.A. Auroux, A. Manz, *Anal. Chem* **2002**, 74, 2623.

[5] H.J. Chung, T.G.Park, *Adv. Drug Deliv. Rev*. **2007**, 59, 249.

[6] W.J. Kao, *Biomaterials* **1999**, 20, 2213.

[7] M.B. Gorbet, M.V. Sefton, *Biomaterials* **2004**, 25, 5681.

[8] B.D. Ratner, A.S. Hoffman, F.J. Schoen, J.E. Lemons, "Biomaterials Science", 2nd edition, Elsevier Inc., **2004**, p. 332-338.

[9] [9a] M. Yoshida, R. Langer, A. Lendlein, J. Lahann, *Poly. Rev*. **2006**, 46, 347. [9b] D.J. Mooney, E.A. Silva, *Nat. Mate*r. **2007**, 6, 327.

[10] F.F. Shi, *Surf. and Coatings Tech*. **1996**, 82, 1.

[11] [11a] R.G. Nuzzo, D.L. Allara., *J. Am. Chem. Soc*. **1983**, 105, 4481; [11b] S. Onclin, B.J. Ravoo, D.N. Reinhoudt. *Angew. Chem. Inter. Ed*. **2005**, 44, 6282.

[12] M. Chen, H. Liang, Y. Chiu, Y. Chang, H. Wei and H. Sung, *J. Contr. Release* **2005**, 108, 178.

[13] B.D. Ratner, A.S. Hoffman, F.J. Schoen, J.E. Lemons, "Biomaterials Science", 2nd edition, Elsevier Inc., **2004**, p. 1-3.

[14] G. Mani, M.D. Feldman, D. Patel, C.M. Agrawal, *Biomaterials* **2007**, 28, 1689.

[15] J. Lahann, H. Hocker, R. Langer, *Angew. Chem. Int. Ed.* **2001**, 40, 726.

[16] J. Lahann, R. Langer, *Macromolecules* **2002**, 35, 4380; H. Nandivada, H.Y. Chen, L. Bondarenko, J. Lahann, *Angew. Chem. Int. Ed*. **2006**, 45, 3360; X. Jiang, H.Y. Chen, G. Galvan, M. Yoshida, J. Lahann, *Adv. Func. Mater*. **2008**, 18, 27; J. Lahann, M. Balcells, T. Rodon, J. Lee, I.S. Choi, K.F. Jensen, R. Langer, Langmuir **2002**, 18, 3632; J. Lahann, R. Langer, *Macromol. Rapid Commun*. **2001**, 22, 968.

[17] J. Lahann, *Polym. Int*. **2006**, 55, 1361.

[18] J. Lahann, W. Plüster, T. Rodon, M. Fabry, D. Klee, H.-G. Gattner, H. Höcker, *Macromol. Biosci*. **2002**, 2, 82.

[19] P. Simon, S. Mang, A. Hasenhindl, W. Gronski, A. Greiner, *Macromolecules* **1998**, 31, 8775; C. Schmidt, V. Stuempflen, J. Wendorff, A. Hasenhindl, W Gronski, M. Ishaque, A. Greiner, *Acta Polym* **1998**, 49, 232; L. You, G. Yang, C. Lang, P. Wu, J. Moore, J. McDonald, et. al., *J. Vac. Sci. Tech*. A **1993**, 11, 3047.

[20] H. Nandivada, H.Y. Chen, J. Lahann, *Macromol. Rapid Commun*. **2005**, 26, 1794.

[21] H. Y. Chen, J. M. Rouillard, E. Gulari, J. Lahann. *Proc Natl Acad Sci U S A*. **2007**. 104, 11173.

[22] H.Y. Chen, J. Lahann, *Adv. Mater*. **2007**, 19, 3801; S. Thévenet, H.-Y. Chen, J. Lahann, F. Stellacci, *Adv. Mater.* **2007**, 19, 4333.

[23] K.Y. Suh, R. Langer, J. Lahann, Adv. Mater. **2004**, 16, 1401; H.Y. Chen, J. Lahann, *Anal. Chem*. **2005**, 77, 6909.

[24] J. Lahann, D. Klee, H. Hocker, *Macromol. Rapid Commun.* **1998**, 19, 441.

[25] M. Morgen, S.H. Rhee, J.H. Zhao, I. Malik, T. Ryan, H.M. Ho, M.A. Plano, P. Ho, *Macromolecules* **1999**, 32, 7555; J.J. Senkevich, S.B. Desu, V. Simkovic, *Polymer* **2000**, 41, 2379; S.Y. Park, S.N. Chvalun, A.A. Nikolaev, K.A. Mailyan, A.V. Pebalk, I.E.

Kardash, *Polymer* **2000**, 41, 2937; D. Klee, N. Weiss, J. Lahann. Vapor-Based Polymerization of Functionalized [2.2]Paracyclophanes: A Unique Approach towards Surface-Engineered Microenvironments" Chapter 18, Modern Cyclophane Chemistry, Wiley-VCH, Weinheim 2004, p463.

[26] Y. Elkasabi, H.Y. Chen, J. Lahann, *Adv. Mater*. **2006**, 18, 1521.

[27]; D.R. Critchley *Biochem Soc Trans* **2004**, 32, 831; E. Zamir, B. Geiger. *J Cell Sci* **2001**, 114, 3583.

[28] J.A. Gardella, S.A. Ferguson, R.L. Chin, *Appl. Spectrosc*. **1986**, 40, 224.

[29] S. Beguin, R. Kumar, *Thromb. Haemost.* **1997**, 78, 590.

[30] Z. Zhang, K. Apse, J. Pang, R.C. Stanton, *J. Biol. Chem.* **2000**, 275, 40042.

[31] J.F. Schmedtje Jr., M.S. Runge, D. Baykal, Am. *J. Cardiol.* **1995**, 75, 82B.

[32] J. Lahann, D. Klee, W. Pluester, & H. Hoecker, *Biomaterials* **2001**, 22, 817.

[33] H. Chen, Y. Chen, H. Sheardown, M.A. Brook, *Biomaterials* **2005**, 26, 7418.

CHAPTER 5

**POLYMER COATINGS WITH REACTIVE SURFACE COMPOSITION
GRADIENTS**

The materials in this chapter have been adapted with minor modifications from

the following published article: Y. Elkasabi, J. Lahann, *Macromolecular Rapid*

Communications **2009**, 30, 57-63.

5.1 Background and Motivations

In nature, biological information is typically encoded and displayed in the form of

continuous gradients mitigating important cellular events, such as cell signaling, cell

development, or chemotaxis. Mimicking surfaces with natural, spatially continuous

gradients is therefore of decisive importance to a range of biological applications

including studies of neuronal growth and differentiation,[1-3] the design of cell migration[4-6] and inflammation[7] assays, microfluidic cell culture,[8] or discovery-driven

(bio)materials research.[9,10] In spite of the importance of surface gradients for biological

applications, their realization, especially with biomedically relevant polymers, has been

challenging. Methods of making gradients are often relatively undifferentiated and are

potentially associated with a number of limitations: (i) Translation of chemical gradients

into biological gradients requires immobilization of biomolecules, which is often not

possible with existing gradient materials.[11,12] (ii) Due to technical constraints, such as

chemical resolution, resulting gradients are often intrinsically discontinuous with

potentially steep transitional steps.[13-15] (iii) Methods for making gradients are in many cases restricted to a particular surface chemistry, such as thiols to gold or siloxanes to glass or silicon. (iv) As a consequence, the range of materials, to which a given protocol can be applied, may become rather limited.[16,17] Although a range of methods have been developed that have the potential to address some or all of these challenges, experimental deficiencies are still in gross discrepancy to the rather elaborated approaches that have been developed over the last two decades for inorganic surface gradients. There, the use of vapor-based fabrication methods for inorganic materials resulted in efficient, high-throughput screening for catalytic activity, conductivity, or luminescence.[18] Where fabrication of gradients in inorganic materials has greatly benefited from anisotropic chemical vapor deposition,[18] polymer gradients have been so far prepared by solution-based processes, such as bulk diffusion,[11,19] microfluidic pathways,[13,14] lithography,[15,16,20] or combinations thereof.[12,17]

By taking advantage of vapor-based polymers, we have now established a simple method for polymer gradients with continuously changing surface compositions. Given the wide-range applicability of CVD polymerization to a diverse set of different substrates,[21] polymer gradients based on CVD polymer technology have the potential to expedite biomaterials discovery, much like it has been witnessed for inorganic materials over the last decades.[22]

Our approach towards polymer gradients takes advantage of chemical vapor deposition (CVD) polymerization of substituted [2.2]paracyclophanes to prepare polymer coatings with identical backbone chemistries, but different functional side groups.[21] Compared to plasma polymerization, which has been previously used to prepare polymer

gradients,[23] CVD polymerization of functionalized poly-*p*-xylylene has the potential to create robust, chemically well-defined polymers with a diverse range of reactive side groups – typically without appreciable side reactions. Recently, co-polymerization of two different [2.2]paracyclophanes resulted in surfaces with fine-tunable composition ratios.[24] With the concept of CVD co-polymerization demonstrated, the fundamental feasibility of a vapor-based gradient fabrication tool that mimics the processes developed for inorganic materials discovery is now within reach for soft materials.

5.2 Experimental Methods

CVD Copolymerization – CVD depositions were carried out in a custom-built chemical vapor deposition system, equipped with two inlet sources. Each source consisted of a quartz tube encased in a 3-zone tube furnace, and both tubes entered the deposition chamber directly opposite to each other. 4-trifluoroacetyl[2,2]paracyclophane monomer (**1**) was synthesized using an established synthesis route.[25] 4-Aminomethyl[2,2]paracyclophane monomer (**2**) was purchased from Uniglobe Kisco, Inc. (White Plains, NY) and used as-received. Monomer **1** and monomer **2** were loaded separately into two feed dishes, with each dish loaded into its own source. A system pressure of 0.165 Torr and sublimation temperatures between 80-110 $^{\circ}$C were used to ensure sublimation. Argon carrier gas was used to independently control the flow velocities of sublimated monomer (**1**) and monomer (**2**). Three different process conditions produced gradients with differing compositional rates of change. Condition 1: M_1 = 160 mg, M_2 = 205 mg, Ar_1= 6.5 sccm, Ar_2 = 32 sccm. Condition 2: M_1 = 200 mg, M_2 = 205 mg, Ar_1 = 7.2 sccm, Ar_2 = 29.7 sccm. Condition 3: M_1 = 120 mg, M_2 = 205 mg,

Ar$_1$ = 5.7 sccm, Ar$_2$ = 35 sccm. The sample holder was set 4 inches below the position of both sources. To ensure gradient formation, the sample holder was not rotated. Although the sample holder remained at 15 ^{o}C, a copper plate was set on top of the sample holder, in order to control the sample's angle of inclination. Deposition occurred on silicon, gold, and glass substrates. To minimize wall deposition, the chamber wall was heated to 120 ^{o}C.

Surface Characterization – X-ray photoelectron spectroscopy (XPS) was performed on CVD-coated silicon substrates (1cm x 1cm). XPS data were recorded on an Axis Ultra X-ray photoelectron spectrometer (Kratos Analyticals, UK) equipped with a monochromatized AlKα X-ray source. All spectra were calibrated with respect to the non-functionalized aliphatic carbon with a binding energy of 285.0 eV and were corrected for atomic sensitivity factors. Thicknesses were recorded at a wavelength of 532 nm using an EP^3-SW imaging ellipsometry (Nanofilm Technologie GmbH, Germany). Four-zone nulling experiments were performed at an angle of incidence of 70°, and an anisotropic Cauchy model was used to model the ellipsometric parameters psi and delta. Infrared spectroscopy was performed on a Nicolet 6700 spectrometer utilizing the grazing angle accessory (Smart SAGA) at a grazing angle of 85°. FTIR spectra were corrected for any residual baseline drift. Au-coated Si substrates were used for FTIR measurements, using blank Au-coated Si as a reference.

Surface Modification – Surface reactions were performed on CVD-coated glass microscope slides (3'' x 1'', Fisher Inc.). Biotin hydrazide and rhodamine-linked streptavidin were purchased from Pierce Inc., and Atto 655 NHS ester was purchased from Sigma Aldrich. All surface reaction experiments were performed on glass

substrates. A PDMS membrane was molded and cut in the shape of a long rectangle made for holding fluid within its boundaries. The membrane was placed on the film and allowed to seal, and the reaction buffer filled the membrane. Then the entire slide was immersed in washing buffer, with the PDMS still remaining on the surface. Reactions were carried out in a closed Petri dish, to prevent the reaction mixtures from drying out. All surfaces were rinsed with DI water after applying the ligands and using the washing buffers. Consecutive surface reactions were conducted at each location. Fluorescence images and intensities were acquired using a GenePix 4000B scanner with 532 nm (17 mW) and 635 nm (10 mW) lasers. Both excitation wavelengths were scanned simultaneously at 100 μm spatial resolution. Colors shown in the scanning images were not true colors, but were set for best visualization.

Ligand 1: 0.5 ml of anhydrous dimethylformamide was added to 1 mg Atto 655 NHS ester. From this, 5.0 μl were diluted with 7 ml 0.1 M sodium bicarbonate buffer (pH 8.3), containing 0.02% (v/v) Tween 20. NHS esters are time-sensitive in aqueous solution, so the buffer was applied to the film immediately upon dilution. The solution was incubated for 1 hour at room temperature, after which the surface was rinsed with ethanol for 10 minutes and with PBS/Tween solution for 30 minutes.

Ligand 2: Biotin hydrazide was diluted to 10 mM in phosphate buffered saline (PBS pH 7.4). The solution was acid-catalyzed (HAc) prior to surface application. Incubation time lasted 7 to 10 minutes, which was followed by a wash of PBS containing 0.02% (v/v) Tween 20. The area was then applied with rhodamine-linked streptavidin solution (0.075 mg/ml in PBS; 0.02% (v/v) Tween 20; 0.1% (w/v) bovine serum albumin) for 15

minutes. Finally, the entire glass slide was immersed for 1 hour in a PBS/Tween/BSA solution.

5.3 Results and Discussion

5.3.1 Polymer Gradient Deposition

The experimental setup for gradient co-polymerization of functionalized [2,2]paracyclophanes is illustrated in Figure 5.1. Instead of the traditional single-source CVD system,[26] a polymerization chamber with two sources at an 180° angle has been designed. Each source can independently provide different types of starting materials. During CVD copolymerization using dual sources, each ring-constrained [2.2]paracyclophane is thermally converted into corresponding quinodimethanes and transferred into the reaction chamber. Next, the quinodimethanes spontaneously copolymerize below a certain threshold temperature onto a temperature-controlled substrate (typically 40 to 60 ºC depending on the chemical structure of the [2.2]paracyclophane). While the monomer flows over a substrate with a temperature below this threshold temperature, gradual depletion of the monomer from the gas phase occurs, resulting in a gradual decrease in polymer composition of the vapor phase. If two monomers are deposited in a countercurrent manner to each other, each monomer's concentration should decrease with increasing distance from the respective source. As a consequence, the relative ratio of the components, which make up the polymer film, will form a continuous gradient. In order for gradient deposition to occur in this manner, however, the mass transport properties of both monomers must allow for sufficient manipulation.
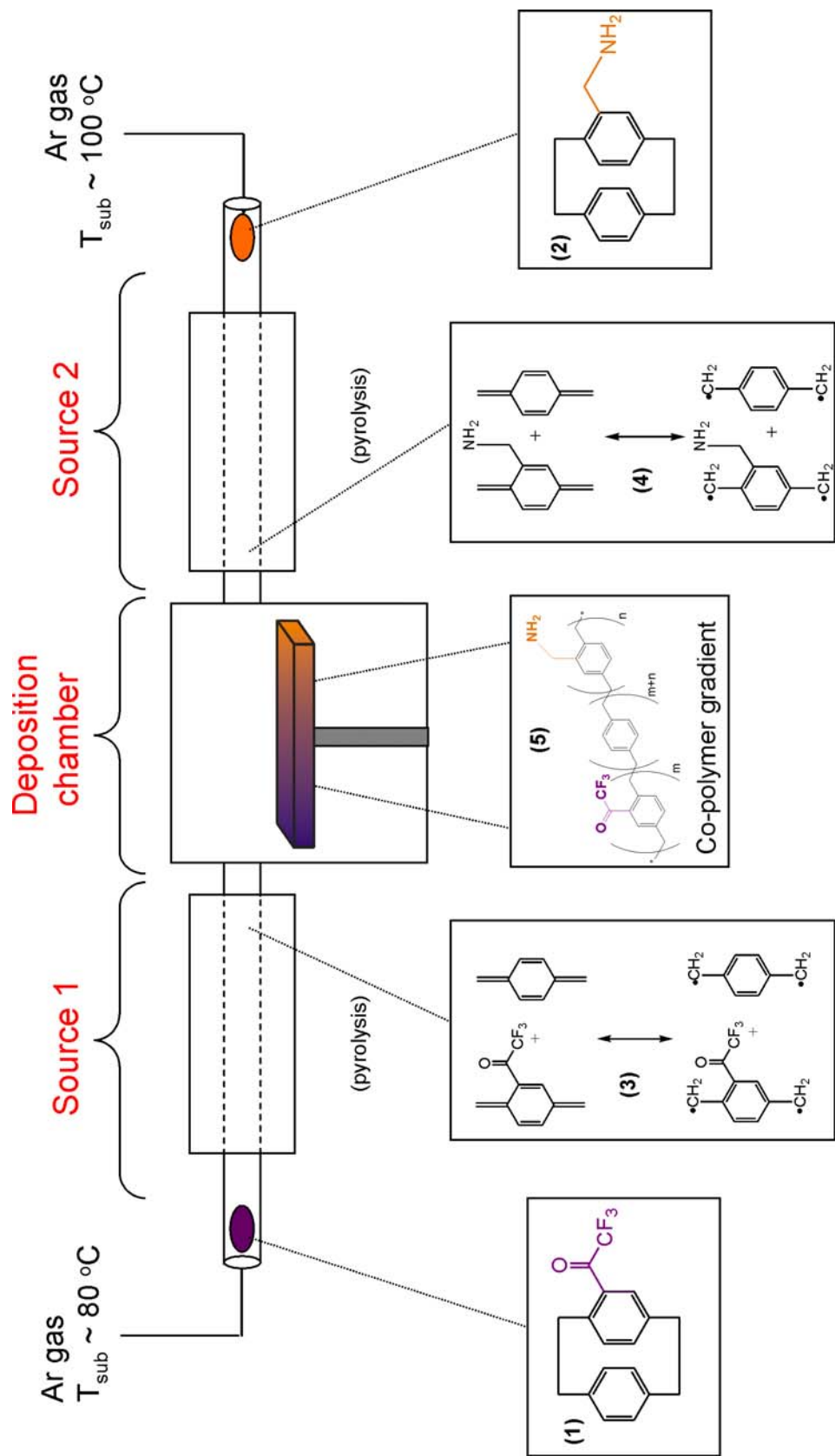
Figure 5.1. A side-view schematic of the custom-built two-source CVD system. Each source consists of a quartz tube that passes through a 3-zone furnace and then connects into the deposition chamber. Both the tubes and the chamber together are held at 0.16 Torr. (**1**) and (**2**) sublimate, undergo pyrolysis, and then copolymerize to deposit on the sample holder. The specified process conditions create a poly(*p*-xylylene) (PPX) film possessing a functional composition gradient.

Some process variables that can affect the gradient formation include system pressure, argon flow rates, substrate temperature, sample height, monomer loading, and pyrolysis temperatures. The CVD-based gradient experiments were conducted in a vacuum chamber, which accommodates a 30.5 cm diameter sample holder placed between the two source inlets. Starting material 4-trifluoroacetyl-[2.2]paracyclophane (**1**) was loaded into source 1, while 4-aminomethyl-[2.2]paracyclophane (**2**) was loaded into source 2. Pyrolysis temperatures of 670 ^{o}C were used in both source systems. Under these conditions, paracyclophanes **1** and **2** were converted into the corresponding quinodimethanes **3** and **4**. Deposition rates were adjusted by controlling the sublimation rates of starting material **1** and **2,** so that sublimation of both dimers started and finished simultaneously after a 10-minute period. Dimer sublimation rates were controlled by changing the amount of loaded starting material, while keeping sublimation temperatures and pressure constant. In addition, rapid venting of the deposition chamber with argon after CVD deposition improved gradient quality. Gradient co-polymerization yielded continuous polymer films with thicknesses varying between 120-190 nm. Thickness differences were occasionally observed along the polymer gradient, but did not compromise the chemical composition gradients or the gradient reactivity.

Steady gradient formation with respect to bulk composition across the polymer films was evaluated using a combination of surface analytical methods. Fourier transform infrared (FTIR) spectroscopy was chosen because of its ability to detect relative changes in characteristic bond vibrations. The trifluoroacetyl functional group of homopolymer **6** resulted in characteristic vibrational modes at 1716 cm^{-1} associated with the carbonyl group and at 1200, 1152, 973 cm^{-1} (C-F stretches). Aminomethyl groups have

characteristic N-H and C-N signals at 3368, 3302, 1640, and 829 cm^{-1}, respectively. During CVD co-polymerization, gold substrates were placed at specific positions along the length of the sample holder, and the polymer coating was deposited using the two-source system (Figure 5.1). Relative ratios of vibrational signal intensities associated with trifluoroacetyl and aminomethyl groups were determined for each substrate. Samples were placed at various locations on a 12'' diameter sample holder. Figure 5.2 shows IR spectra at various locations along the sample holder. A detailed FTIR analysis of these

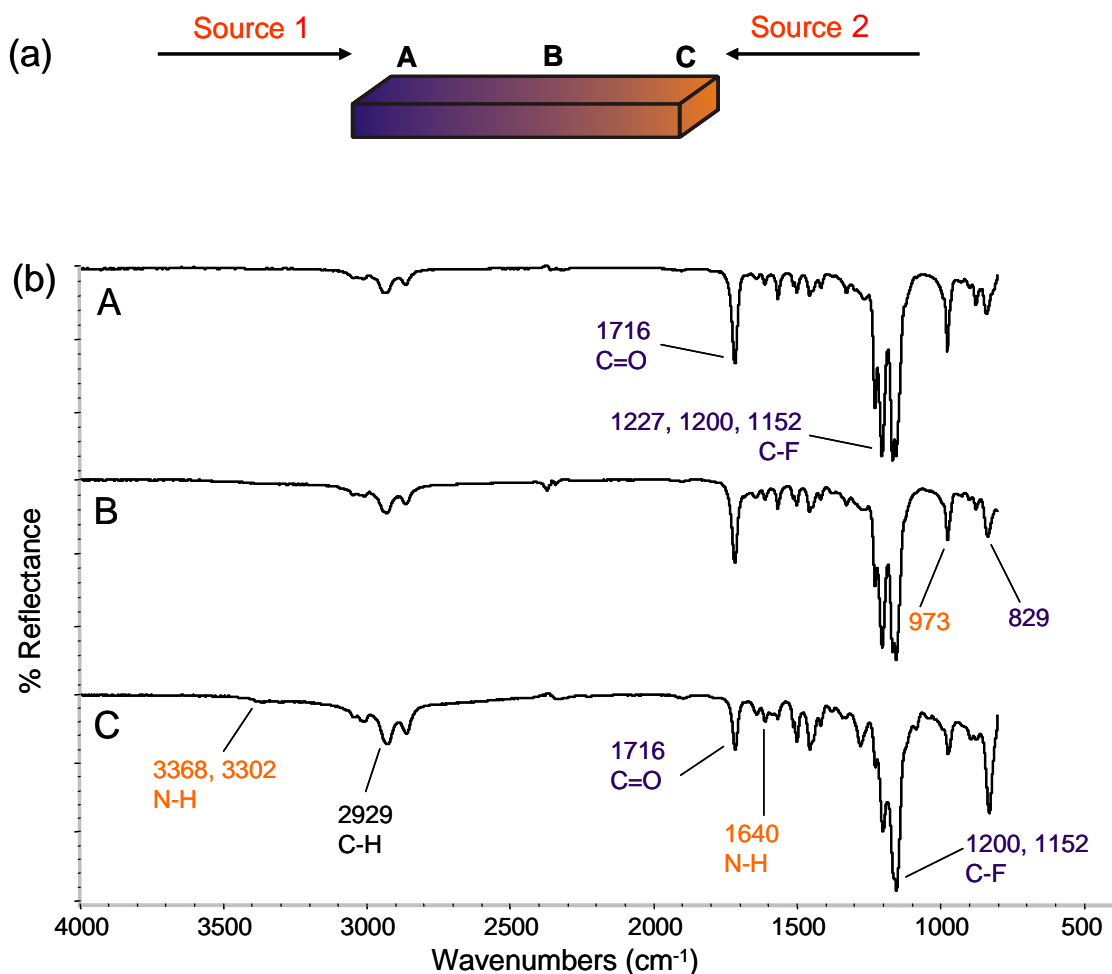**Figure 5.2.** (a) Side view of the CVD sample holder. AB = BC = 7.6 cm. AC = 15.2 cm. (b) FTIR spectra of CVD copolymers produced from the conditions of scheme 1. The bulk ratio of CVD copolymer changes with respect to position along the sample holder.
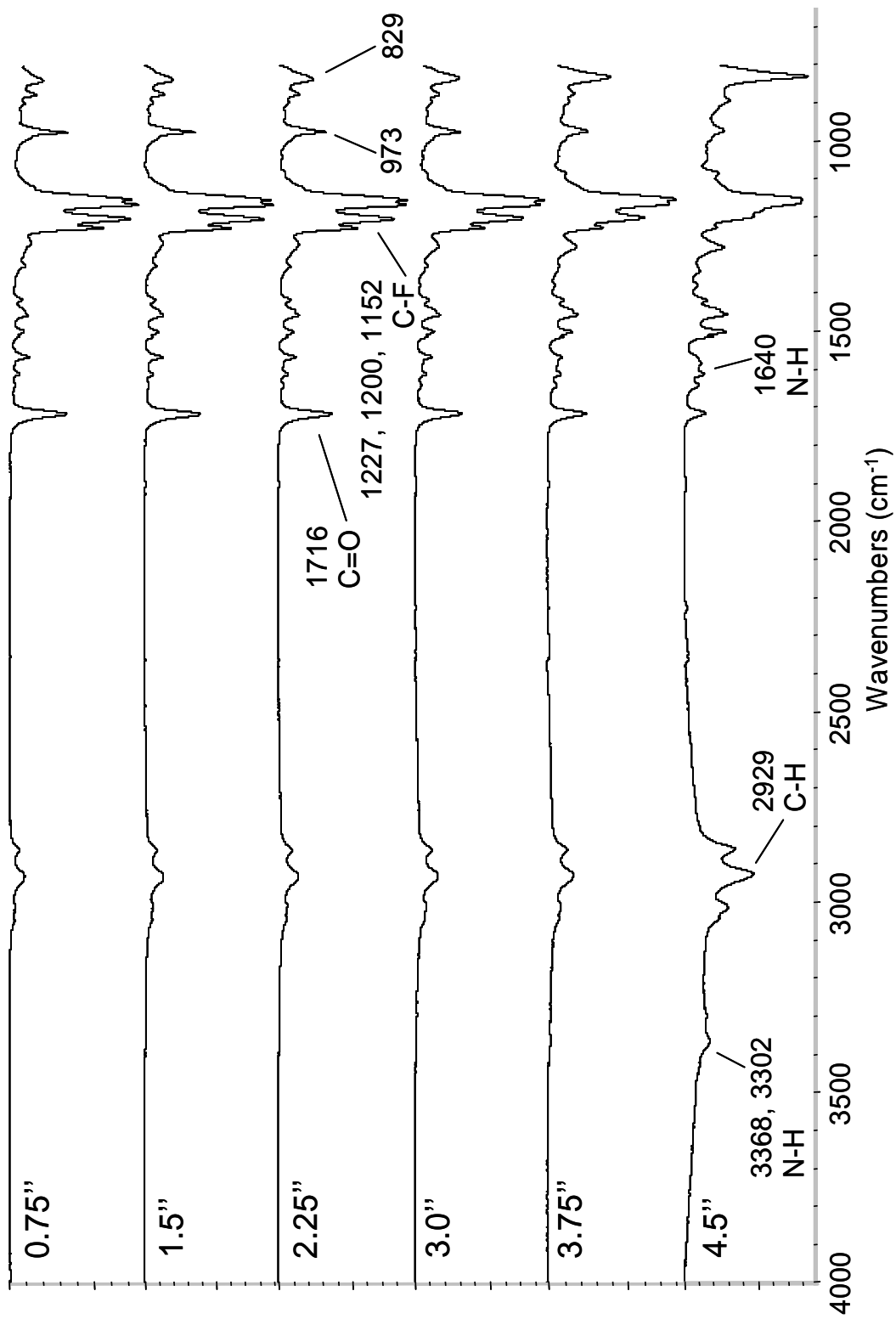
109

Figure 5.3. FTIR spectra of CVD copolymer gradients, using condition 2

110

samples revealed a transition from strong trifluoroacetyl signals to strong aminomethyl signals, most evidently from the band vibrations at 973 and 829 cm^{-1}. Correlation between FTIR and XPS data provides access to polymer compositions at the surface.[24] Upon calibration using the FTIR technique, sample point A was related to a molar ratio of 1:2 (PPX-CH$_2$-NH$_2$: PPX-COCF$_3$), sample point B corresponded to the equimolar ratio of the two building blocks, and sample point C was related to a 5:1 excess of PPX-CH$_2$-NH$_2$, at fixed flow rates of 6.5 sccm source A and 32.0 sccm source B. FTIR spectra from other CVD deposition conditions revealed analogous results, indicating different rates of change across the substrate (Figure 5.3). Differences in the chemical side groups of the starting materials had a profound impact on the spreading of the resulting polymer films. This agrees well with a recent study on penetration of CVD coatings into confined microchannels.[27]

The FTIR study was complemented by a detailed X-ray photoelectron spectroscopy (XPS). In general, XPS provides information about the polymer composition within the top 5-10 nm of a polymer film.[28] We used XPS in its survey spectrum mode to study the composition of three different CVD films made by gradient copolymerization on a silicon substrate. Fluorine and nitrogen were selected as reporter atoms for monomers **3** and **4**, respectively. On the basis of these reporter atoms, relative surface ratios were calculated for each film. Figure 5.4 shows the copolymer concentration profiles based on the XPS results. Upon inspection of the surface composition from Figure 5.2, gradually changing concentrations can be observed ranging from 26% of compound **4** at positions A (closest to source 1) to 44% at position B, to 85% at position C (closest to source 2). A detailed analysis on the basis of 14 data points

along the trajectory between the two source inlets revealed a linear change in surface composition over a distance of 15.2 cm. Simple modulation of the process parameters allowed for controlled manipulation of the gradient compositional slope. To vary the compositional slope of the gradients, cooperative control of argon flow rates and
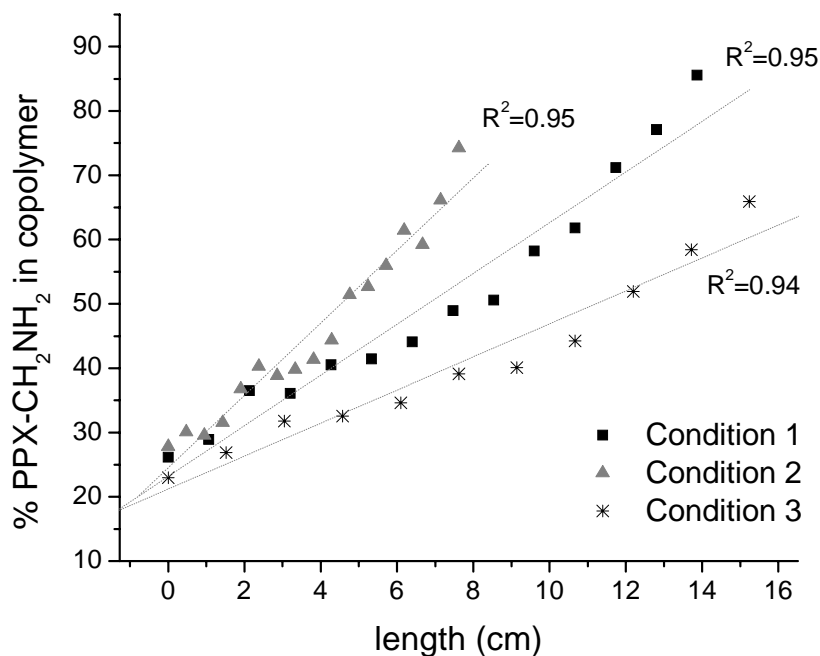
Figure 5.4. Copolymer compositions along the surface gradient, based upon XPS survey spectra. Copolymer ratios are calculated based upon the percentage of fluorine and nitrogen, both characteristic of (**1**) and (**2**), respectively. The concentration of aminomethyl groups increases with respect to position along the substrate. The compositional rate of change can be controlled by manipulating argon flow rates and sublimation rates.

monomer sublimation rates resulted in substantially different gradient slopes as shown in Figure 5.4. As the ratio of argon flow rates increases (Ar_1/Ar_2), an increase in compositional slope of the gradients was observed. Fundamentally, effective gradient formation required the deposition zones of both PCP's to sufficiently overlap on the substrate, which was placed onto a cooled sample holder to enhance deposition pressure.

If the deposition zones were identical for both PCP's, the sample had to be placed in the center between both sources to obtain optimum deposition. However, it has already been shown for CVD polymerization within microchannels,[27] that trifluoroacetyl-functionalized PCP possesses a higher mobility as compared to the amine-functionalized dimers, which effectively moves the deposition zone away from the source of the trifluoroacetyl-functionalized PCP and closer to the source of the amino-functionalized PCP. When samples were placed outside of the region of overlapping deposition zones, the resulting gradients were flat and very difficult to control. Moreover, modulation of parameters associated with the CVD polymerization of trifluoroacetyl-functionalized PCP can be expected to be more effective when controlling gradient properties, such as compositional profiles and slopes. Increasing the mass and argon flow of paracyclophane **1**, while decreasing the argon flow of paracyclophane **2**, increased the compositional slope of the gradient, as long as the mass of compound **2** was held constant. Because of the different monomer mobility, changes made to flow rates of the amine were small enough, to ensure that the aminomethyl-rich end of the gradient remains unaffected by the increase in trifluoroacetyl-functionalized monomers. Assuming that the sublimation temperatures remain constant, the aforementioned trends in deposition conditions can be used to produce compositional gradients with predictable slopes.

To verify this, three plots are shown in Figure 5.4, which represent three CVD conditions outlined in the experimental section. Linear trends can be fitted to each plot, each with an R^2 value of at least 0.94. In spite of the steeper compositional gradient, the actual range of realizable compositions remains approximately unaltered. The ability to

predict surface compositions along the surface gradient solely on the basis of its location with such accuracy is a critical attribute of this gradient synthesis process.

There exist limitations on the gradient length. The maximum gradient length is primarily determined by the CVD chamber size. CVD coatings deposit everywhere inside the chamber, so if argon flow rates are optimized accordingly, the gradient can span the entirety of the sample holder. The intrinsic transport characteristics of each monomer also affect the feasibility of forming longer gradients. If a monomer exhibits greater mobility, then smaller argon flow rates are needed to ensure its presence on the opposite side of the chamber, resulting in thinner coatings. This phenomenon may then compromise the overall gradient thickness profile.

The minimum gradient length possible would be constrained by the mean free path,[29] given by equation 5.1

$$\lambda = \frac{3.2\mu}{P}\sqrt{\frac{RT}{2\pi M}} \quad \text{(Equation 5.1)}$$

where λ is in m, μ is viscosity in Pa-s, P is the pressure in N/m^2, T is the absolute temperature in K, R is the universal gas constant (8.3143 x 10^3 N-m/kg-mol-K), and M is the molecular weight in kg/kg-mol. As the gradient length decreases, it will approach the mean free path (~0.5-2 mm). Hence, maintaining a concentration gradient in the vapor phase will increase in difficulty. Concentration fluctuations increase as gradient length decreases, and the XPS concentration profiles of Condition 2 (Figure 5.4) exhibit this behavior. One recommended action for further experimentation is to simultaneously 1) increase the system pressure and 2) decrease temperatures of the substrate and chamber wall. Doing so would decrease λ, which would increase the gradient resolution. This, in

combination with the aforementioned trends in deposition parameters, could allow for the deposition of gradients shorter than 8 cm.

5.3.2 Surface Reactions

To confirm that free amino and trifluoroacetyl groups are available at the surface in the expected ratios, we reacted the polymer gradients with two fluorescence-based reporter reactants with orthogonal reactivity. Model surface reactions were employed, which followed previously established reactions.[24] First, Atto 655 NHS ester was reacted with the primary amines of monomer **4,** followed by reaction of the trifluoroacetyl groups of monomer **3**, with biotin hydrazide to form the corresponding hydrazones. Rhodamine-linked streptavidin was then used to visualize biotin

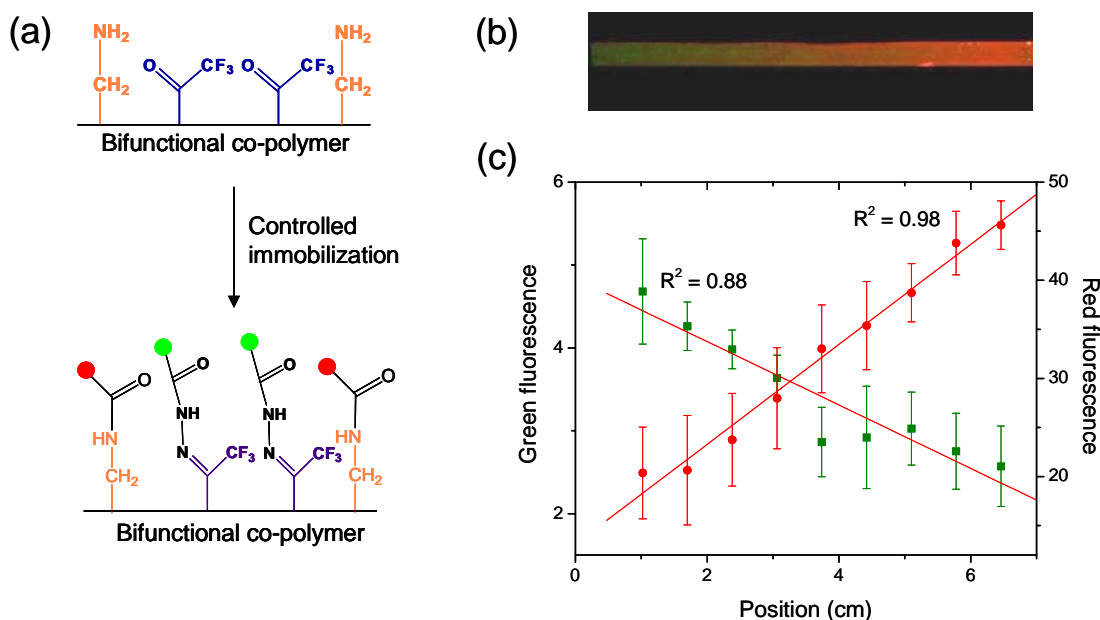
Figure 5.5. (a) Schematic of the biomolecular immobilization process (b) Fluorescence image and (c) intensity profiles of immobilized fluorescent dyes across a CVD polymer gradient. Both Atto 655 NHS ester (red) and biotin hydrazide with rhodamine-tagged streptavidin (green) reacted over the same regions, showing that the composition gradient can be converted into immobilization gradients.

attachment.[30] Figure 5.5 shows a fluorescence scanning image and normalized fluorescence profiles for a surface gradient, which was reacted with two fluorescent dyes. To obtain fluorescence profiles, actual fluorescence values within areas of ligand immobilization were divided by the polymer background fluorescence. As the concentration changes across the substrate, the ratio of red versus green fluorescence intensities is altered correspondingly. The fluorescence gradient changed linearly and correlated well with the surface composition ratios obtained by XPS. This is important, because XPS provides information that averages over the outermost 5 to 10 nm, while the fluorescence titration only reflects chemical groups incidentally available at the surface. Thus, the gradient surfaces not only have well predictable surface composition gradients, but these gradients also correspond to a gradual change in surface reactivity.

5.4 Conclusions

In summary, we have developed a straightforward process for the fabrication of continuous, reactive composition gradients based on vapor-deposited polymer thin films. These poly(*p*-xylylene) coatings consist of a uniform polymeric backbone, with gradually changing functional side groups present at the surface. The films possess a gradient of two reactive functional groups, allowing for independent manipulation of physical and/or chemical properties. By controlling CVD polymerization parameters, such as argon flow rates and sublimation rates, the slope of the compositional gradients can be adjusted, while maintaining a linear trend. Most importantly, we were able to selectively immobilize fluorescently-labeled ligands onto the reactive polymer gradients. Not only is CVD polymerization conformal over complex geometries, but the deposition can occur

over various substrate materials. In addition, the CVD co-polymerization approach used for preparing the polymer gradients is not limited to the two functionalities discussed herein. A range of different functionalities including alcohols,[31] amines,[32] ketones,[33] esters,[34] alkynes,[35] and aldehydes[36] can be incorporated into these coatings and selecting dimeric precursor(s) with the appropriate functional group may create gradients of a wide range of different functionalities. CVD composition gradients have the potential to address many common setbacks and limitations of currently employed methods for polymer gradients and may find applications in a range of biotechnological devices. Specific applications of PPX gradients will vary depending on the gradient characteristics, including the gradient length. Longer gradients (7 – 12'') would be useful for generating combinatorial libraries for high-throughput experimentation. A large number of relatively small substrates can be loaded onto the sample holder, within the region of gradient deposition. The local composition within each substrate would be a homogeneous copolymer. Moderately short gradients (2 – 7'') of biochemical signals have greater application in tissue regeneration and scaffold constructs.[37] Relevant signals include growth factors and peptide sequences. Shorter gradients (< 2''), if successfully fabricated with CVD, have potential use in microfluidic bioassays and regulation of cellular migration and differentiation of most cell lines.

References

[1] H.J. Song, M. Poo, *Curr. Opin. Neurobio*., **1999**, 9, 355-363.

[2] S.K.W. Dertinger, X. Jiang, Z. Li, V.N. Murthy, G.M. Whitesides, *Proc. Natl. Acad. Sci*., **2002**, 99(20), 12542-12547.

[3] A.C. von Philipsborn, S. Lang, J. Loschinger, A. Bernard, C. David, D. Lehnert, F. Bonhoeffer, M. Bastmeyer, *Development,* **2006**, 133, 2487-2495.

[4] C. A. Parent, P.N. Devreotes, *Science* **1999**, 284, 765-770.

[5] R.T. Tranquillo, D.A. Lauffenburger, S.H. Zigmond, *J. Cell Biol*. **1988**, 106, 303-309.

[6] H. Mao, P.S. Cremer, M.D. Manson, *Proc. Natl. Acad. Sci. U.S.A*. **2003**, 100, 5449.

[7] R.J. Mrsny, A.T. Gewirtz, D. Siccardi, T. Savidge, B.P. Hurley, J.L. Madara, B.A. McCormick, *Proc. Natl. Acad. Sci*., **2004**, 101, 7421.

[8] L. Ionov, N. Houbenov, A. Sidorenko, M. Stamm, S. Minko, *Adv. Func. Mater*. **2006**, 16, 1153-1160.

[9] [9a] J.C. Meredith, J.L. Sormana, B.G. Keselowsky, A.J. Garcia, A. Tona, A. Karim, E.J. Amis, *J. Biomed. Mater. Res*. **2003**, 66A, 483-490; [9b] P. Zapata, J. Su, A.J. Garcia, J. C. Meredith, *Biomacromol*. **2007**, 8, 1907.

[10] [10a] J. Genzer, R.R. Bhat, *Langmuir* **2008**, 24, 2294; [10b] T. Winkler, N. Ballav, H. Thomas, M. Zharnikov, A. Terfort, *Angew. Chem. Int. Ed*. **2008**, 47, 7238.

[11] M.K. Chaudhury, G.M. Whitesides, *Science* **1992**, 256(5063), 1539.

[12] T.M. Keenan, C.H. Hsu, A. Folch, *Appl. Phys. Lett*. **2006**, 89, 114103.

[13] N.L. Jeon, S.K.W. Dertinger, D.T. Chiu, I.S. Choi, A.D. Stroock, G.M. Whitesides, *Langmuir* **2000**, 16, 8311.

[14] J.A. Burdick, A. Khademhosseini, R. Langer, *Langmuir* **2004**, 20(13) 5153.

[15] N.D. Gallant, K.A. Lavery, E.J. Amis, M.L. Becker, *Adv. Mater.* **2007**, 19, 965.

[16] N. Ballav, A. Shaporenko, A. Terfort, M. Zharnikov, *Adv. Mater*, **2007**, 19, 998-1000.

[17] [17a] C. Xu, S.E. Barnes, T. Wu, D.A. Fischer, D.M. DeLongchamp, J.D. Batteas, K.L. Beers, *Adv. Mater.* **2006**, 18, 1427; [17b] I. Luzinov, S. Minko, V.V. Tsukruk, *Soft Matter* **2008**, 4, 714.

[18] E. Danielson, J. H. Golden, E. W. McFarland, C. M. Reaves, W. H. Weinberg, X.D. Wu, *Nature* **1997**, 389, 944.

[19] M. Zelzer, R. Majani, J.W. Bradley, F.R.A.J. Rose, M.C. Davies, M.R. Alexander, *Biomaterials* **2007**, 29, 172.

[20] [20a] M.S. Kim, G. Khang, H.B. Lee, *Prog. Polym. Sci.* **2008**, 33, 138; [20b] P. Burgos, M. Geoghegan, G.J. Leggett, *Nano Letters* **2007**, 7, 3747; [20c] N. Ballav, S. Schilp, M. Zharnikov, *Angew. Chem. Int. Ed.* **2008**, 47, 1421; [20d] M. Steenackers, A. Kuller, N. Ballav, M. Zharnikov, M. Grunze, R. Jordan, *Small* **2007**, 3, 1764.

[21] A. Greiner, *Trends Poly. Sci.* **1997**, 5, 12.

[22] V. Murphy, A.F. Volpe Jr., W.H. Weinberg, *Curr. Opin. Chem. Bio.* **2003**, 7, 427-433.

[23] [23a] J.D. Whittle, D. Barton, M.R. Alexander, R.D. Short, *Chem. Commun.* **2003**, 14, 1766; [23b] D.E. Robinson, A. Marson, R.D. Short, D.J. Buttle, A.J. Day, K.L. Parry, M. Wiles, P. Highfield, A. Mistry, J.D. Whittle, *Adv. Mater.* **2008**, 20, 1166.

[24] Y. Elkasabi, H.Y. Chen, J. Lahann, *Adv. Mater.* 2006, 18, 1521-1526.

[25] J. Lahann, D. Klee, H. Höcker, *Macromol. Rapid Commun.* **1998,** 19, 441.

[26] J. Lahann, *Polym. Int.* **2006**, 55, 1361-1370.

[27] H.Y. Chen, Y. Elkasabi, J. Lahann, *J. Amer. Chem. Soc.* **2006**, 128, 374-380.

[28] *Biomaterials Science: An Introduction to Materials in Medicine* (Eds: B.D. Ratner, A.S. Hoffman, F.J. Schoen, J.E. Lemons), Academic, San Diego, CA **1996**.

[29] C.J. Geankoplis, *Transport Processes and Unit Operations*, Prentice Hall PTR, Englewood Cliffs, NJ **1993**.

[30] L. Haeusling, B. Michel, H. Ringsdorf, H. Rohrer, *Angew. Chem. Int. Ed*. **1991**, 30, 569.

[31] J. Lahann, R. Langer, *Macromolecules* **2002,** *35*, 4380.

[32] J. Lahann, H. Hocker, R. Langer, *Angew. Chem. Int. Ed.* **2001,** *40*, 726.

[33] K. Suh, R. Langer, J. Lahann, *Advanced Materials* **2004** *16*, 1401.

[34] J. Lahann, I.S. Choi, J. Lee, K. Jensen, R. Langer, *Angew. Chem., Int. Ed.* **2001**, 40, 3166.

[35] H. Nandivada, H.Y. Chen, L. Bondarenko, J. Lahann, *Angew. Chem. Int. Ed*. **2006**, 45, 3360-3363.

[36] H. Nandivada, H.Y. Chen, J. Lahann, *Macromol. Rapid Commun*. **2005**, *26*, 1794.

[37] L. Liu, Z. Xiong, Y. Yan, R. Zhang, X. Wang, L. Jin, *J. Biomed. Mater. Res. B: Appl. Biomater*. **2008**, 88B, 254.

CHAPTER 6

CONCLUSIONS

6.1 Summary

The work described in this dissertation investigated vapor-deposited polymer coatings, which are multifunctional in performance. Polymer coatings were synthesized and deposited via chemical vapor deposition polymerization. CVD coatings possess many unique features that distinguishes them from solvent-based methods, such as their conformal deposition within confined microgeometries and the absence of impurities. Functionalized derivatives of [2.2]paracyclophane (PCP) were polymerized into their poly(*p*-xylylene) analogues. Past research investigated the synthesis and characterization of functionalized poly(*p*-xylylenes) (PPXs).[1] The copolymerization studies detailed in this dissertation serve as a fundamental extension of the previous work, which primarily examined polymerization and immobilization on homofunctionalized poly(*p*-xylylenes). The following aims have been demonstrated: 1) Partially fluorinated PCPs were brominated, allowing for further addition of reactive groups onto a hydrophobic PCP monomer. The contact angle of reactive PPX coatings can be changed independently of the polymer reactivity, allowing for the formation of a superhydrophobic reactive coating. 2) Two differently-functionalized PCPs can be CVD copolymerized to produce a PPX coating, bearing two functional groups on the coating surface. These functional

groups react orthogonally towards two different molecules, allowing for independent co-immobilization of multiple biomolecules onto a substrate. 3) CVD copolymers exhibit biofunctionality in short-term assays and cell adhesion experiments. HUVECs and NIH 3T3s adhere and spread onto reactive PPX copolymers, even though one of the copolymer functional groups may be cytophobic. Immobilization and activity of two antithrombotic drugs was achieved on a bifunctional CVD copolymer. 4) A CVD system was modified to accommodate a second source for monomer flow, and process conditions were optimized for the deposition of PPX composition gradients. The gradient coatings can be deposited onto any substrate material of planar and/or three-dimensional geometry. Futhermore, the surface gradients are reactive and are capable of immobilizing two dyes as a two-component gradient. The aforementioned results have the potential to improve performance of bioanalytical devices, as well as to facilitate cell adhesion onto artificial implants. The following are some suggested directions for future investigations into the dissertation topic.

6.2 Future Directions and Potential Applications

6.2.1 Superhydrophobic Reactive Coatings

A superhydrophobic PPX has been sought after for its potential impact on self-cleaning and water-repellant surfaces.[2] The traditional method of increasing hydrophobicity is to heavily fluorinate the PCP dimer, in hopes that the fluorine bonds retain stability throughout the CVD process. Dolbier and coworkers[3,4] have demonstrated the synthesis of a [2.2]paracyclophane that contains a perfluorinated bridge; recently, they successfully synthesized a completely perfluorinated

[2.2]paracyclophane dimer. Our work on brominated tetrafluoro[2.2]paracyclophanes was an attempt to increase hydrophobicity of PPX polymers, before augmenting reactive functional groups onto the benzene ring. Future experiments should include the replacement of the bromine atom with a reactive group, such as an aldehyde.

The development of superhydrophobic reactive polymer coatings opens the door for more advanced combinatorial studies, with respect to more than one type of surface property (reactivity, wettability, topography, etc.). By systematically varying the PPX functional groups and concentrations of surface nanoparticles, one can screen surfaces bearing many different combinations of roughness, hydrophilicity, and chemical functionality. Doing so would effectively decouple these variables from each other, and it would facilitate a more fundamental understanding of how these surface properties correlate with the variable of interest (non-fouling, cytophilicity, etc.). Furthermore, a wettability gradient which ranges from superhydrophilic to superhydrophic would simplify these combinatorial experiments. Rather than synthesizing multiple combinations of fibers and CVD coatings in a serial manner, gradient deposition onto a surface gradient of nanoparticles will produce one sample which encompasses all combinations of roughness and surface chemistry. For example, this dual gradient can be used in one single experiment to determine optimal non-fouling characteristics for proteins and bacteria (see Appendices for preliminary data).

As a preliminary experiment, the CVD copolymer gradient described in Chapter 5 was deposited onto a silicon substrate bearing polymeric nanofibers and/or nanoparticles (produced as described in Chapter 2). Succinic anhydride was allowed to react with the aminomethyl functional group. Due to the increased surface roughness, contact angles of

succinic anhydride and trifluoroacetyl-PPX are expected to dramatically decrease and increase, respectively. Figure 6.1 shows preliminary results from this procedure. Because the contact angles on both ends do not qualify as superhydrophobic or superhydrophilic ($>155^o$ and $< 10^o$, respectively), several experimental conditions need to be optimized, such as the molecule of choice for immobilization, CVD coating thickness, and nanoparticle/fiber morphology. For this purpose, a two-dimensional gradient would serve well – one axis would contain the polymer gradient after succinic anhydride reaction, and perpendicular to this gradient would be a roughness gradient.
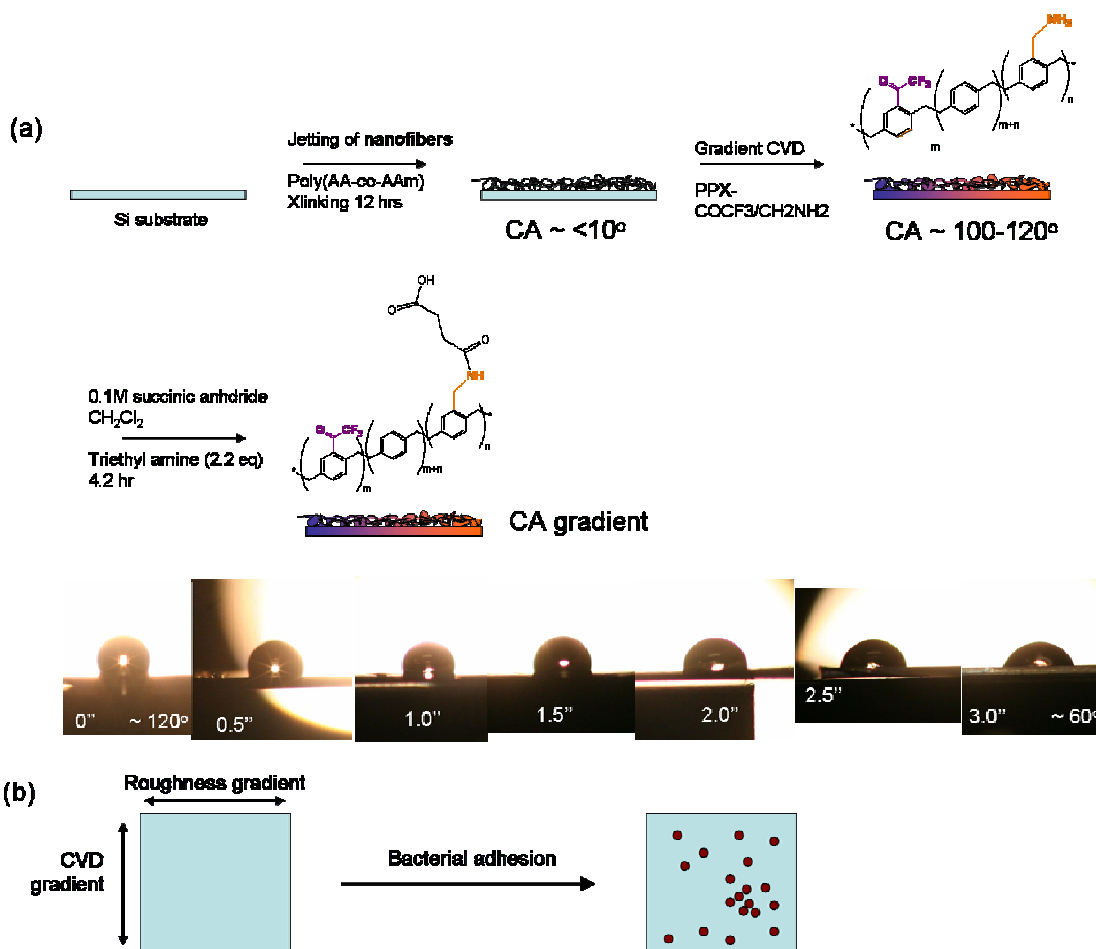

Figure 6.1 Preliminary experimental protocols for (a) contact angle gradient fabrication and (b) screening gradient surfaces for non-fouling characteristics.

6.2.2 Multipotent Copolymer Coatings

It was demonstrated that a bifunctional CVD copolymer can immobilize two biomolecules.[5] Each functional group reacts independently from the other. Although the proof of concept bodes well for biological applications, a truly advanced surface would accommodate many more surface functionalities (at least 8-10). This order of magnitude could possibly control not only the adhesion of one or two biomolecules, but also could affect biological processes downstream, such as blood coagulation.[6] However, the straightforward procedure developed in chapter 3 is easily hindered by certain CVD process variables. Ten differently-functionalized paracyclophanes would easily cross-
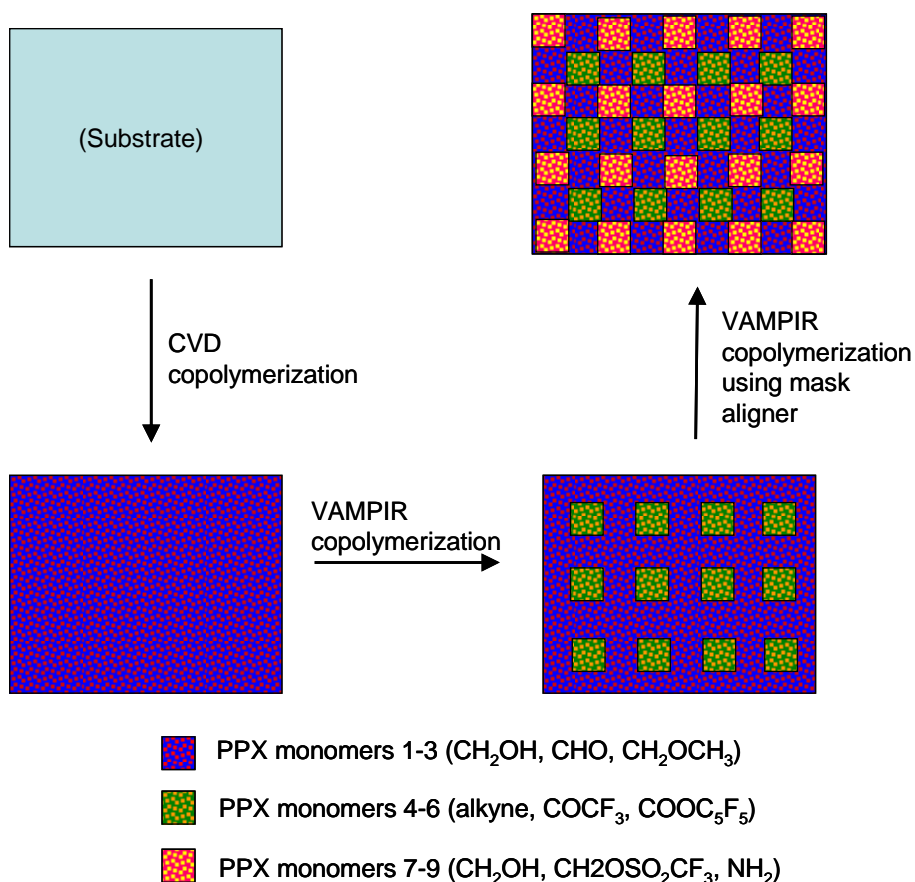

(Substrate)

CVD copolymerization

VAMPIR copolymerization

VAMPIR copolymerization using mask aligner

PPX monomers 1-3 (CH_2OH, CHO, CH_2OCH_3)

PPX monomers 4-6 (alkyne, $COCF_3$, $COOC_5F_5$)

PPX monomers 7-9 (CH_2OH, $CH2OSO_2CF_3$, NH_2)

Figure 6.2 Procedure for fabrication of copolymer surface potentially bearing 8-10 functional groups

react *in situ*. Also, the ratios would be very difficult to control, regardless if a one-source or two-source CVD was used.

One possible way to bypass such problems is to employ a combination of the VAMPIR procedure (described in chapter 1) and CVD copolymerization. As shown in Figure 6.2, a copolymer (3-5 different dimers) is homogeneously deposited onto a substrate. Following this, a micropatterned PDMS stamp is applied to the substrate, after which VAMPIR copolymerization is performed, using 3-5 dimers different than that of the base copolymer. What results is a copolymer surface comprising of 8-10 functional groups, provided that the pattern features are sufficiently small. By using a mask aligner to apply a second VAMPIR stamp, another VAMPIR deposition step can be employed, such that its pattern is misaligned from the first. This procedure could produce a surface which bears three patterns simultaneously (Figure 6.2), and it would allow the user to divide the 10-component copolymerization into three steps. Such a process, if accomplished successfully, could also transform DNA/protein microarrays into highly advanced and highly selective devices. Efficient bioassays and diagnostic devices rely on the specific binding of analytes and biomolecules.[7] Thus, the more analytes one can bind in a specific manner, the more detailed and specific the detection will be. Within each group of monomers in the VAMPIR pattern (Figure 6.2), one functional group serves as the binding site, whereas the other two are meant to inhibit adhesion of other molecules. Also, in gene therapy applications, multiple virus vectors can be immobilized in specific predefined areas, a necessity for directing tissue regeneration of organs such as bone.[8] The protocol specified in Figure 6.2 could be used to regenerate organ tissue and blood vessels.

6.2.3 CVD Copolymer Gradients

The two-source CVD system is as adaptable as the chamber structure. As long as ports exist in the chamber wall, the user can augment additional hardware into the system. For example, the two-source system used accommodates an *in situ* mass spectrometer, which can be used to gauge the stability and degree of monomer pyrolysis. However, if the angle between the two existing sources is decreased to 120° instead of 180°, a third source can be installed, allowing for the production of ternary copolymer gradients. Figure 6.3 illustrates the idea with a possible outcome. One limitation of the existing equipment has been a lack of *in situ* imaging. XPS would become too cumbersome for examining samples over a large 2-dimensional area. FTIR or Raman imaging would also be an important supplement to a 3-source deposition system.

Further expansion of the available range of gradient concentrations will be another area of further study. Although CVD parameters control the gradient slope with ease, a decrease in gradient slope will also be valuable. However, some hurdles block the facile decrease of polymer gradient slope. One hurdle is the fluctuation of polymer gradient composition. Decreasing the polymer gradient slope to 1.5 inches may be possible by decreasing the system mean free path, as suggested in Chapter 5. Also, if a 3-source CVD system is employed, one could conceivably load an identical monomer into two sources, with a different monomer loaded into the third source. Such a protocol may offset the aforementioned obstacle. In any event, the immobilized biomolecular gradient(s) have an effectively greater slope than the base polymer gradient, due to steric hindrances of immobilized biomolecules.
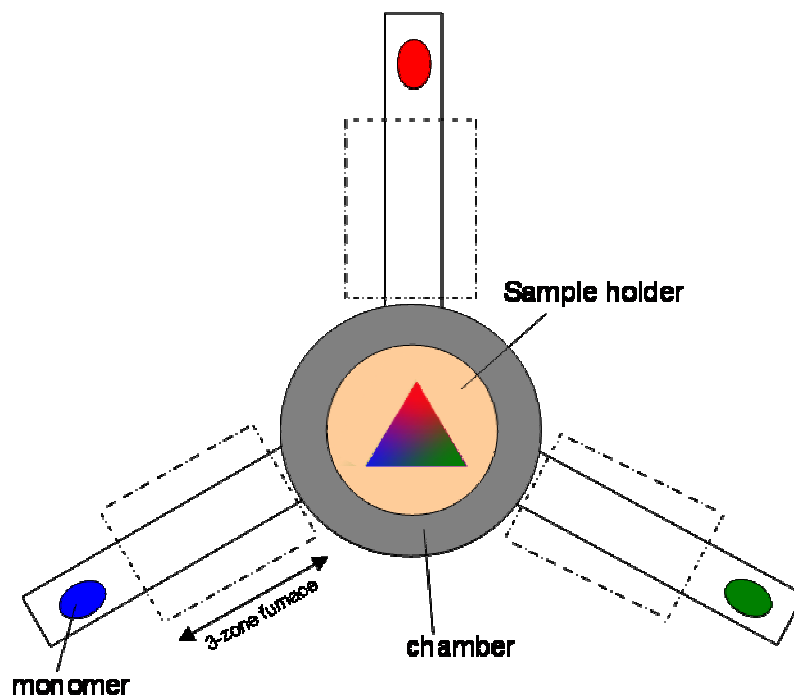
Figure 6.1 Overhead-view schematic of a potential three-source CVD system.

While the work described illustrates the immobilization of a biomolecular gradient, CVD polymer gradients can be used as a platform for other types of gradients. If a hydrophilic molecule selectively reacts with one of the gradient components, a contact angle gradient would result. Also, a binary and/or ternary gradient can be used in high-throughput combinatorial experiments. Rather than depositing homogeneous copolymer compositions in a serial manner, one copolymer gradient can simultaneously screen for cellular responses towards many different surface compositions. Most importantly, the gradient can potentially induce cell chemotaxis and differentiation. The ability to deposit high-slope gradients would greatly benefit cell chemotaxis studies. As an application, one could immobilize a gradient of morphogens, which is necessary for tissue development.[9] The gradient would be useful post-surgery in accelerating patient recovery and preventing autoimmune responses towards implants.

References

[1] J. Lahann, *Polym. Int*. **2006**, 55, 1361.

[2] J.A. Lee, T.J. McCarthy, *Polymer Preprints* **2007**, 48, 464.

[3] W.R. Dolbier Jr., M.A. Asghar, H.Q. Pan, L. Celewicz, *J. Org. Chem*. **1993**, 58, 1827.

[4] W.R. Dolbier Jr., P. Xie, L. Zhang, W. Xu, Y. Chang, K.A. Aabboud, *J. Org. Chem.* **2008**, 73, 2469.

[5] Y. Elkasabi, H.Y. Chen, J. Lahann, *Adv. Mater.* **2006**, 18, 1521.

[6] A.K. Bajpai, *J. Mater Sci. Mater. Med*. **2008**, 19, 343.

[7] H. Tani, K. Maehana, T. Kamidate, *Anal. Chem*, **2004**, 76, 6693-6697.

[8] R.M. Schek, E.N. Wilke, S.J. Hollister, P.H. Krebsbach, *Biomater*. **2006**, 27, 1160.

[9] J.B. Gurdon, P.Y. Bourillot, *Nature* **2001**, 413, 797.

APPENDICES

APPENDIX A
Protocol for *Escherichia coli* Adhesion onto Poly(*p*-xylylene) Coated Surfaces

<u>Using CVD-coated 8-well glass slides</u>
1. Sterilize in 95% EtOH for >5 minutes. Sonicate briefly above each well
2. Cells grown in liquid culture
    a. Spin down 1mL of saturated overnight culture at 16,000g for 1 minute.
    b. Wash pellet with 1mL of PBS pH 7.4 by flicking and pipetting up/down.
    c. Spin down again at 16,000g 1 minute.
    d. Resuspend pellet in 1mL of PBS by flicking and pipetting up/down.
    e. Dilute to 1OD with PBS.
3. Cells grown on a YESCA plate
    a. Pull cells from plate and resuspend in 1mL of PBS.
    b. Wash with 1mL of PBS pH 7.4 by flicking and pipetting up/down.
    c. Spin down again at 16,000g for 1 minute.
    d. Resuspend pellet in 1mL of PBS by flicking and pipetting up/down.
    e. Dilute to 1OD with PBS
4. Place 20uL of cells suspensions on plate and incubate at room temperature for 2 hours (or vary).
5. Wash plate by dropping into 50mL of PBS in a large wash tray.
6. Wash 5 minutes by shaking at '5' speed. Remove PBS and wash 2 more times
7. Put plates on a blotting paper and remove excess solutions.
8. Let plate dry >30 minutes at 37 $^{\circ}$C.
9. OPTIONAL: Heat fixation. Wave plate over flame for a few seconds to dry it.

<u>Staining</u>:
DAPI
1. Add 200μL of 200X DAPI stain to 40mL of PBS
2. Drop plates in stain and cover. Incubate for 5 minutes on benchtop.
3. Wash 3X in 50mL of PBS for 5 minutes. Keep covered
4. To view slide (should be some liquid left) cover with a slip and view with DAPI filter set

Crystal Violet
1. Add 50mL of 1% Crystal Violet (CV) to large wash tray.
2. Drop plates into CV and stain for 1 hour. Keep covered
3. Wash 3X in 50mL of PBS for 5 minutes.
4. Take a picture

Live/Dead Assay
    (Cells in suspension)
1. Add 6μL of Component A to 2mL of MilliQ water to make 2X staining solution.

2. Take OD 670 of cells used in above solution
3. Dilute to OD670 of 0.12 in PBS
4. Add 100μL of cells into a 96 well plate and add 100μL of staining solution.
5. Incubate the sample in the dark for 15 minutes.
6. Excite at 485 and Read from 500 to 700 in 5 nm Steps using a 495 Cutoff
7. Be sure to duplicate samples and do a buffer control

   (On a plate)
1. After drying dilute 2X staining solution to 1X with PBS
2. Add 50μL of 1X staining solution to each depression.
3. Incubate in the dark for 15 minutes.
4. Remove ~45μL of solution with a pipette
5. Add coverslip and view with fluorescent microscope

Attached cell number/ml
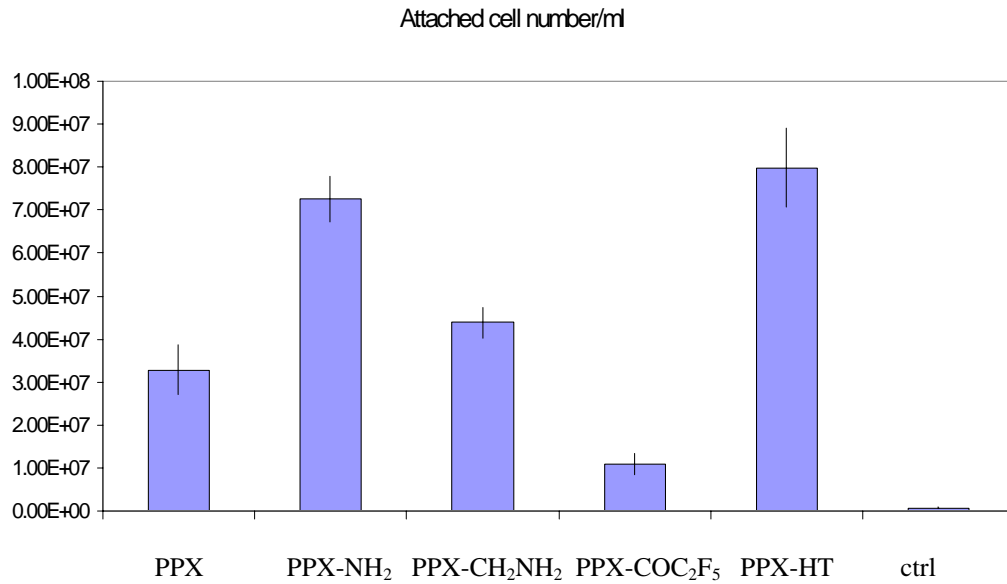
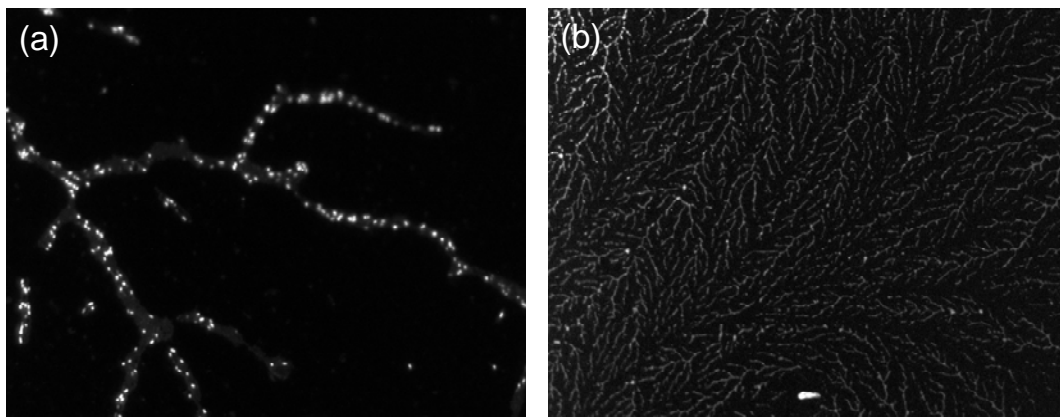**Figure B.1**. Cell counts of *E. coli* adhered onto various functionalized PPX coatings.

Figure B.2. Fluorescence images of MC4100 *E. coli* strain cultured over PPX-CH_2NH_2 surface. Images acquired at (a) 400X and (b) 40X magnification
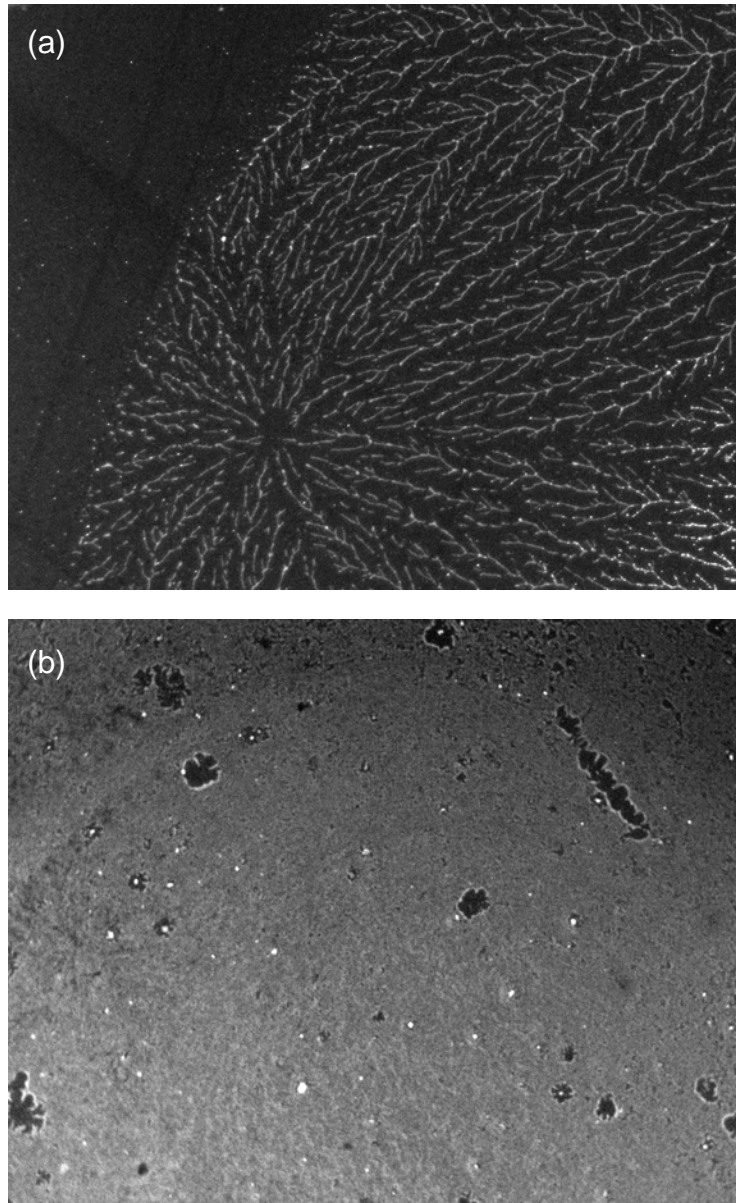
133

Figure B.3 Fluorescence images (40X magnification) of LSR11 *E. coli* strain cultured over (a) PPX-COC$_2$F$_5$ and (b) PPX-HT surfaces.
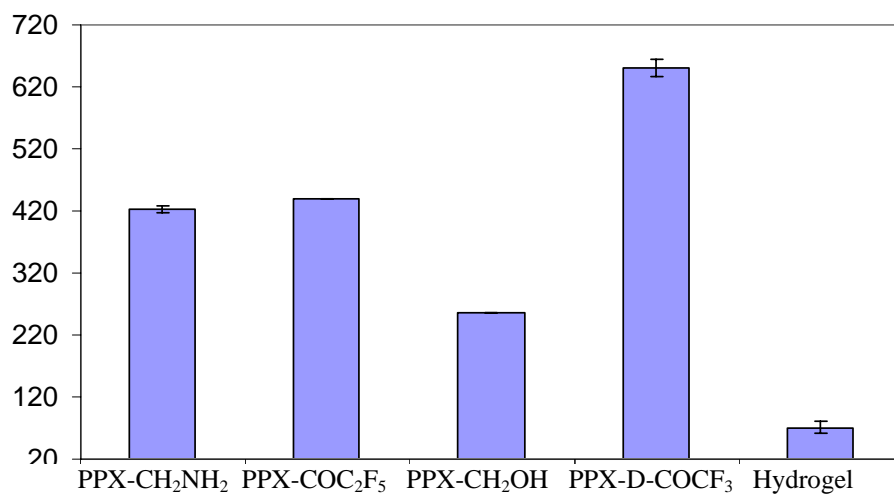
Figure B.4 Quantified fluorescence readings of MC4100 *E. coli* strain adhered onto various functionalized PPX coatings. Cells were grown initially from YESCA plate.
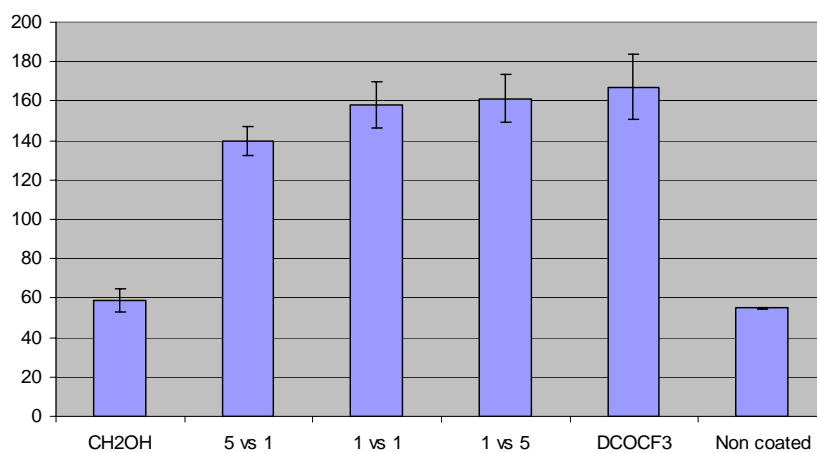

Figure B.5 Quantified fluorescence readings of MC4100 *E. coli* strain adhered onto PPX-CH$_2$OH/PPX-D-COCF$_3$ copolymer coatings